BELL CREEK TEST SITE – SIMULATION REPORT

Plains CO_2 Reduction (PCOR) Partnership Phase III
Task 9 – Deliverable D66, Update 5

Originally Submitted: August 2011; Update 1 Submitted: August 2012; Update 2 Submitted: August 2013; Update 3 Submitted: August 2014; Update 4 Submitted: August 2015

Prepared for:

Andrea M. Dunn

National Energy Technology Laboratory
U.S. Department of Energy
626 Cochrans Mill Road
PO Box 10940
Pittsburgh, PA 15236-0940

DOE Cooperative Agreement No. DE-FC26-05NT42592

Prepared by:

Lu Jin
Nicholas W. Bosshart
Benjamin S. Oster
Steven B. Hawthorne
Kyle J. Peterson
Matthew E. Burton-Kelly
Ian K. Feole
Tao Jiang
Lawrence J. Pekot
Wesley D. Peck
Scott C. Ayash
Charles D. Gorecki

Energy & Environmental Research Center
University of North Dakota
15 North 23rd Street, Stop 9018
Grand Forks, ND 58202-9018

August 2016
Approved

2019-EERC-10-04

EERC DISCLAIMER

LEGAL NOTICE This research report was prepared by the Energy & Environmental Research Center (EERC), an agency of the University of North Dakota, as an account of work sponsored by the U.S. Department of Energy (DOE) National Energy Technology Laboratory (NETL). Because of the research nature of the work performed, neither the EERC nor any of its employees makes any warranty, express or implied, or assumes any legal liability or responsibility for the accuracy, completeness, or usefulness of any information, apparatus, product, or process disclosed or represents that its use would not infringe privately owned rights. Reference herein to any specific commercial product, process, or service by trade name, trademark, manufacturer, or otherwise does not necessarily constitute or imply its endorsement or recommendation by the EERC.

ACKNOWLEDGMENTS

This work was performed under DOE NETL Cooperative Agreement No. DE-FC26-05NT42592. The EERC would like to thank Denbury Resources Inc. (Denbury) for providing necessary data to perform this work. Special thanks go to the members of Denbury's Bell Creek team for their valuable input and fruitful discussions.

DOE DISCLAIMER

This report was prepared as an account of work sponsored by an agency of the United States Government. Neither the United States Government, nor any agency thereof, nor any of their employees, makes any warranty, express or implied, or assumes any legal liability or responsibility for the accuracy, completeness, or usefulness of any information, apparatus, product, or process disclosed, or represents that its use would not infringe privately owned rights. Reference herein to any specific commercial product, process, or service by trade name, trademark, manufacturer, or otherwise does not necessarily constitute or imply its endorsement, recommendation, or favoring by the United States Government or any agency thereof. The views and opinions of authors expressed herein do not necessarily state or reflect those of the United States Government or any agency thereof.

TABLE OF CONTENTS

LIST OF FIGURES

Continued . . .

LIST OF FIGURES (continued)

Continued . . .

LIST OF FIGURES (continued)

LIST OF TABLES

BELL CREEK TEST SITE – SIMULATION REPORT

EXECUTIVE SUMMARY

The Plains CO_2 Reduction (PCOR) Partnership has been working with Denbury Resources Inc. (Denbury) in the Bell Creek Field to evaluate the effectiveness of large-scale CO_2 injection for CO_2 enhanced oil recovery (EOR) and study the long-term CO_2 storage potential within the field.

As part of the PCOR Partnership's adaptive management approach to developing the CO_2 storage program, modeling and numerical simulation activities continue toward the goal of providing a comprehensive assessment of associated CO_2 storage behavior. This goal, while not a new objective at Bell Creek Field, has been guiding recent efforts discussed in this report (work completed since August 2015). The overarching themes for the research discussed in this report include 1) increasing our understanding of the subsurface of Bell Creek Field through the acquisition of new data and 2) modeling and simulation activities to achieve predictions of fluid flow, pressure response, oil sweep and CO_2 storage efficiency, and determining the long-term fate of injected CO_2.

More specifically, discussion from this reporting period includes the 1) acquisition of new geologic characterization data, including pulsed-neutron logs (PNLs) and surface seismic data, to reduce uncertainty in model construction; 2) modeling of the reservoir and shallow subsurface aquifers, both within and surrounding the field, to provide the basis for numerical simulations of CO_2 injection; 3) development of a pressure, volume, and temperature (PVT) model (to be applied in compositional simulations) to predict the miscibility behavior of the system with varying injection gas compositions (i.e., recycled gas injection, CO_2 with varying amounts of impurities); 4) investigation of the effects of recycled gas injection on EOR and CO_2 storage performance; 5) history-matching of reservoir models; and 6) running of predictive simulations to aid in monitoring long-term behavior of injected CO_2.

Additional characterization data have been acquired in this reporting period to gain further insight into the static and dynamic nature of the Bell Creek Field subsurface environments. Seventeen PNLs were acquired in late 2015, providing baseline characterization data and delineation of fluid saturation changes (CO_2, water, and oil). Seismic data acquired in 2015 have enabled further geologic characterization and interpretation. The 2012, 2014, and 2015 surface seismic surveys show consistency and repeatability of geologic features (indicating the seismic data sets are reliable). Permeability barriers noted in amplitude summation maps (discussed in Burnison and others[1] and Bosshart and others[2]) are shown clearly in time-lapse images of seismic difference volumes. The morphology of these features substantiates the revised interpretation of the erosional/depositional processes through which they were created. As noted in Bosshart and others[2], hydraulic connectivity appears to exist between Phases 1 and 2 (across the north–south

incised channel permeability barrier) in 4-D seismic analyses. These analyses also suggest the presence of limited hydraulic connectivity between Phases 1 and 3.

The data acquired over the last year have provided further verification of the revised understanding of Muddy Formation deposition at Bell Creek. Reservoir modeling efforts are focused on integrating this interpretation to create more accurate facies and petrophysical property distributions, enabling a better history match and more accurate predictive simulations.

Regional-scale, basin-scale, and near-surface (shallow aquifer) models were constructed to determine the long-term CO_2 migration potential in the greater Bell Creek Field region. The regional- and basin-scale models were developed to assess CO_2 migration potential in the reservoir interval, while the near-surface model was developed to investigate CO_2 migration potential in Bell Creek's shallow aquifers (Fox Hills and Hell Creek Formations). To clarify, there is no evidence of unintended CO_2 saturation in shallow aquifer units or any regions outside of the field, nor any reason to believe this will ever be the case. These investigations aim to inform where MVA (monitoring, verification, and accounting) efforts may best be implemented for rapid detection and response. These models have not yet been subjected to simulation efforts.

Three simulation models with different scales (quarter five-spot, subphase-, and phase-scale) and a nine-component PVT model were developed to simulate the impact of impurities on recycled gas EOR and CO_2 storage performance. Impurities in Bell Creek produced gas samples were analyzed to provide data necessary for these simulations. Results showed methane (CH_4) was the main impurity, which varied from 1 to 4 mol%, and the quantity of impurities appears to be decreasing as the CO_2 flood continues. A series of minimum miscibility pressure (MMP) measurements were conducted for the Bell Creek oil and CH_4–CO_2 mixtures under reservoir conditions using the vanishing interfacial tension (VIT) method, which produced similar results to the slim-tube method (but the testing was faster and more cost-effective). The measured MMPs of the Bell Creek oil increased from 1403 to 4085 psi as the CH_4 mol% increased from 0% to 100% in the solvent phase. The recycled gas EOR simulations performed with the new PVT model discussed above indicated a range of impurities (up to 30 mol%) can be tolerated in the recycled gas without significant impairment of EOR efficiency or CO_2 storage performance.

A simulation model encompassing the Phases 3–7 areas was also constructed for investigation of long-term CO_2 migration behavior. Two case studies were simulated considering the effects of fluid density differences (buoyancy) within the reservoir's geologic structure. These cases simulated a 5000-year interval and showed that CO_2 migration (under the effects of buoyancy only) would be a slow process in the Bell Creek Field, around 3 ft/year to the east–southeast. However, these simulations excluded the effects of mineral trapping, the pinchout of reservoir quality sand updip of the field, and natural hydrodynamics operating in the direction opposite to the CO_2 migration vector. These additional factors would likely further hinder CO_2 migration potential, suggesting that injected CO_2 is likely to remain contained within the field for thousands of years.

[1] Burnison, S.A., Burton-Kelly, M.E., Zhang, X., Gorecki, C.D., Steadman, E.N., and Harju, J.A., 2014, Bell Creek test site – 3-D seismic and characterization report: Plains CO_2 Reduction (PCOR) Partnership Phase III Task 4 Deliverable D96 for U.S. Department of Energy National Technology Laboratory Cooperative Agreement No. DE-FC26-05NT42592, March.

[2] Bosshart, N.W., Jin, L., Dotzenrod, N.W., Burnison, S.A., Ge, J., He, J., Burton-Kelly, M.E., Ayash, S.C., Gorecki, C.D., Hamling, J.A., Steadman, E.N., and Harju, J.A., 2015, Bell Creek test site – simulation report: Plains CO_2 Reduction (PCOR) Partnership Phase III Task 9 Deliverable D66 Update 5 for U.S. Department of Energy National Energy Technology Laboratory Cooperative Agreement No. DE-FC26-05NT42592, August.

BELL CREEK TEST SITE – SIMULATION REPORT

INTRODUCTION

The Plains CO_2 Reduction (PCOR) Partnership, led by the Energy & Environmental Research Center (EERC), is working in conjunction with operator Denbury Resources Inc. (Denbury) to evaluate the effect of large-scale carbon dioxide (CO_2) injection into a clastic reservoir in the Bell Creek Field in southeastern Montana for CO_2 enhanced oil recovery (EOR) and to monitor the storage of CO_2. A technical team consisting of the EERC, Denbury, and others is conducting a variety of investigations used to determine baseline reservoir characteristics, perform predictive simulations of CO_2 injection, and monitor the migration of injected CO_2 within the reservoir. Injection and production operations are being carried out by Denbury with the EERC providing site characterization; modeling and simulation; risk assessment; and the continual development of monitoring, verification, and accounting (MVA) plans to address key technical subsurface risks (Gorecki and others, 2012).

The Bell Creek Field in the northeastern Powder River Basin (PRB) (Figure 1) has been producing oil from the Muddy Formation for nearly 50 years. Denbury's employment of the tertiary technique of CO_2 EOR is progressing through nine phases of development (regions within the Bell Creek Field; Figure 2). This operation is being supplied with CO_2 from ExxonMobil's Shute Creek gas-processing plant in LaBarge, Wyoming, and ConocoPhilips' Lost Cabin natural gas-processing plant via the 232-mile Greencore Pipeline (Figure 1). There is approximately 55 million standard cubic feet (MMscf) of CO_2 being delivered to Bell Creek Field every day for EOR operations.

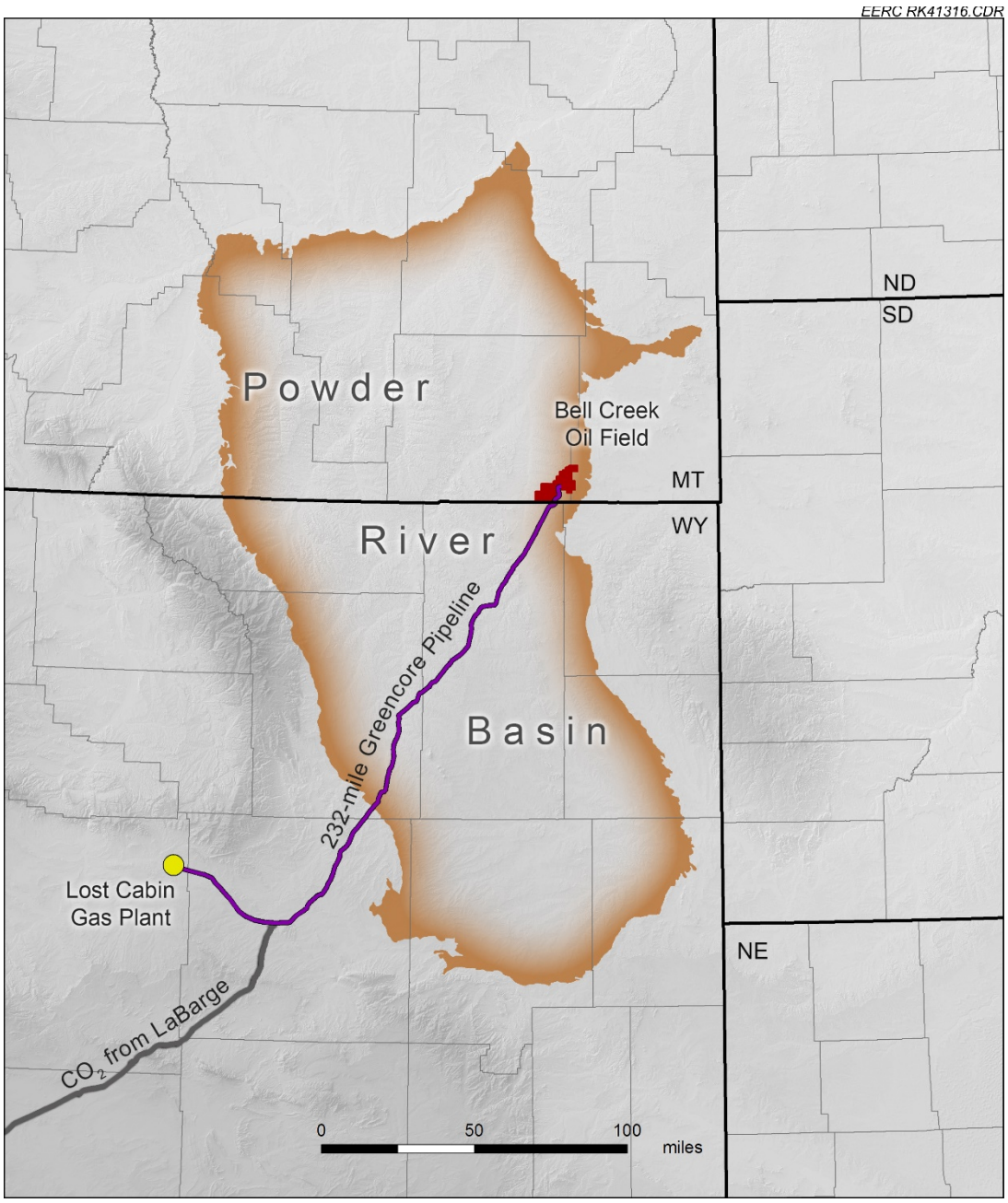

Figure 1. Map of the Bell Creek Field in relation to the PRB and the pipeline from the Lost Cabin gas plant.

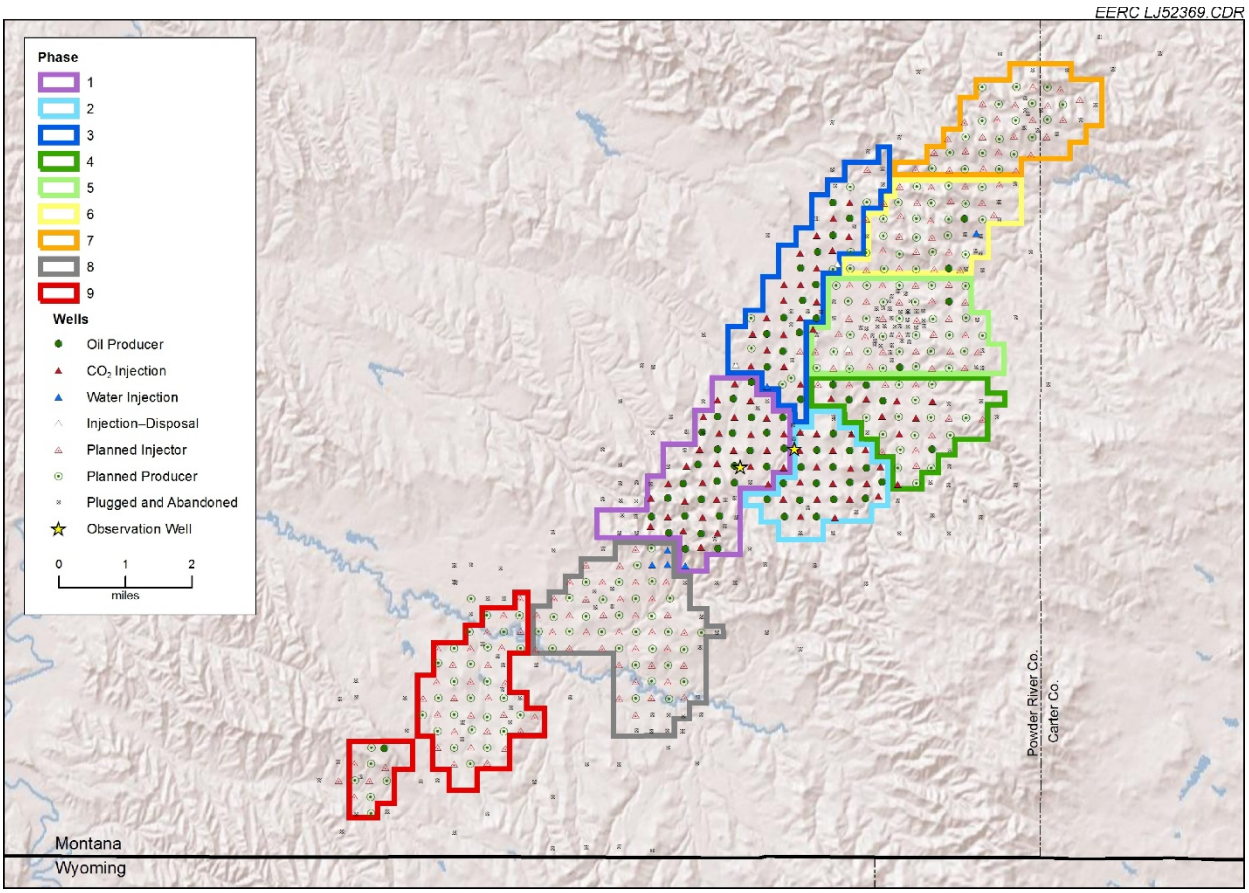

Figure 2. Study area of the Bell Creek Field showing the nine phase areas of scheduled injection.

PURPOSE

Four main components (site characterization, modeling and simulation, risk assessment, and MVA) are being employed by the PCOR Partnership as an Adaptive Management Approach (Gorecki and others, 2012; Figure 3) for large-scale CO_2 storage projects. The Bell Creek Field is currently in the injection/operation phase, where MVA efforts are focused on risk assessment and risk management through modeling and simulation activities, as well as intermittent acquisition of key monitoring data sets (such as seismic surveys and pulsed-neutron well logging (PNL) campaigns). The PCOR Partnership's Adaptive Management Approach allows the site-specific nature of a carbon capture and storage project to be taken into account. Modeling and simulation activities 1) identify areas where site characterization efforts could be increased or a denser data distribution is desired, 2) identify and characterize potential subsurface risks such as fluid migration away from the reservoir, and 3) aid in the development of effective monitoring strategies.

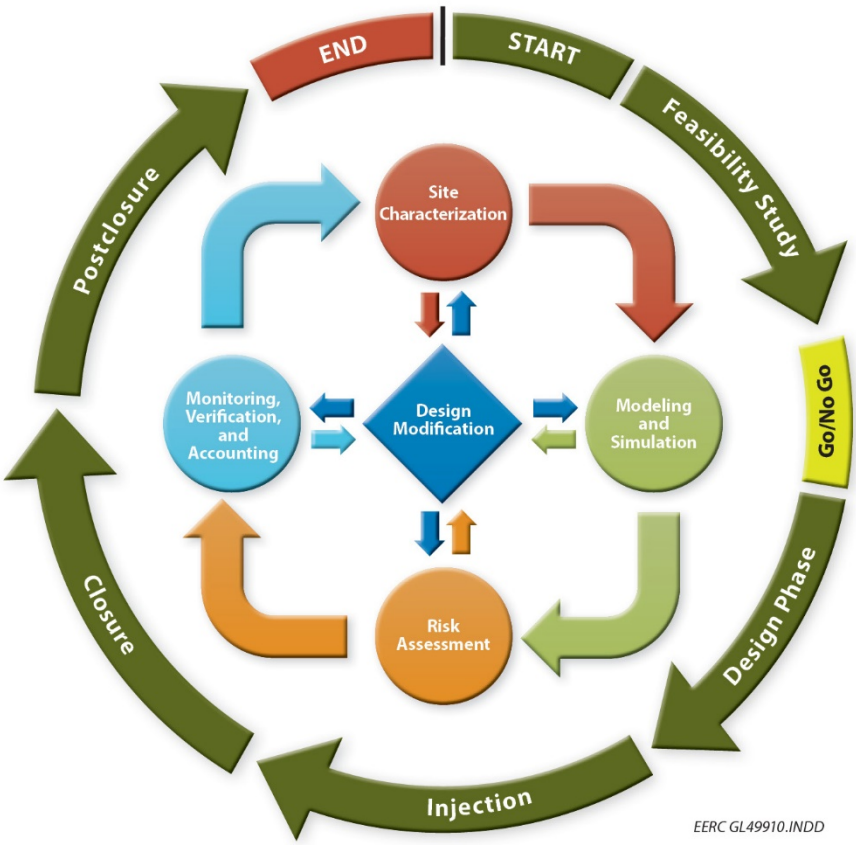

Figure 3. Project elements of the Bell Creek CO_2 storage and EOR project. Each element feeds into another, iteratively improving results and efficiency of evaluation (modified from Gorecki and others, 2012).

The EERC's geocellular modeling of the subsurface enables increased understanding and prediction of the behavior of injected CO_2 and reservoir fluids over the injection and postinjection period. History matching is performed on a numerically tuned dynamic reservoir model (constructed from a static geologic model) for validation and increased accuracy in predictive simulations. This history-matching process is followed by the simulation of multiple scenarios pertaining to fluid migration and pressure response within the reservoir. Additionally, these simulation activities provide a means to evaluate the sweep and storage efficiency and the applicability of various monitoring activities related to CO_2 injection.

Geologic characterization, geocellular modeling, and numerical simulation are essential inputs for risk identification and an excellent guide for MVA techniques. This approach lays the foundation for a project's site-specific, risk-based, goal-oriented MVA plan to effectively monitor the behavior of injected CO_2 and reservoir fluids as the project progresses. Predictive simulations assist with targeted deployment of MVA data acquisitions at optimal surface and subsurface locations in relevant temporal context for (time and cost) efficiency in risk management. The results and experience gained at the Bell Creek oil field will provide insight and knowledge that

can be directly and readily applied to similar projects within the PCOR Partnership region and throughout the world (Steadman and others, 2011; Hamling and others, 2013).

BACKGROUND

Following the adaptive management philosophy developed by the PCOR Partnership (Figure 3), modeling and simulation activities have been updated annually based on available site characterization data and field injection/production records to improve risk identification and the MVA plan. All elements have been integrated into an iterative process to produce meaningful results for large-scale CO_2 storage and EOR projects. To date, five versions of the modeling and simulation reports have been produced to cover the highlights of activities since 2011. A brief description of each report follows:

- **Bell Creek Test Site Simulation Report: PCOR Partnership Phase III Task 9 Deliverable D66, 2011, approved (Pu and others, 2011)**

  The Version 1 (V1) 3-D geologic model was developed based on the available site characterization data and was focused on the Phase 1 area. A generalized lithology and stratigraphic framework in the Bell Creek oil field were interpreted that include four distinct lithofacies: Springen Ranch shale, coastal plain, Bell Creek sand, and Rozet shale in the Muddy Formation. The structure and properties were populated based on the 154 wells within the study boundary. Available data were analyzed, interpreted, and incorporated into the 3-D static geologic and dynamic reservoir models to represent geologic and reservoir properties in order to provide a solid groundwork for simulation activities.

  The PVT (pressure, volume, and temperature) data from three fluid samples were analyzed and lumped as seven components that matched the laboratory data. The results indicate that miscibility for oil samples can be achieved at approximately 2800 psi.

- **Bell Creek Test Site Simulation Report: PCOR Partnership Phase III Task 9 Deliverable D66, 2012, approved (Saini and others, 2012)**

  A 1-D compositional simulation of the experimental slim-tube tests was performed to ensure the robustness of the seven-component Peng–Robinson (PR) equation of state (EOS) developed in 2011. Minimum miscibility pressure (MMP) estimated from slim-tube simulation is about 2750 psia at 108°F, which agrees with the experimental results.

  The constructed geologic model was validated through history matching of oil rate, water cut, and gas/oil ratio (GOR) and was used for various predictive simulation scenarios for the Phase 1 area. A total of 12 cases based on a five-spot, a quarter five-spot, and the entire Phase 1 pattern were designed to address associated CO_2 storage and CO_2 breakthrough at the monitoring well, 05-06 OW, from a CO_2 water-alternating-gas (WAG) injection scenario.

- **Bell Creek Test Site Simulation Report: PCOR Partnership Phase III Task 9 Deliverable D66, 2013, pending approval (Braunberger and others, 2013)**

  A revised and more detailed 3-D static geocellular model of the Bell Creek oil field area (V2 model) was constructed using pertinent reservoir characterization data gathered in an extensive literature review and existing core analysis work for the entire Bell Creek oil field and surrounding area. Seven hundred forty-eight wells with wireline logs and many with core data were analyzed, interpreted, and incorporated into the 3-D static geocellular and dynamic reservoir models to represent geologic stratigraphy, petrophysical facies, and reservoir properties for simulation activities.

  The seven-component PR EOS model was tuned and matched to both original oil and depleted oil from slim-tube test and laboratory data. This produced an acceptable EOS for both matching historic production/injection and for performing predictive simulations.

  The Phase 1 area and immediately adjacent area were clipped from the V2 model and matched to production and injection historical records for a total of 46 years to validate the model and to get a good estimate of the current saturations and pressures in the model. Five predictive simulation cases were run to evaluate WAG and continuous CO_2 injection (CCI) at two injection bottomhole pressure (BHP) constraints and varying WAG cycle lengths.

- **Bell Creek Test Site Simulation Report: PCOR Partnership Phase III Task 9 Deliverable D66, 2014, pending approval (Liu and others, 2014)**

  Thirty-three baseline PNLs and seven repeat PNLs were used to update the stratigraphy and formation thicknesses from the reservoir to the surface throughout the V2 geologic model. Changes in fluid saturations for CO_2, water, and oil were identified through the repeat logs and incorporated into the model. In addition, a comprehensive reference model was created to serve as a repository for all relevant Bell Creek data used in the modeling and simulation activities. The existing V1 and V2 models, PNLs, historic and newly acquired logs, and core data were included in the reference model.

  A Phase 2 area simulation model was created from the V2 fieldwide 3-D geologic model and validated by history-matching oil, water, and gas production; water injection; and reservoir pressure data. The history-matched Phase 1 and 2 models were used to conduct predictive simulations to estimate the CO_2 storage potential of the Bell Creek Field as well as better understand sweep efficiency, recovery factors, and CO_2 utilization. Five simulation cases for Phases 1 and 2 (ten cases total) were performed to investigate WAG and CCI for two injection BHP constraints and varying WAG cycle lengths. Results indicated that WAG yields faster oil recovery and better sweep efficiency than CCI in Phases 1 and 2, while CCI results in more CO_2 being stored.

- **Bell Creek Test Site Simulation Report: PCOR Partnership Phase III Task 9 Deliverable D66, 2015, pending approval (Bosshart and others, 2015)**

  The Bell Creek reference model, constructed to house key data sets and enable consistency and efficiency in data sharing across various modeling efforts, was updated with new PNLs and seismic data that complemented the existing Bell Creek data (field and processed logs, core analyses, structural tops, cultural/political boundaries, completed simulation results, and ground surface elevation from lidar measurements).

  Previously developed Phase 1 and 2 simulation models were combined to simulate the fluid migration between the phases. Field records of primary production, waterflooding, and CO_2 injection were history-matched. The distributions of fluid saturations within the model were analyzed. Fluid flow between Phases 1 and 2 was identified. Predictive simulations of CCI and WAG were used to estimate oil recovery, CO_2 storage, and CO_2 utilization. It was concluded that, in the EOR process, WAG operations exhibit a higher sweep efficiency and can utilize CO_2 better than CCI. In terms of storage, CCI can store approximately double the amount of CO_2 in comparison to WAG.

  Previously developed geologic models (V1 and V2) were constructed in support of the historical Bell Creek depositional model (Galveston Island style barrier bar deposits with depositional strike oriented northeast–southwest). Investigations discussed by this report (history-matching results, interpretation of 3-D and 4-D seismic surveys, and comparison of PNL data) warranted the construction of a V3 model based upon a new geological interpretation. The V3 model, under construction at the time of this report, was supported by a depositional model which included a local, transgressive barrier bar in Phases 1 and 2. This interpretation indicated a large (90 degree) shift in the inferred shoreline orientation (approximately northwest–southeast) from previous studies.

SCOPE OF WORK

In order to evaluate the efficiency of large-scale CO_2 injection for EOR and to monitor the associated CO_2 storage in the Muddy Formation at the Bell Creek Field, several iterations of 3-D geologic modeling coupled with dynamic simulation work were completed as submitted in the previous five D66 reports (Pu and others, 2011; Saini and others, 2012; Braunberger and others, 2013; Liu and others, 2014; Bosshart and others, 2015). This report documents the modeling and simulation activities completed over the course of the past year (August 2015 – August 2016).

The updates pertaining to static modeling include 1) expanding on the revised geological interpretation first discussed in Bosshart and others (2015) based on the newly acquired PNL, seismic, and existing core data; 2) updating of the Bell Creek reference model with recently acquired PNL and seismic data; 3) continuing efforts in the construction of the V3 geologic model being developed to more accurately capture the reservoir heterogeneity; 4) completion of the Bell Creek regional- and basin-scale models; and 5) completion of the Bell Creek near-surface model.

The reservoir engineering and simulation activity updates for this reporting period pertain to 1) measuring of MMP for produced gas samples; 2) determining (bulk) recycled gas properties as the quantity of impurities varies; 3) conducting EOR simulations (WAG and continuous gas injection [CGI] operations) using recycled gas with varying amounts of impurities in the injection gas to assess both oil recovery and CO_2 storage performance; 4) conducting simulations on multiple hypothetical (varying geologic heterogeneity and resulting property distributions) quarter five-spot models to gain greater insight into the effects of geologic conditions, pressure constraints, and injection gas compositions on EOR and CO_2 storage performance; 5) history-matching the primary, secondary (waterflooding), and tertiary (EOR) production and injection data for Phase 3 of Bell Creek Field; and 6) conducting long-term simulations (thousands of years) to investigate the migration potential and long-term fate of injected CO_2 within Bell Creek Field.

Bell Creek Field Geology, New Data, Revised Interpretation, and Modeling Efforts

The Lower Cretaceous Mowry Formation overlies the Muddy Formation (reservoir and CO_2 injection target formation) and provides the primary seal, preventing the migration of fluid to overlying aquifers and to the surface (Figure 4). Overlying the Mowry, several thousand feet of low-permeability strata (Belle Fourche, Greenhorn, Niobrara, and Pierre Formations) provide secondary seals that will retard, if not prevent, upward fluid migration in the unlikely event that the primary seal fails.

Deposited in nearshore marine environments (Bosshart and others, 2015), high-porosity (25%–35%), high-permeability (150–1175 mD) sandstones dominate the Muddy Formation reservoir within the Bell Creek oil field. The initial reservoir pressure, approximately 1200 psi, is significantly lower than the regional hydrostatic pressure regime of 2100 psi at 4500 feet. Structurally, the field is on a shallow monocline dipping less than 2° to the northwest with a strike trending southwest to northeast. Stratigraphically, the Bell Creek sand interval pinches out in the updip direction against the overlying Springen Ranch Member and the underlying Rozet Member of the Muddy Formation.

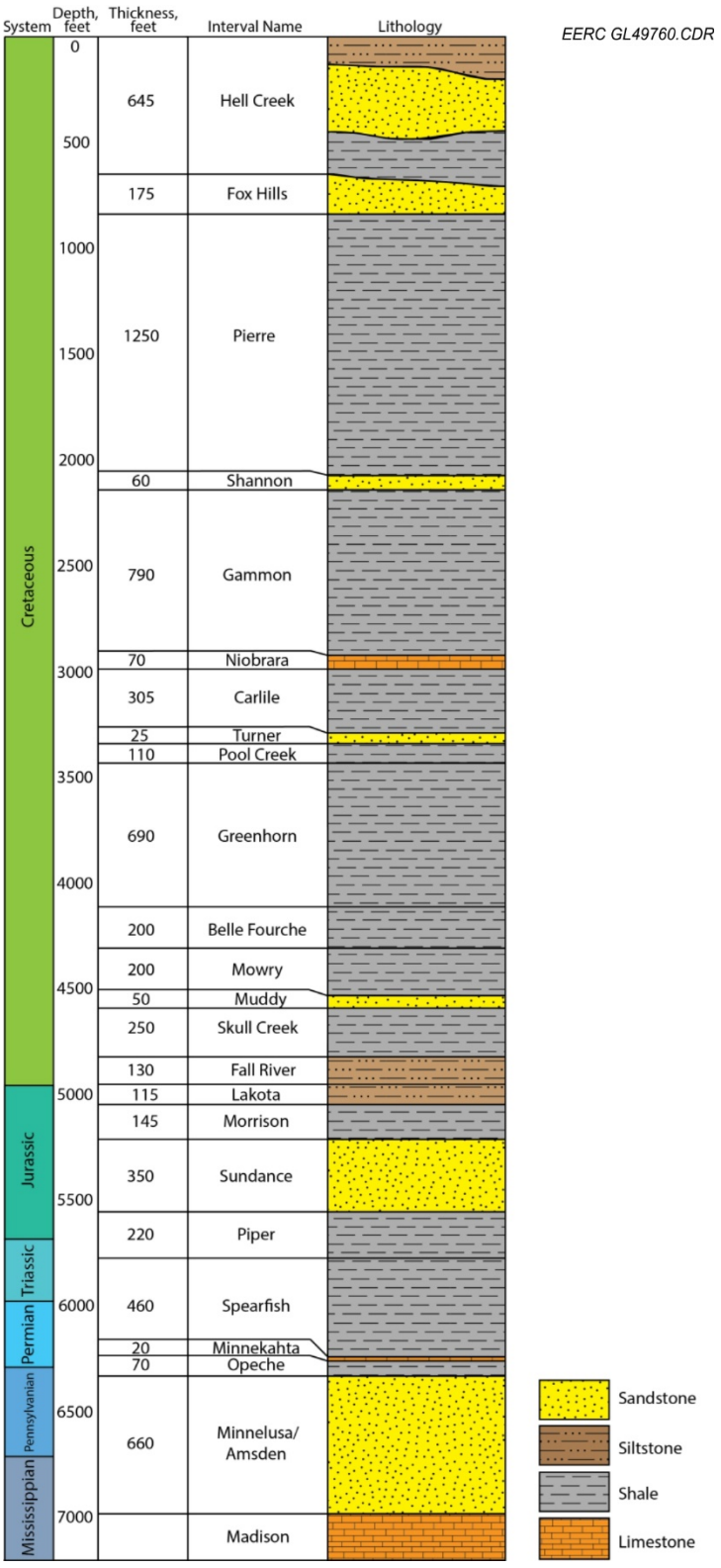

Figure 4. Local stratigraphy of the Bell Creek development area.

The Muddy Formation in Bell Creek Field can be subdivided into four intervals/members based on well log and core analysis. These members include (in ascending order) the Rozet Member (lowermost silty interval overlying the Skull Creek shale), overlain by the Bell Creek sand interval (reservoir), overlain by (if present) the Coastal Plain interval (included as the uppermost strata of the Bell Creek sand interval in this study), and the Springen Ranch Member (estuarine and shallow marine siltstone/shale; Figure 5).

From Bosshart and others (2015):

"The Bell Creek sand interval can (generally) be divided (in ascending order) into as many as four facies: 1) at the base, a laterally extensive sand that has been interpreted from well logs to have high connectivity throughout the field and is thought to have been deposited during deltaic/shoreline progradation occurring during a period of relative sea level fall; 2) a relatively thin, fine-grained layer representing a slight deepening in water depth (relative sea-level rise); 3) a sand interval that appears similar in lithology to the lower Bell Creek sand and was likely deposited in a similar fashion (regression/relative sea-level fall) but appears to contain an erosional unconformity at the top (as made evident by change in grain sorting, composition, bedding character and, in some places, the inclusion of thin coals, indicating subaerial exposure); and 4) an upper transgressive sheet sand (where present) deposited in barrier bar-to-shoreline environments as the seas transgressed (relative sea level rise). As sea level continued to rise, the estuarine/shallow marine siltstone of the lower Springen Ranch was deposited atop the Bell Creek sand interval."

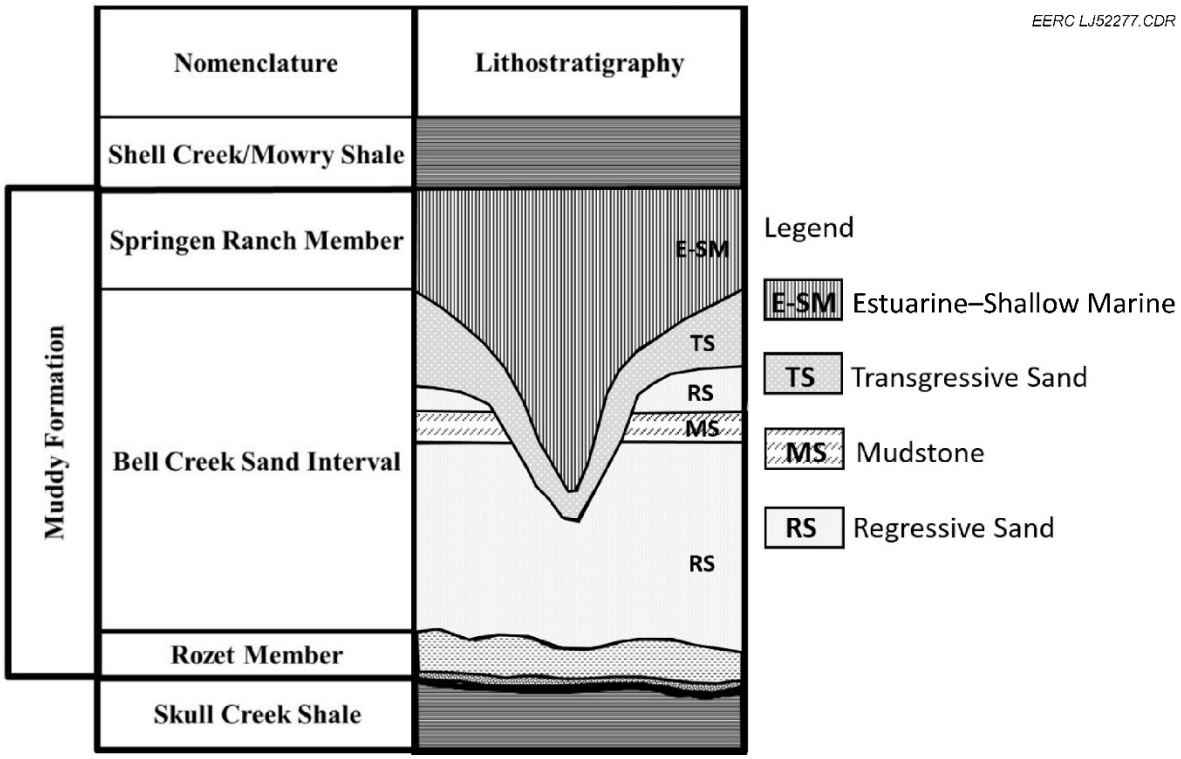

Figure 5. Muddy Formation reservoir stratigraphy (adapted from Molnar, 1990).

New Data Acquired

Since August 2015, new data have been acquired from a PNL campaign and a combined baseline/monitor seismic survey. All newly acquired data, along with previous data (e.g., well logs, core analysis, structural tops, etc.), are stored in the Bell Creek reference model (Liu and others, 2014; Bosshart and others, 2015).

PNL Data

During the 2015 PNL campaign (October–November), baseline and repeat/monitor logging was completed on 17 wells in the Phase 1, 3, and 4 areas (Figure 6). Within the Phase 1 area, repeat/monitor PNLs were acquired in five wells to investigate the water, oil, and CO_2 saturation responses associated with WAG injection and operational issues within the field. Figure 7 displays the saturation responses for WAG Injection Well 05-01 (injecting water at the time of acquisition, note the decrease in CO_2 saturation from previous measurement). Baseline PNLs in the Phase 3 area were acquired after CO_2 injection had already begun. Three production wells were chosen to determine near-wellbore CO_2 saturations. Nine wells in the Phase 4 area had baseline PNLs acquired prior to CO_2 injection. These wells were chosen to investigate a possible connection between the Phase 2 and 4 areas and to provide additional characterization data. Figure 8 shows the baseline log for the Phase 4 area Production Well 03-08 (penetrating interpreted lagoonal deposits within the upper Bell Creek sand interval [4327.5–4337.5 ft]).

Since 2013, monitor and baseline PNL surveys have been acquired on 45 wells in the Bell Creek Field (Figure 9). These PNL campaigns contributed large amounts of data to various investigations, such as monitoring CO_2 breakthrough between production and injection wells, improving the Bell Creek MVA program by monitoring saturations in overlying formations (Bosshart and others, 2015), calibrating history-matching efforts during dynamic simulation, and updating reservoir properties.

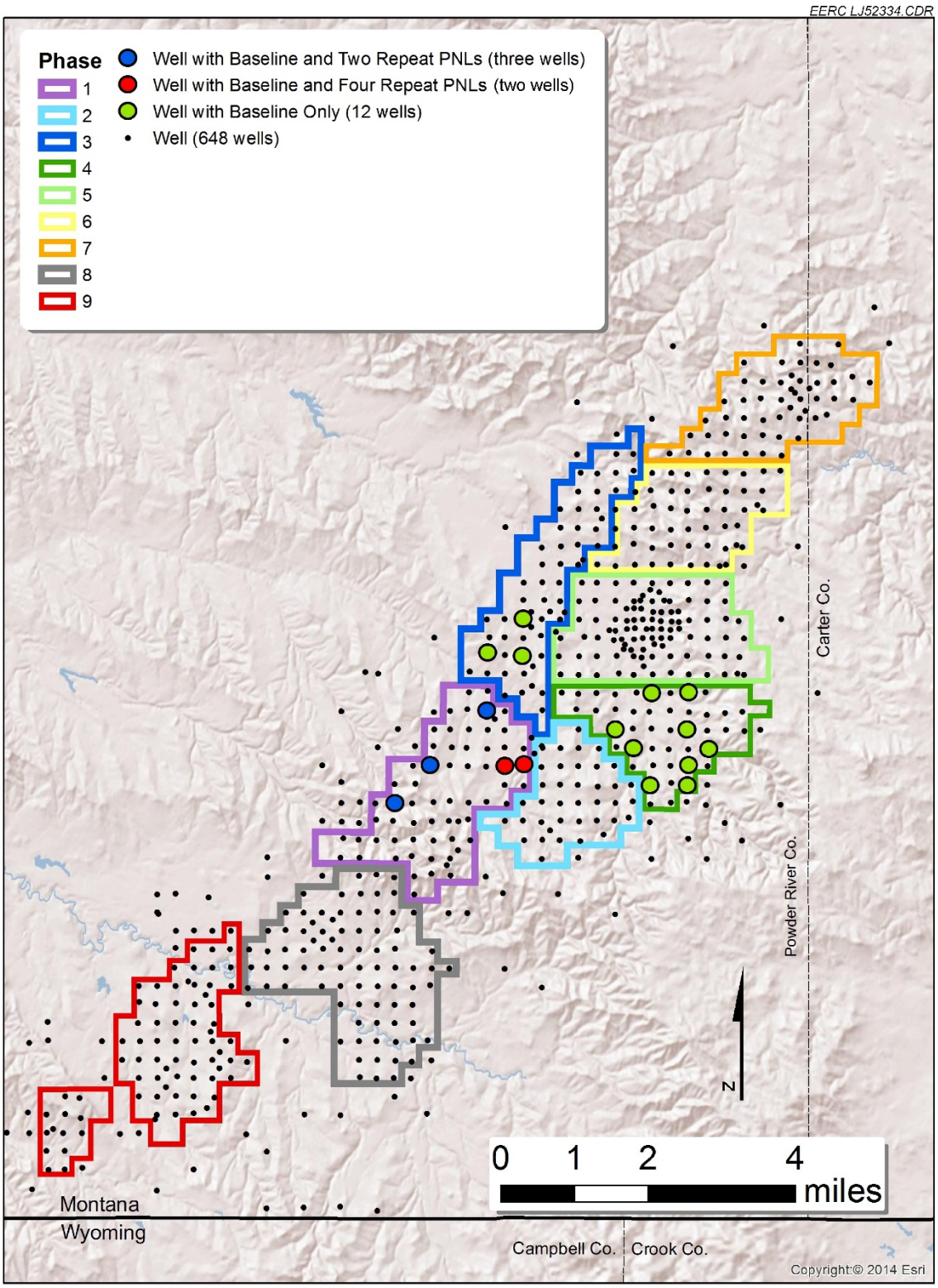

Figure 6. Map of Bell Creek Field wells logged during the 2015 PNL campaign.

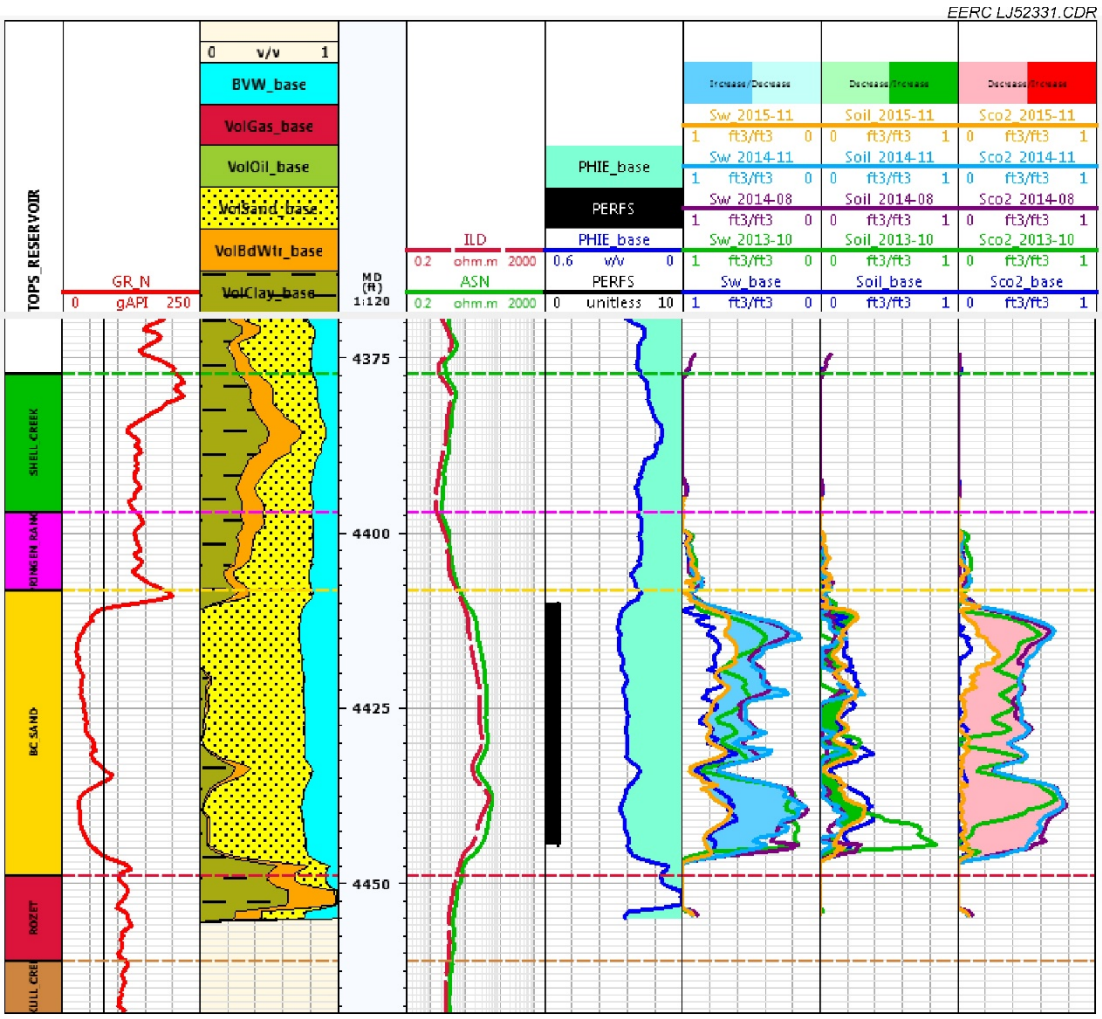

Figure 7. 05-01 injection well (Phase 1) PNL display within the Muddy Formation. Track descriptions are (from left to right) Muddy Formation subintervals (members), gamma ray (GR) log, component volumes, measured depth reference track (feet), resistivity log, perforations and effective porosity, water saturation, oil saturation, and CO_2 saturation. Regarding the saturations, color fill is indicative of increase or decrease in repeat PNL measurement (from November 2014 to November 2015). Interval tops shown are (from bottom to top) Skull Creek, Rozet, Bell Creek sand, Springen Ranch, and Shell Creek shale. This well was undergoing water injection at the time of measurement (note the decrease in CO_2 saturation and increase in water saturation).

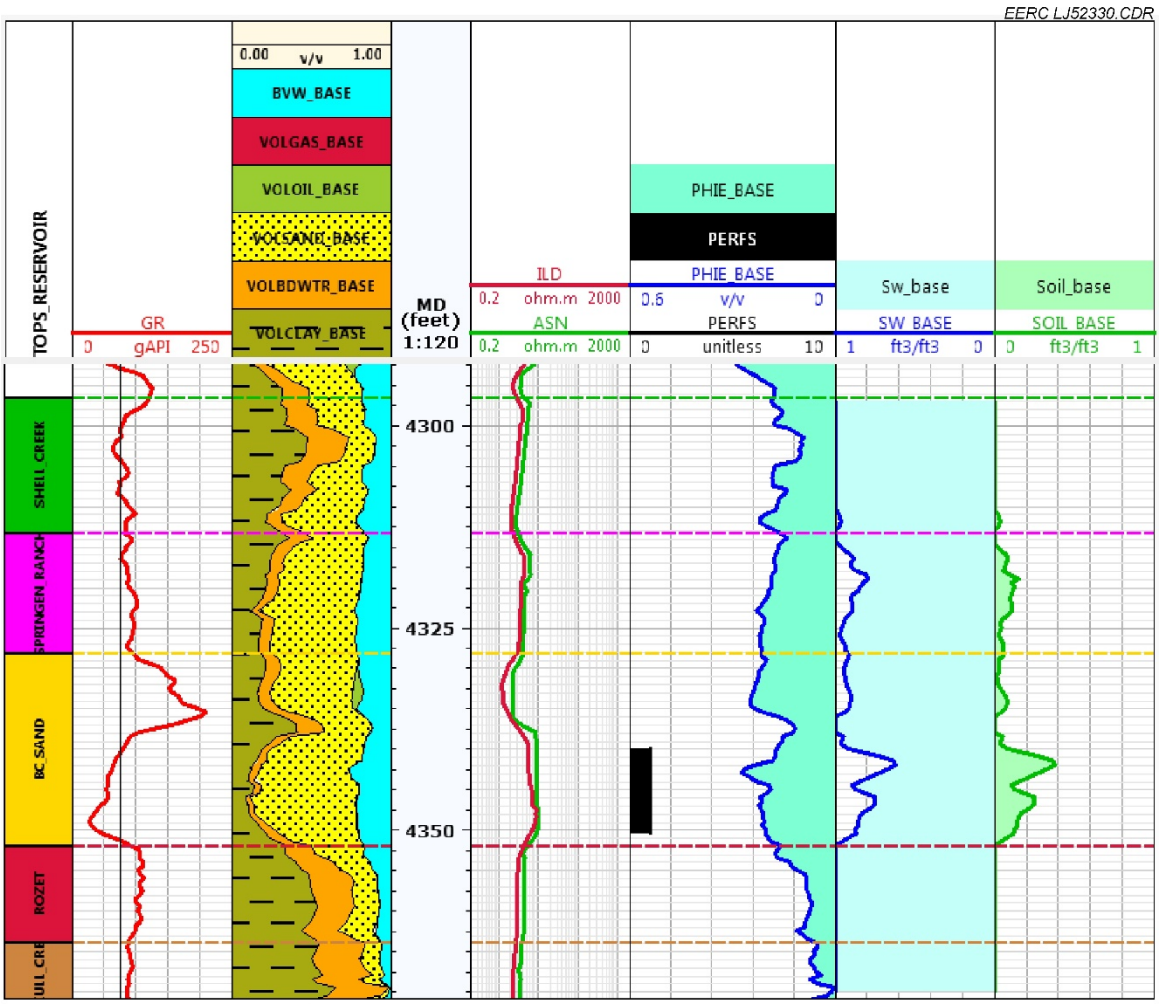

Figure 8. 03-08 production well (Phase 4) baseline PNL display within the Muddy Formation interval. Track descriptions are (from left to right) Muddy Formation subintervals (members), GR log, component volumes, measured depth reference track (feet), resistivity log, perforations and effective porosity, water saturation, and oil saturation. Interval tops shown are (from bottom to top) Skull Creek, Rozet, Bell Creek sand, Springen Ranch, and Shell Creek shale. This well penetrates interpreted lagoonal deposits in the upper Bell Creek sand member with high GR signature (depths 4327.5–4337.5 ft).

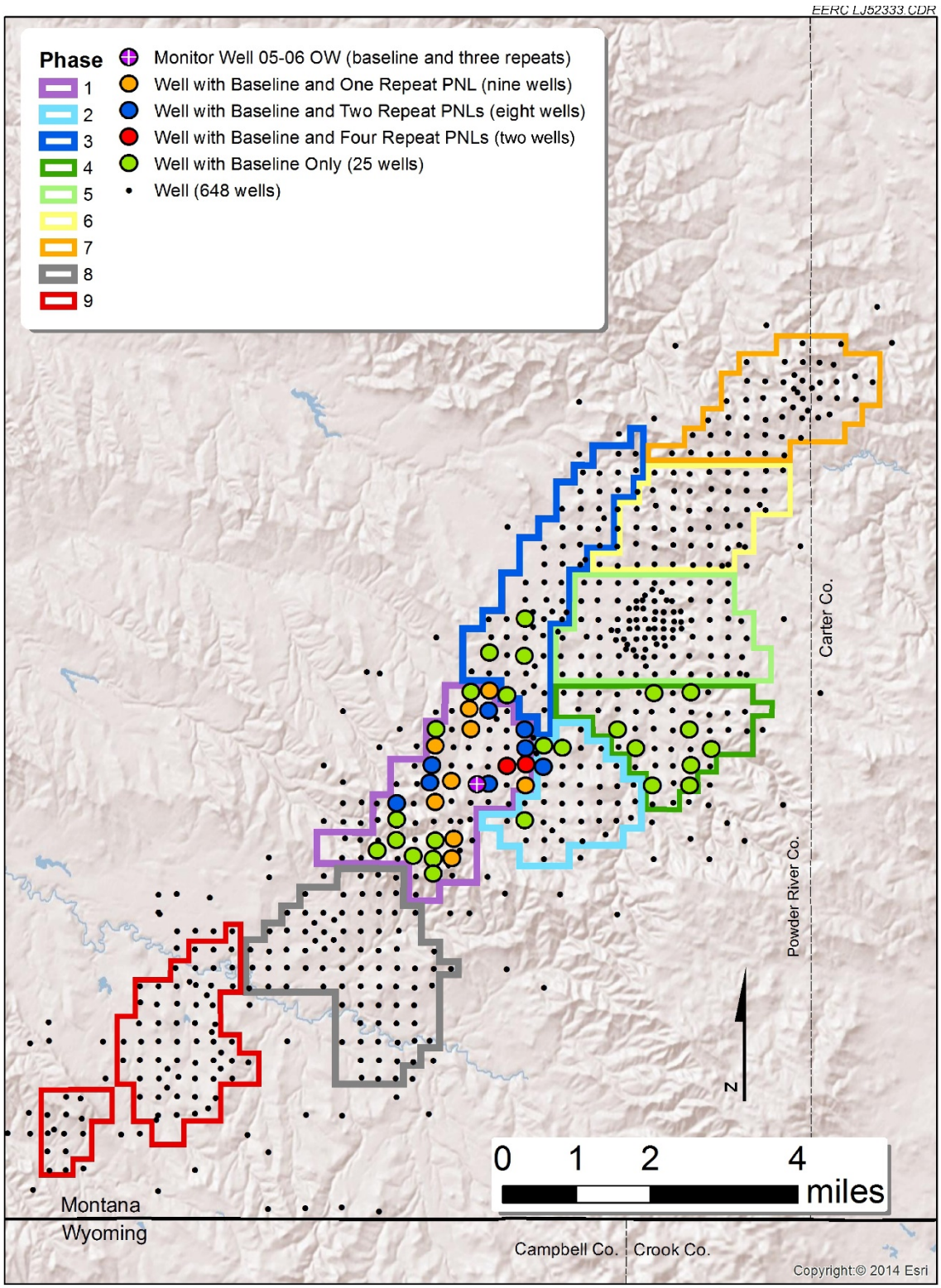

Figure 9. Map of wells showing where baseline and monitor pass PNLs have been collected in Bell Creek Field.

Seismic Survey Data

Previous 3-D surface seismic data acquired at Bell Creek began with a baseline survey (prior to CO_2 injection) acquired in 2012, centered on the Phase 1 and 2 areas (and containing portions of the surrounding Phases 3, 4, 5, and 8). A smaller repeat/monitor survey was acquired in 2014 centered on the Phase 1 and 2 areas. In 2015, a combined baseline and repeat/monitor survey was acquired (Figure 10). The 2015 survey was a repeat/monitor survey over the Phase 1, 2, and 4 areas, as well as the southern part of the Phase 3 area. This survey also expanded baseline coverage in the Phase 5, 6, and 7 areas. Integration of the baseline and monitor 3-D seismic data sets has provided an increased understanding of the Muddy Formation deposition and enabled a higher degree of accuracy in capturing the reservoir geology in V3 modeling efforts (discussed in the following sections). The 2015 seismic data have also been compared with 2012 and 2014 seismic data in an effort to identify changes in fluid saturation and pressure related to CO_2 injection.

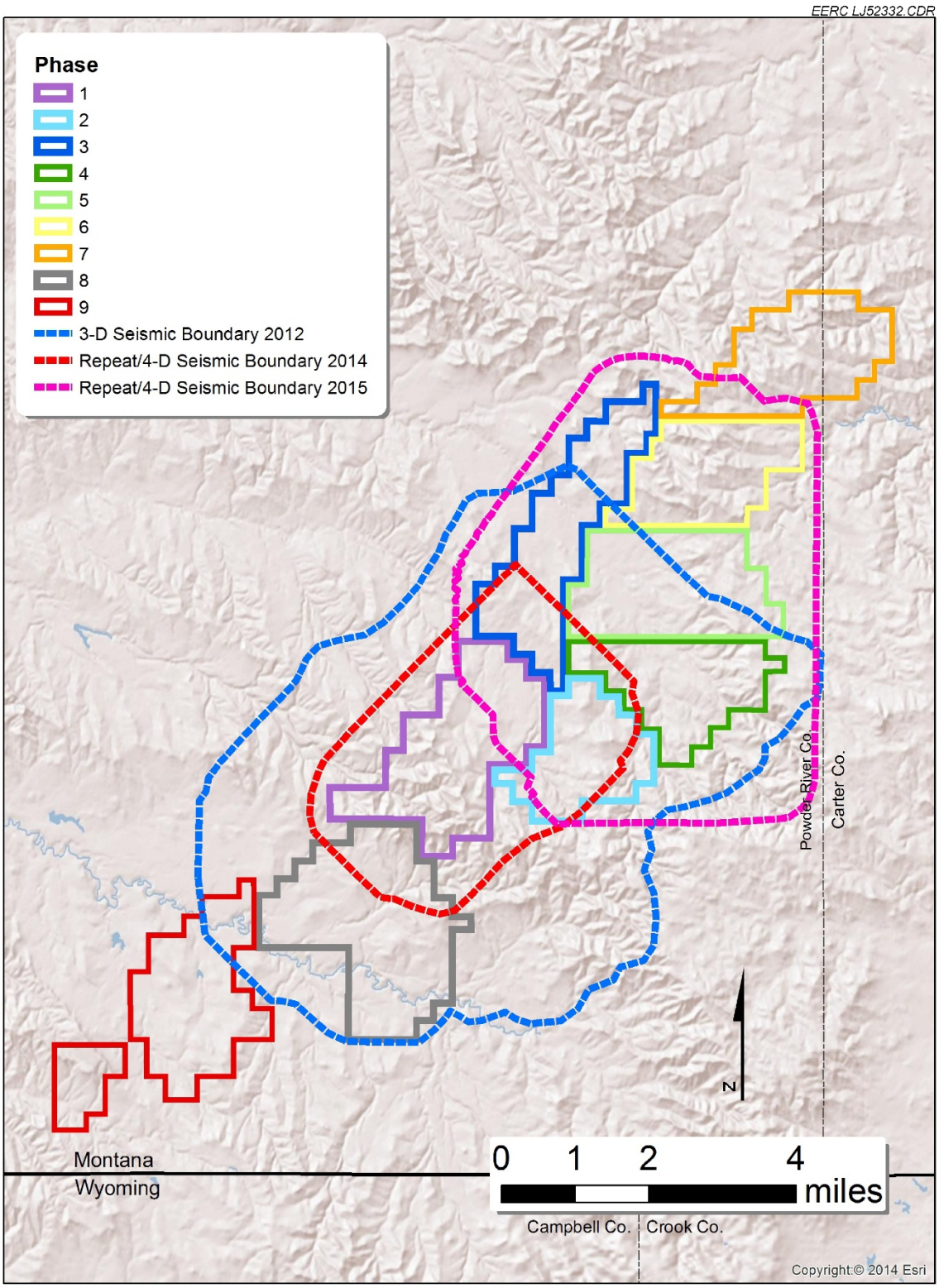

Figure 10. Map showing the approximate areal extent of the Bell Creek baseline and repeat 3-D surface seismic surveys: 2012 (outlined in blue), 2014 repeat seismic survey (outlined in red), and 2015 repeat seismic survey (outlined in pink).

Seismic Data Interpretation and Revised Depositional Model

To build upon previous seismic interpretation within Bell Creek, the 2015 seismic survey has been assessed in a similar manner as that described by Burnison and others (2014) and Bosshart and others (2015). Burnison and others (2014) created a surface attribute map from the 2012 baseline seismic data by summing amplitudes from the Skull Creek seismic horizon to the Springen Ranch seismic horizon after a 90° phase shift. Bosshart and others (2015) showed an annotated (depicting labeled geobodies) version of this amplitude summation map. A similar amplitude summation surface attribute map was constructed from the recently acquired 2015 surface seismic data (Figure 11).

Integration of this new seismic data has enabled a continuation of the interpretation detailed in Bosshart and others (2015). The Bell Creek sand within the Bell Creek Field appears to have been deposited as two stratigraphic units resulting from a regressive–transgressive sequence split by lowstand subaerial exposure and erosion.

The lower Bell Creek sand was deposited as deltaic/shoreline progradation (regression) from the northeast toward the southwest during a period of relative sea level fall. The higher seismic amplitude feature(s) on the eastern edge of the field in Phases 4, 5, and 6 (Figure 11; Geobody F) likely represent the finer-grained material deposited at the margins of the prograding delta/shoreline during early Bell Creek sand deposition. Following relative sea level fall, there is evidence of a brief sea level rise producing a relatively thin, fine-grained (siltstone/mudstone) layer overlying the regressive/prograding deposits below. This layer can vary within the Bell Creek sand interval both in stratigraphic position and thickness (3 to 5 feet thick on average). A period of relative sea level fall and subaerial exposure is interpreted to follow, as evidenced in core as a thin layer of coarser sand, disrupted bedding, and (in some locations) the presence of thin coals (either intact or plant fragments).

Following relative sea level fall and the deposition of regressive sands, the seas began to transgress from the southwest, forming barrier bar and lagoonal environments in the southwest part of the field. The seas continued to rise, causing the barrier bar and lagoonal environments to migrate to the northeast, and a tidal channel complex was formed in the southwest lagoonal region (Figure 11; Geobody D). A brief still stand allowed a local barrier bar to form in Phases 1 and 2 (Figure 11; Geobody A), along with an associated lagoon to the northeast along the boundaries between Phases 1–3 and Phases 2–4 (Figure 11, Geobodies B1 and B2). These features, as noted in the seismic data, suggest the shoreline orientation at this time to be approximately northwest–southeast.

Visible in the seismic is a high-amplitude feature with sinuous character trending generally north to south along the Phase 1 and 2 boundary, cross-cutting the Phase 1 and 2 barrier bar and lagoonal deposits in a perpendicular manner (Figure 11, Geobody C1). This feature coincides with a previously inferred permeability barrier (interpreted from pressure compartmentalization effects; Farnham and Haddenhorst, 1972; Molnar, 1990). From well log analysis, this hydraulic disconnection is due to erosion of nearly all reservoir-quality sand. The shape and scale of this feature resembles a fluvial incised valley, which explains the erosion and decreased sand thickness

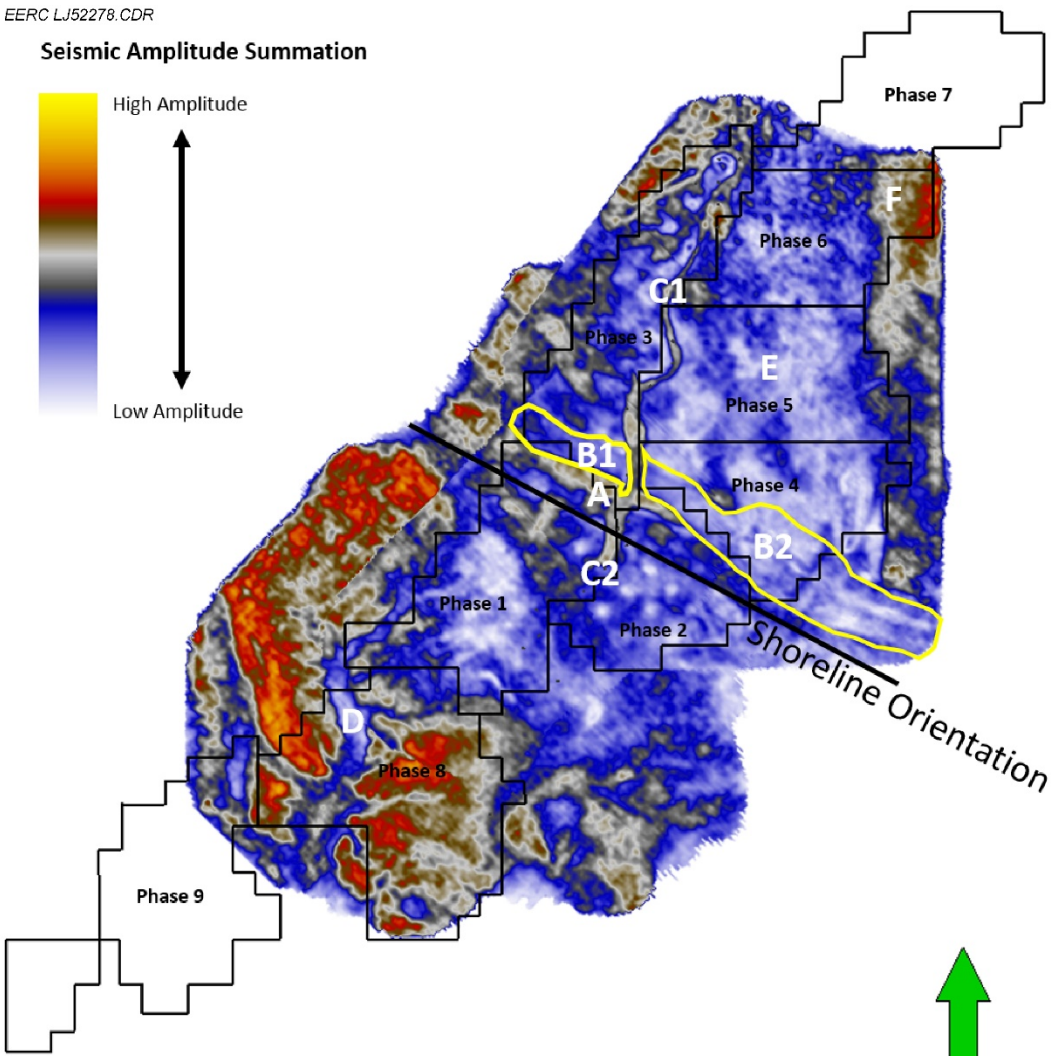

Figure 11. Seismic amplitude root mean squared summation map of the Muddy Formation of Bell Creek Field from the 2015 surface seismic survey with labeled geobodies and shoreline orientation (from Bosshart and others, 2015). Geobody A represents the back-barrier silty sands of the interpreted barrier bar. Geobodies B1 and B2 represent lagoonal deposits that are bisected by the incised fluvial channel represented by C1. Geobody C2 represents shallow marine channel deposits. Geobody D represents an early lagoonal environment repurposed to a tidal channel complex as seas continued to transgress. Geobody E represents generally thicker regressive sands overlain by thinner transgressive sheet sands. Geobody F represents regressive silts, deposited on the margins of the northeast to southwest prograding deltaic/shorefront sands and overlain by thin transgressive sheet sands.

(Bosshart and others, 2015). The 2015 seismic data show this feature continuing along the same north to south trend between Phases 3 and 4, Phases 3 and 5, and Phases 3 and 6. In the northernmost part of Phase 3, the high-amplitude channel feature becomes indistinguishable from surrounding seismic amplitudes and challenging to track with limited well control.

Fluvial sediment, transported to the shallow marine environment seaward of the barrier bar (Figure 11; Geobody C2), was carried southeast by longshore currents, draped into the incised channel (developed previously during lowstand subaerial exposure), and provided a hydraulic link between Phases 1 and 2 (which can be seen in the figures of the following section, Seismic Volume Differences). After the establishment of this Phase 1 and 2 hydraulic connection, relative sea level rise resumed, resulting in the deposition of (mostly continuous) transgressive sheet sands in the northern regions of the field (Figure 11; Geobody E; generally thicker in the southwest, thinning and pinching out in the northernmost part of the field). These transgressive sands of the upper Bell Creek sand interval vary in thickness but are typically between 5 and 10 feet thick (Figure 12). This final transgression appears to have occurred quickly, burying and preserving all of these features (before wave-reworking made them indiscernible) with the overlying estuarine–shallow marine Springen Ranch deposits.

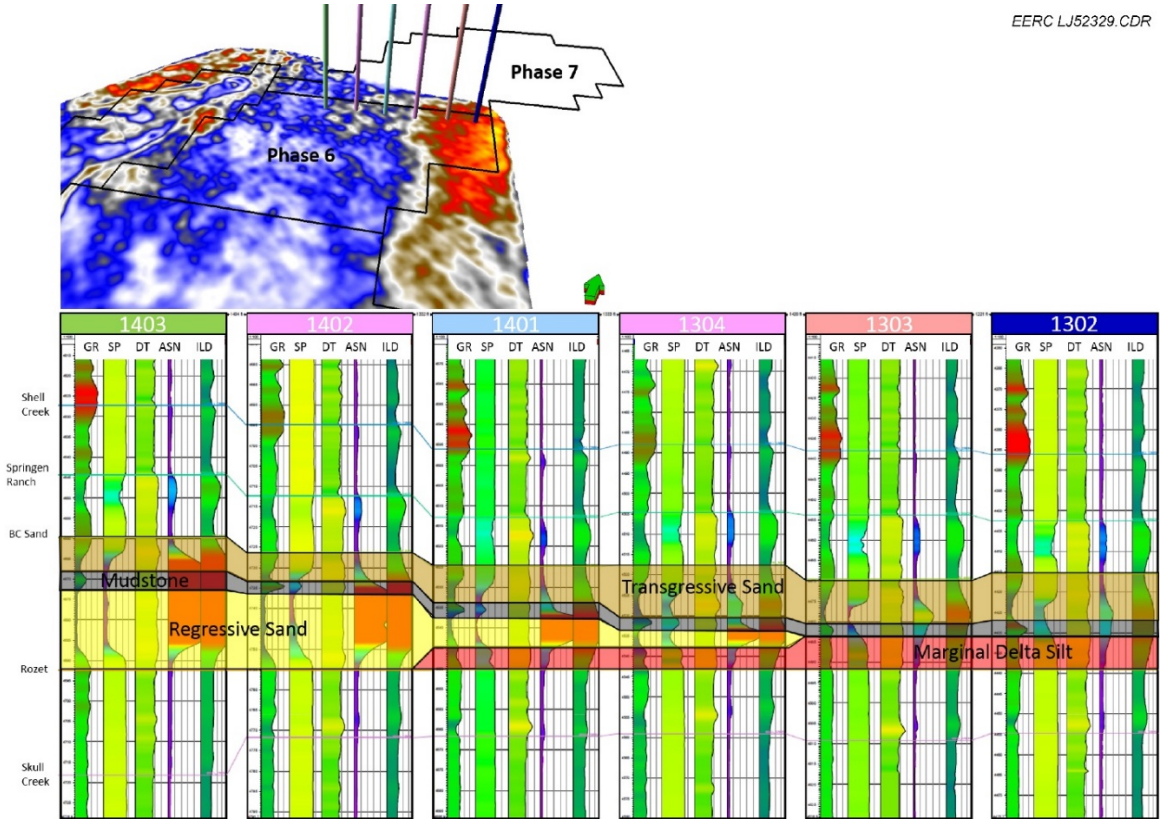

Figure 12. Interpreted well cross section (west–east) through the higher-amplitude seismic geobody found on the eastern margins of Phases 4, 5, 6, and 7. Tracks are (from left to right) GR, spontaneous potential (SP), sonic (DT), amplified short normal (ASN) resistivity, and deep induction log (ILD). The lower, regressive sand thins to the east and becomes silty at the field margin. The regressive deposits are overlain by thin mudstones/siltstones which are overlain by the transgressive deposits that mark the end of Bell Creek sand deposition.

4-D Seismic Analysis and Enhancement to Geological Interpretation

4-D seismic (or time-lapse seismic) analyses in Bell Creek have shown interesting and encouraging results, illustrating the difference in measured amplitude between baseline and repeat/monitor surveys. 4-D amplitude maps and indicative of changes in fluid saturation due to CO_2 injection and the associated pressure plumes. A time-lapse amplitude map between 2012 baseline data (pre-CO_2 injection) and 2014 monitor data (post-CO_2 injection) in the Phase 1 and 2 areas is shown in Figure 13. Similarly, Figure 14 shows the time-lapse amplitude map between 2012 baseline data (pre-CO_2 injection) and 2015 monitor data (post-CO_2 injection) over the Phase 1, 2, and 3 areas. Significant differences can be seen in the Phase 1 and 2 areas in Figures 13 and 14, with greater differences occurring in Figure 14 because of the longer period of CO_2 injection between the baseline and repeat/monitor surveys. In Figure 14, no CO_2 had been injected in Phases 4 and 5 during the 3-year period (2012 to 2015), meaning there is no time-lapse amplitude difference. This provides evidence for the good quality of the seismic data. The permeability barrier between the Phase 1 and 2 areas that is seen in the difference map between 2012 to 2014 (Figure 13) continues along the same north to south trend in the 2012 to 2015 difference map (Figure 14).

As discussed in Bosshart and others (2015), there appears to be a hydraulic connection between Phases 1 and 2 (Figure 13). There also appears to be a permeability barrier trending west to east created by the interpreted lagoonal deposits (between the Phase 1 and 3 areas and also between the Phase 2 and 4 areas). These deposits have been interpreted from well logs as containing more fine-grained sediments and decreased sand thickness. However, there also appears to be some connection between the Phase 1 and 3 areas (near the western flank of the interpreted barrier bar) across the interpreted lagoon (Figure 14).

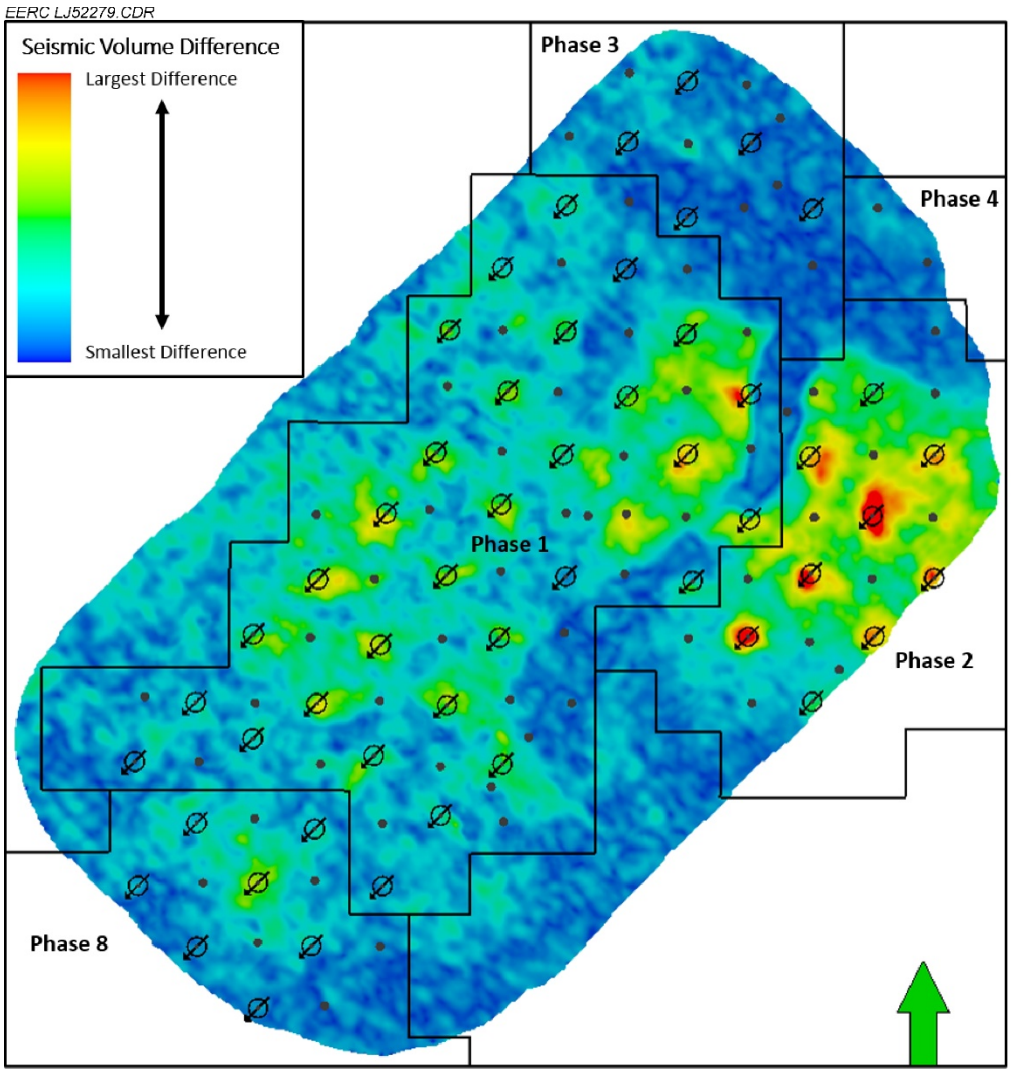

Figure 13. Seismic volume difference from 2012 to 2014. Warmer colors represent greater differences and cooler colors represent smaller differences. Injection wells are shown by black circles bisected by arrows. All other wells are shown as black dots.

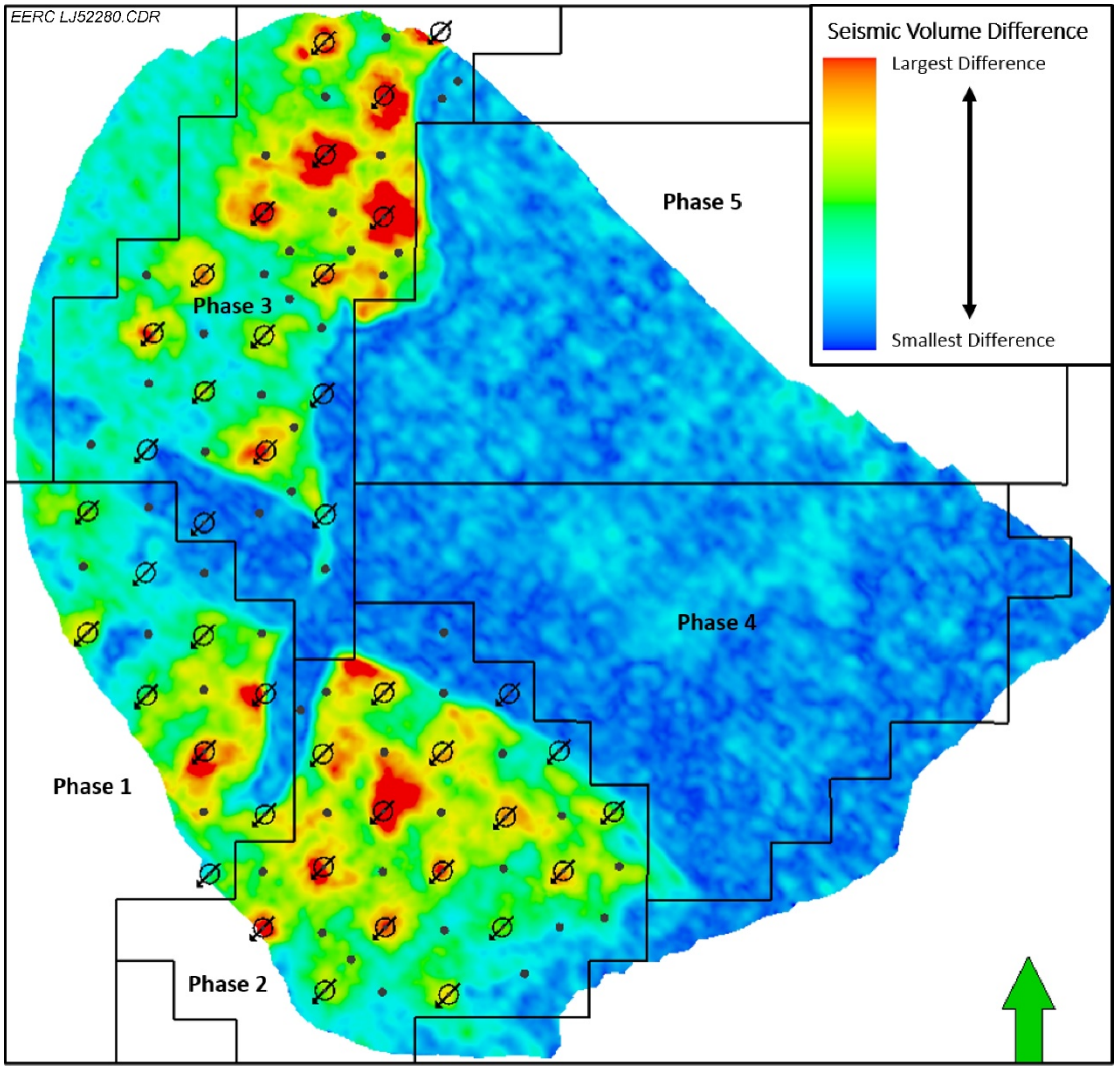

Figure 14. Seismic volume difference from 2012 to 2015. Warmer colors represent greater differences and cooler colors represent smaller differences. Injection wells are shown by black circles bisected by arrows. All other wells are shown as black dots.

Version 3 Geologic Model

Development of the V3 geologic model, first reported in Bosshart and others (2015), began with a different approach and geologic understanding compared to the previous geologic models. Previous geologic models (V1 and V2) were developed based on the historical depositional environment interpretation of the field, which characterized the Muddy sands of the Bell Creek Field as being part of a large, Galveston Island-style barrier bar along a shoreline trending approximately northeast to southwest and were developed prior to acquisition of seismic data within the field. Upon integration of the 3-D seismic data, a revised geologic interpretation (discussed above) was outlined and incorporated into the V3 reservoir modeling efforts.

The incorporation of 3-D seismic data has provided the ability to extract geobodies (areas having similar lithologic properties) Figure 11 described and showed some labeled geobodies which are used to focus investigation and property distribution in the geologic model. Well logs and cross sections have been used to develop an understanding of the lateral and vertical facies associations within each of the different geobodies. Facies logs have been constructed for most wells in the field but are being revisited for accuracy with the 2015 seismic data. Multiple point statistics (MPS) training images have been generated (different training images for each geobody), and MPS facies distributions are being conducted within each respective geobody.

Upon completion, the resulting V3 facies model will be used to constrain further property distributions (porosity, permeability, and water and oil saturations). After completion of property modeling, an upscaled grid will be used for simulation. History-matching efforts will provide insight into the accuracy and further improvements of the static model's property distributions. A comparison will be made with V2 model simulation efforts in an attempt to further support or refute the V3 Bell Creek depositional model.

Regional- and Basin-Scale Reservoir Models

Regional- and basin-scale models were created to investigate the long-term potential for lateral CO_2 migration in the greater Bell Creek Field region. The regional-scale model is approximately 4300 square miles and contains portions of Powder River and Carter Counties of Montana and Campbell and Crook Counties of Wyoming (Figure 15). The basin-scale model spans the extent of the PRB. Both the regional- and basin-scale models contained the Mowry Formation (primary upper seal), the Bell Creek sand interval (reservoir) of the Muddy Formation, and the Skull Creek Formation (lower seal) from west of the field to the Muddy Formation outcrops on the northwestern flank of the Black Hills.

A particularly intractable challenge with these models is the enormous area contained within each. The large area imposes minimum cell size constraints (cell sizes need to be large to keep the total cell count reasonable for efficient simulation), which limits the ability to realistically capture geologic heterogeneity in the Muddy Formation. Thus, the Bell Creek sand interval (in both models) was extrapolated laterally, although lateral equivalents were not necessarily of reservoir quality (a stratigraphic pinchout of reservoir quality sand is noted to the east of Bell Creek Field, providing the hydrocarbon trapping mechanism for the field). This was done to artificially create

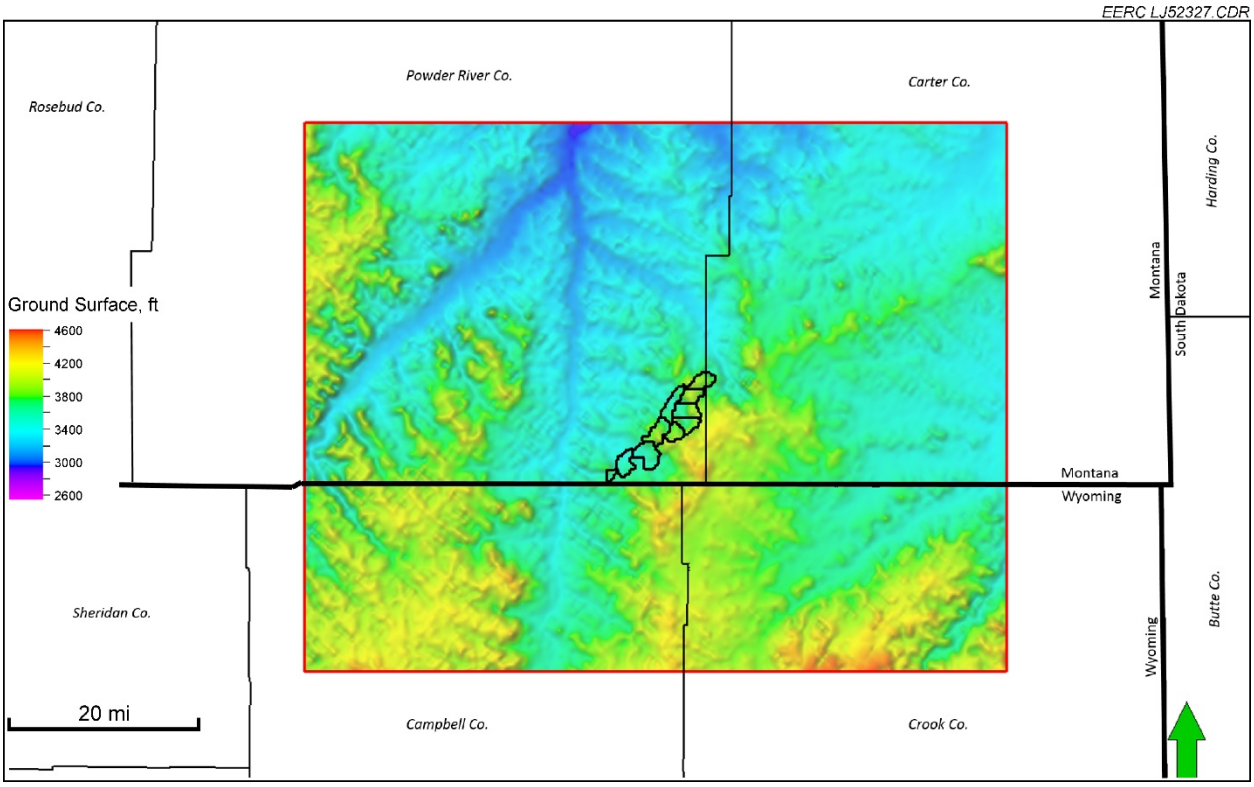

Figure 15. Map view of the regional-scale model extent with the Bell Creek Field and Phase outlines in black. The extent of the model is inset with a lidar ground surface map (V.E. = 10×).

a scenario with CO_2 having the greatest ease of migration assisted by lateral connectivity in order to assess a "worst-case scenario" for CO_2 MVA activities, thereby also creating challenging conditions for MVA. This provided the means to investigate the maximum CO_2 migration potential, to gain visibility if/when unimpeded CO_2 might reach Muddy Formation outcrops and be released to the atmosphere.

Petrophysical property models were created by giving the Bell Creek sand interval porosity and permeability properties average values from within the Bell Creek Field (averaged from core data: 24.8% porosity and 167.5 mD permeability, respectively). These models have not been subjected to simulation as of the time of this report, although similar simulations have been conducted on a reservoir model for the Phase 3–7 areas (and a buffer zone around these phases). The results for these simulations were achieved by considering only the effects of buoyancy and disregarding the effects of mineral trapping, natural hydrodynamic flow, and pinchout of reservoir-quality sands. An important conclusion is that CO_2 may travel up to 3 feet/year. These results are discussed in greater detail in the simulation results text that follows. At this rate, CO_2 would take thousands of years to reach an outcrop for atmospheric release and longer when other effects (noted above) are taken into account. Further simulations are planned that begin to incorporate all these implications regarding long-term CO_2 migration,

Near-Surface Model

The Bell Creek near-surface model, previously reported as under development in Bosshart and others (2015), has been completed. This model provides a structural framework and property model for the Pierre Formation aquitard, Fox Hills and lower Hell Creek Formation aquifers; and exposed upper Hell Creek Formation of the greater Bell Creek Field area (Figure 16). This model was constructed for use in simulations of (potential) unintended CO_2 saturation in shallow aquifer units, helping to inform the MVA program and, ultimately, enable rapid response in the event of out-of-zone CO_2 movement. For clarity, there have been no observations of out-of-zone CO_2 movement, and there is no reason to believe there will be such an event. This investigation is simply aimed at understanding where shallow subsurface monitoring resources might best be allocated to enable rapid detection and response.

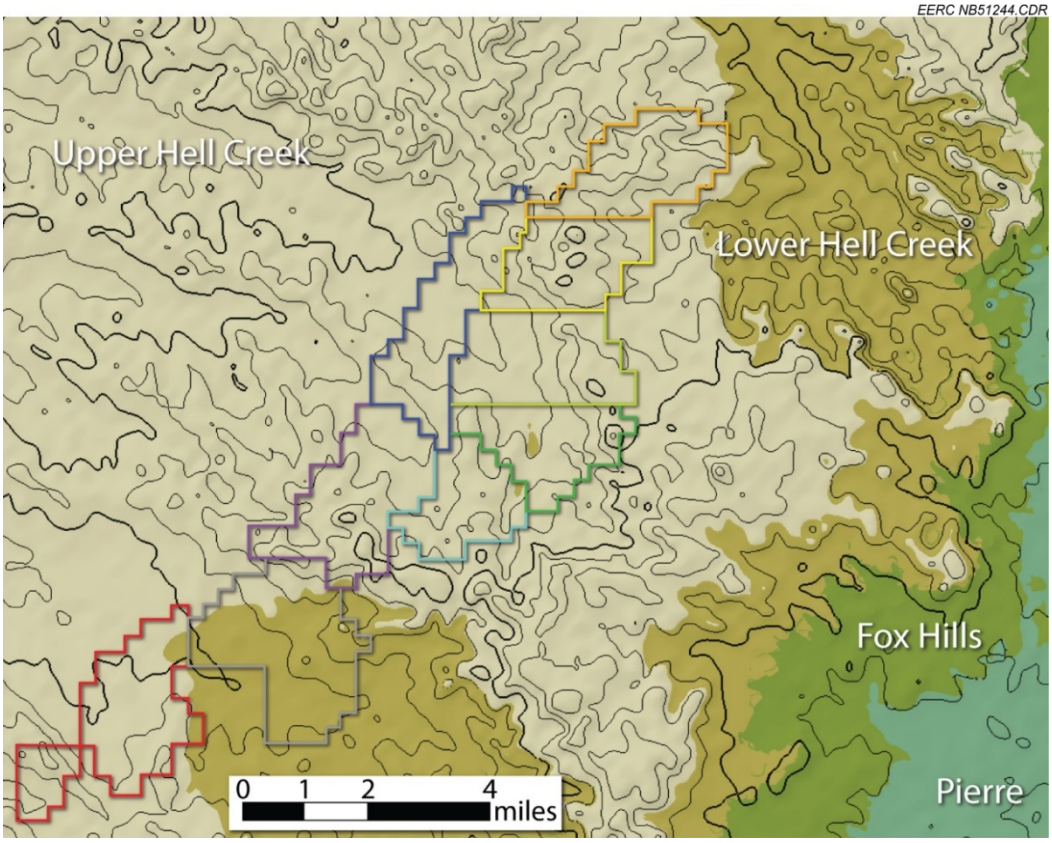

Figure 16. Map view of Bell Creek near-surface model. Relief is that of ground surface. The Fox Hills and Pierre Formations crop out on the east side of the Bell Creek Field and dip to the west–northwest.

Structure and Petrophysical Properties

The Bell Creek near-surface model, including the Pierre Formation to the ground surface, has a maximum depth of approximately 2270 feet. The model has a cell size of 400 feet × 400 feet, 44 layers (with an average layer thickness of 38 feet), and contains nearly 1.7 million cells.

The two most important aquifers (by consumption) in the Bell Creek area are the Fox Hills and the lower Hell Creek intervals (Thanke and others, 2014). The lower Hell Creek interval was deposited in the swamps and floodplains on or near a deltaic front, containing channel deposits and erosional surfaces. The Fox Hills aquifer was deposited in shorefront and nearshore environments, such as beach, bar, tidal channel, bay, and estuarine environments (Thanke and others, 2014). The aquifer sands of the lower Hell Creek and Fox Hills sands are separated stratigraphically by fine-grained (aquitard) deposits (Figures 17 and 18).

The Fox Hills and Hell Creek Formations, as shallow deposits and not targeted for commercial use (but targeted for some beneficial use such as water production for irrigation, livestock, etc.), have a limited amount of accessible data in the Bell Creek Field. To supplement the sparse local data, petrophysical property data from the adjacent Williston Basin was included. However, it is acknowledged that the assumption of similarity between deposits of Bell Creek and equivalent strata in the Williston Basin introduces greater uncertainty in accuracy.

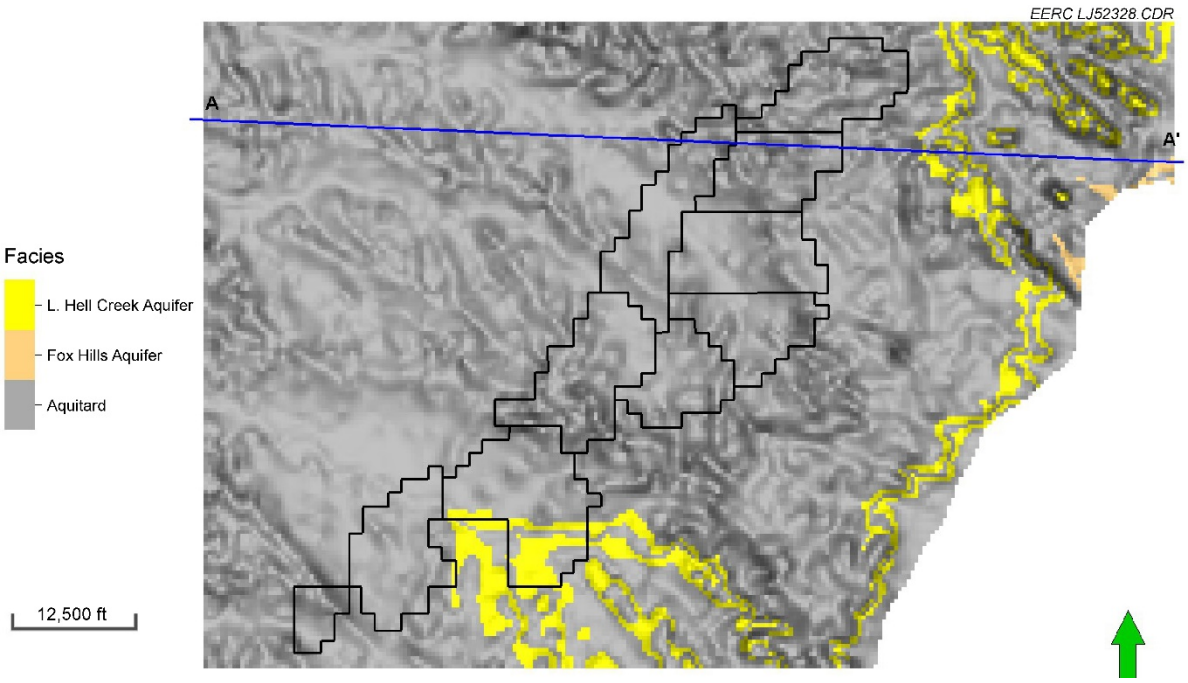

Figure 17. Overhead view of the Bell Creek near-surface model. The outcropping of the modeled formations in the southeast is the reason for the model's truncation.

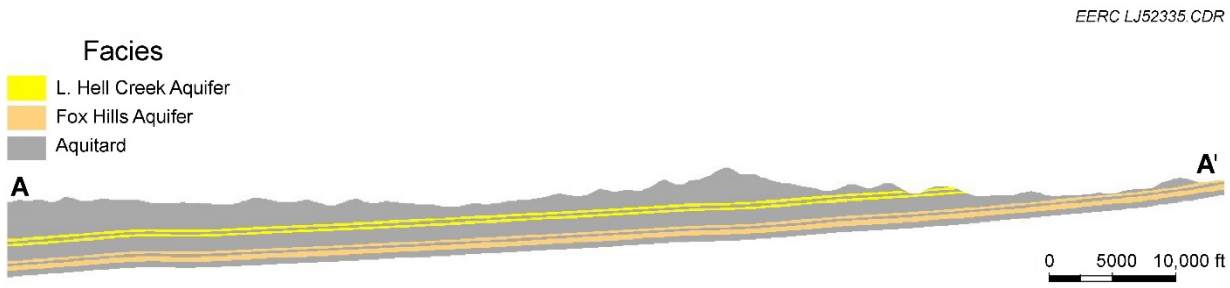

Figure 18. Cross-sectional view of the Bell Creek near-surface model showing the aquifer and aquitard units (V.E. = 10×).

The near-surface model has not been simulated at this time. However, future simulation efforts intend to design and test wellbore failure and vertical CO_2 migration (along natural fractures) scenarios of varying intensities while taking into account natural hydrodynamic flow in these aquifer units. These simulations will provide 1) insight into CO_2 migration velocities in the shallow subsurface, 2) estimates of lag time between a potential CO_2 containment failure and when CO_2 might contaminate agricultural/livestock wells or be released to the atmosphere from outcrop; and 3) an assessment of geographic locations both within and outside of the field where monitoring activities may be best suited for rapid detection.

Reservoir Engineering and Simulation

CO_2 Flood Performance in Bell Creek Field

The Bell Creek Field in southeastern Montana is a subnormally pressured reservoir with significant hydrocarbon charge that lies near the northeastern boundary of the PRB. Since its discovery in 1967, the field has undergone primary production (solution gas drive), waterflooding, and two micellar–polymer pilot tests. These operations produced about 37% of the estimated 353 million barrels (MMbbl) of original oil in place (OOIP) from its nine phase areas. Large-scale miscible CO_2 flooding has been carried out in the field from the Phase 1 area and extended gradually to other phases since May 2013, which is anticipated to recover 30 MMbbl of additional oil from the reservoir.

Figure 19 shows the encouraging oil production performance of the field from the beginning of CO_2 flooding. The oil production rate has increased from about 7 thousand barrels per month (bpm) to about 110 thousand bpm, which has yielded over 2.4 MMbbl of oil in 3 years. Figure 20 shows the water injection and production performance in the field during CO_2 flooding. As shown in Figure 20, the water injection and production rates are nearly identical, indicating the oil is practically in the residual state and the reservoir's fluid flow is water-dominated. Over 40 years of waterflooding in the field has resulted in a reservoir saturated with water.

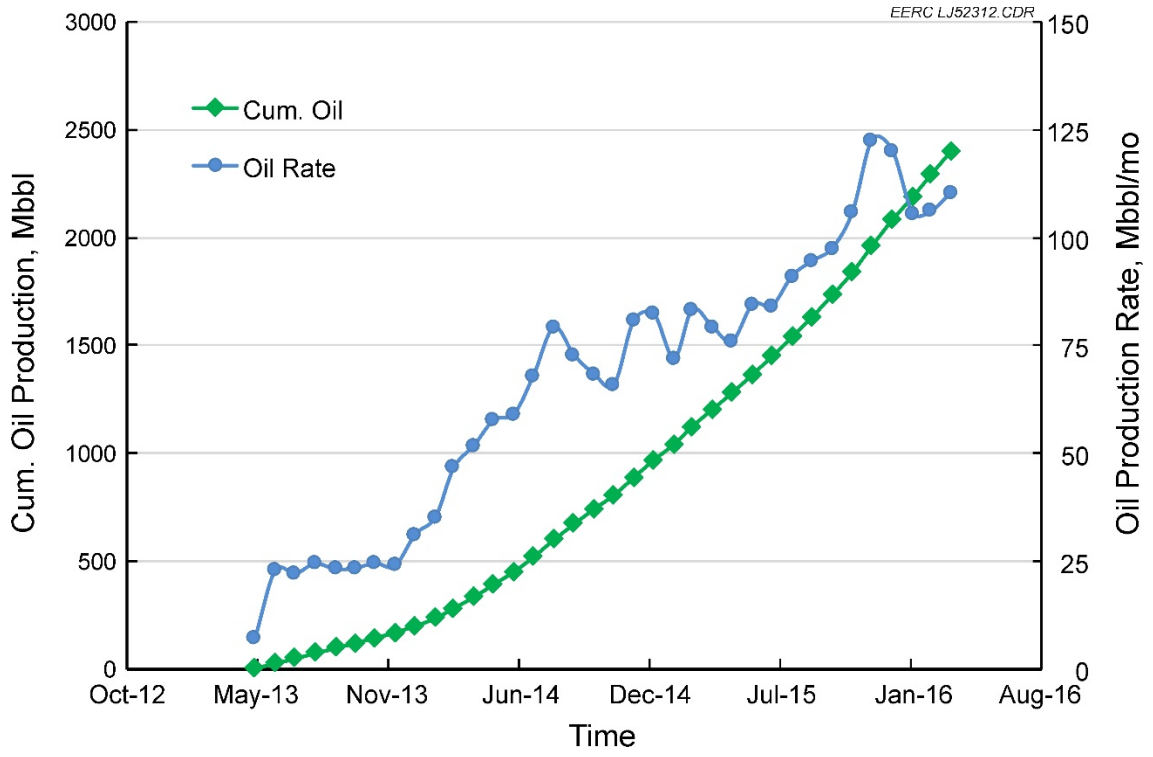

Figure 19. Oil production performance during the Bell Creek CO_2 flooding process.

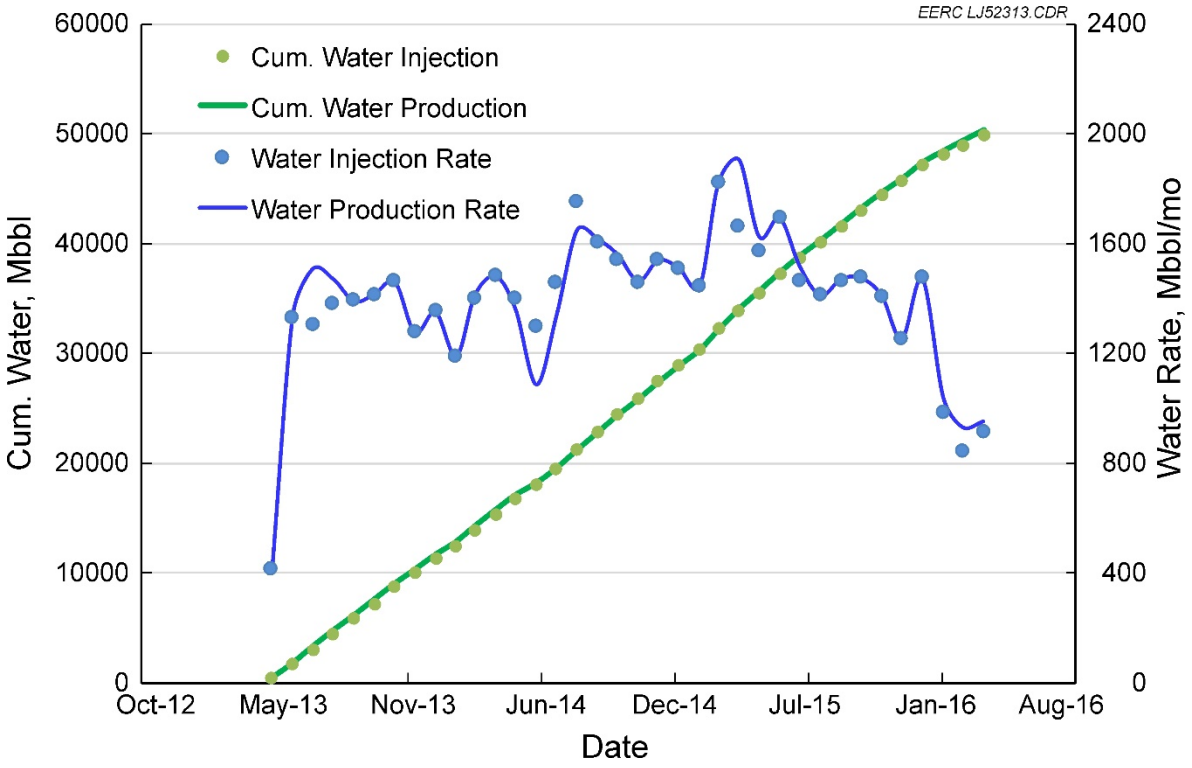

Figure 20. Water injection and production performance during the Bell Creek CO_2 flooding process.

Compared to the water volumes, the CO_2 injection and production performance is quite different (Figure 21). CO_2 injection increased from 9.5 to 234.5 thousand tonnes per month (tpm) in the first 2 years of injection and then fluctuated around 195 thousand tpm after June 2015. CO_2 production lagged behind the injection for about 9 months, indicating that CO_2 can effectively displace oil in the pore space and remain in place during flooding operations. Figure 22 shows cumulative gas injection and production in the field. The difference between them may be considered as gas stored in the reservoir if we use the principle of material balance, as shown in Equation 1:

$$M_{st} = M_{inj} - M_{prod} \quad \text{[Eq. 1]}$$

Where, M_{st}, M_{inj} and M_{prod} are the amounts of CO_2 stored in, injected into, and produced from the reservoir, respectively. Figure 22 shows that about 5 million tonnes of CO_2 have been injected into the reservoir and just over 3 million tonnes have been stored there since the beginning of CO_2 flooding (as of March 2016). Referring back to Figure 21, it is also clear that the gas storage rate related closely to the injection rate, decreasing rapidly when the injection became stable, after June 2015, while the production rate continued increasing. This observation indicates that CO_2

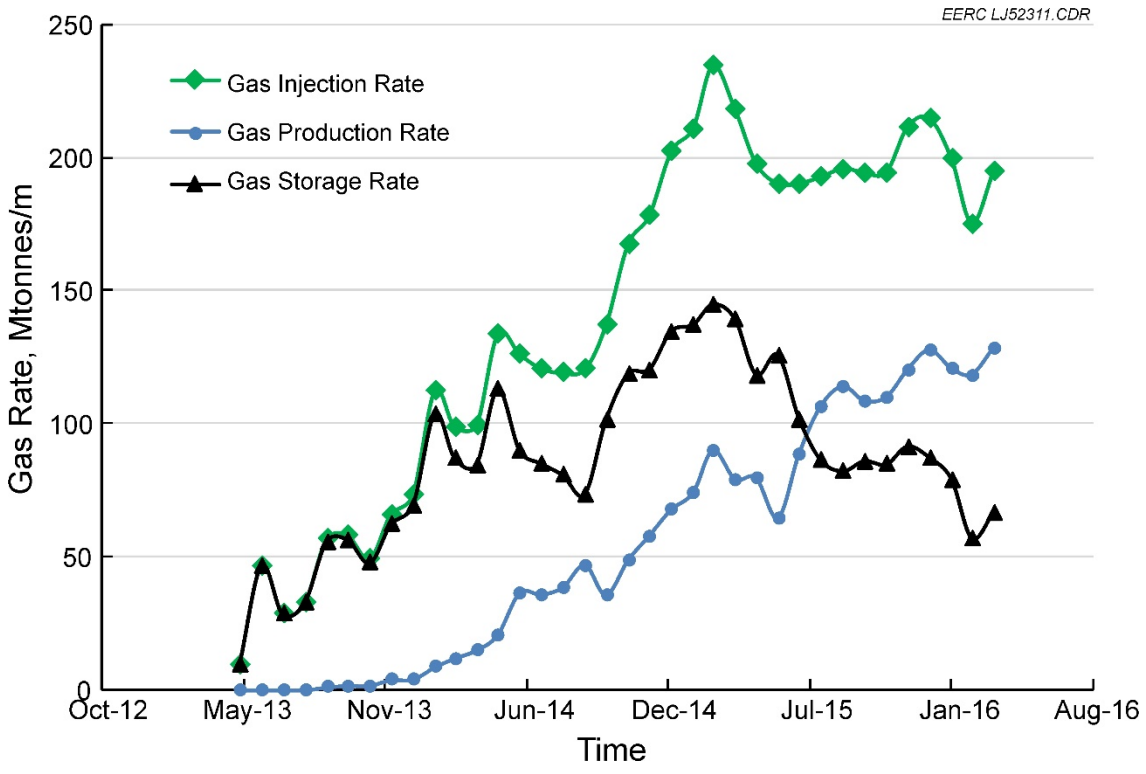

Figure 21. Gas production, injection, and storage rates in the Bell Creek CO_2 flooding process. Note that the term "Gas" refers to CO_2 plus impurities.

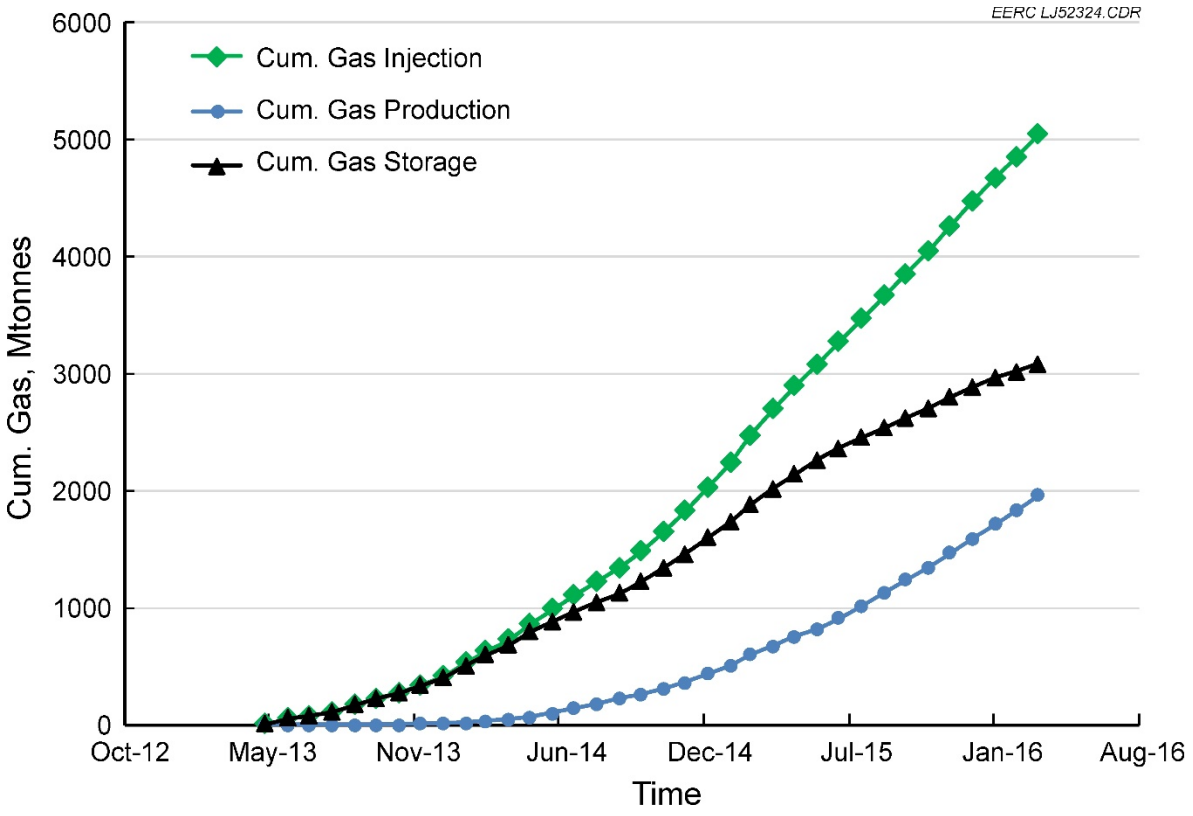

Figure 22. Cumulative gas injection, production, and storage in the Bell Creek CO_2 flooding process. Note that the term "Gas" refers to CO_2 plus impurities.

dominated the flow networks between injection and production wells and likely means gas production will continue to increase as the flooding goes on. Because CO_2 is likely to be produced with mobilized hydrocarbons, impurities (such as light hydrocarbons) are unavoidably mixed with produced CO_2. This mixed gas is recycled back to the injection wells at Bell Creek. A small amount of the impurities noted in the Bell Creek produced gas streams may have been sourced from the upstream capture facilities, with purchased gas measurements indicating generally around 97.5%–98.5% CO_2 (Gorecki, 2016).

Injected solvent composition is a key parameter in the design of miscible CO_2 flooding. Therefore, it is important to investigate the effect of the impurities on CO_2 EOR and storage performance when such a large quantity of produced gas is recycled for injection.

Impurities in the Produced Gas Stream

The Bell Creek Field EOR results are encouraging, while at the same time new challenges are presented. Aside from the produced oil and water, a large amount of CO_2 with impurities (light hydrocarbons; mostly CH_4) is also produced and is available for recycle injection. Studies have shown that most impurities have evident effects on the properties of the injection solvent (Metcalfe, 1982; Shyeh-Yung and Stadler, 1995; Wang and others, 2011; Hawthorne and others,

2016). However, exactly how the impurities may impact a recycle injection performance strongly depends on the geologic conditions, reservoir and fluid properties, operational modes, etc. (Gardner and Ypma, 1984; Pande, 1992; Thomas and others, 1994; Afonja and others, 2012; Jiang and others, 2012; Yin and others, 2014). Therefore, it is important to examine the oil composition and the potential impact of impurities on CO_2 EOR and storage performance to determine whether an impure stream of mixed components may be injected into the reservoir or if the recycled gas must first be purified.

In this study, the impact of CH_4 on CO_2 flood performance in Bell Creek Field was assessed by systematically evaluating the following:

1. Reviewing the production–injection performance of CO_2 flooding in the field.

2. Analyzing the concentration and composition of impurities in the produced gas.

3. Evaluating the behavior and properties of (injection) gas as a function of changing CH_4–CO_2 ratio.

4. Determining the MMP of oil with differing CH_4 fractions in the CO_2 stream.

5. Calibrating a PVT model with an EOS for CH_4 impact evaluation.

6. Assessing the reservoir response to various injection scenarios using a history-matched compositional reservoir model.

The initial and residual oil composition is illustrated in Figure 23, which shows that CH_4 was the main light component in the original oil, accounting for 19 mol% of the total hydrocarbons in the reservoir at discovery. While most of the light components were produced from the original oil, considerable intermediate and heavy components were left in the residual oil, which become the target of recovery in CO_2 flooding. Recycled gas is sampled and analyzed periodically to monitor the change in composition of the produced gas stream during the CO_2 flooding. Figure 24 shows the main components in the recycled gas sampled on October 29, 2014. The gas includes 96 mol% CO_2, 3 mol% CH_4, and 1 mol% of other minor constituents, including C_2–C_5, H_2S, N_2, H_2, etc. It should also be noted that the produced gas composition changes with time, initially containing a greater percentage of light hydrocarbons and little CO_2. This is attributed to molecular selectivity (preferential removal of the lighter hydrocarbon constituents of the oil by CO_2). The CO_2 component of the produced gas increases with time through the effects of dilution as less and less of the light hydrocarbon components remain in the reservoir and more CO_2 is added to the system. The composition of the oil in the reservoir becomes relatively heavier through this process, becoming more difficult to mobilize as the flood matures. Figures 25, 26, and 27 show the change of CO_2, CH_4, and C_2–C_5 in the produced gas through time of the Phase 1 Wells 56-14R, 05-06, and 32-02, respectively. CH_4 is the main impurity within the produced gas with content varying between 1 and 4 mol%. The C_2–C_5 content is relatively stable, varying from 0.5 to 0.8 mol%. The content of CO_2 increased from 94 to 98 mol%.

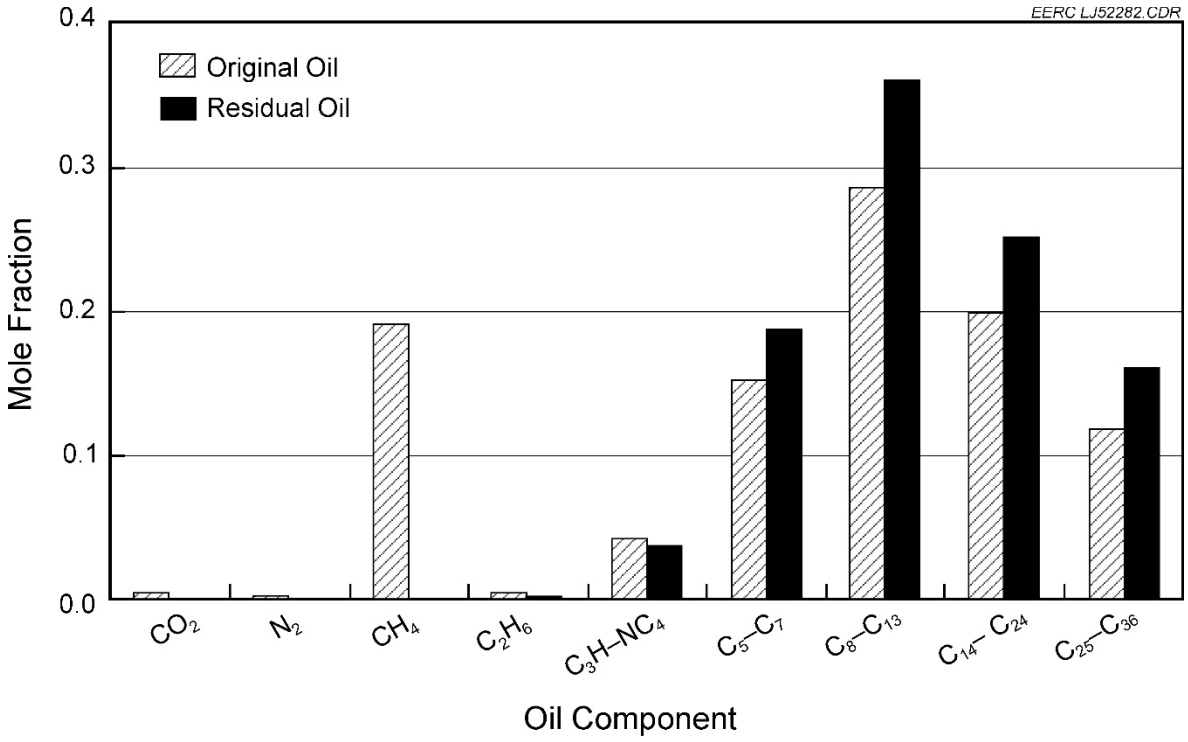

Figure 23. Bell Creek oil composition in original and residual conditions.

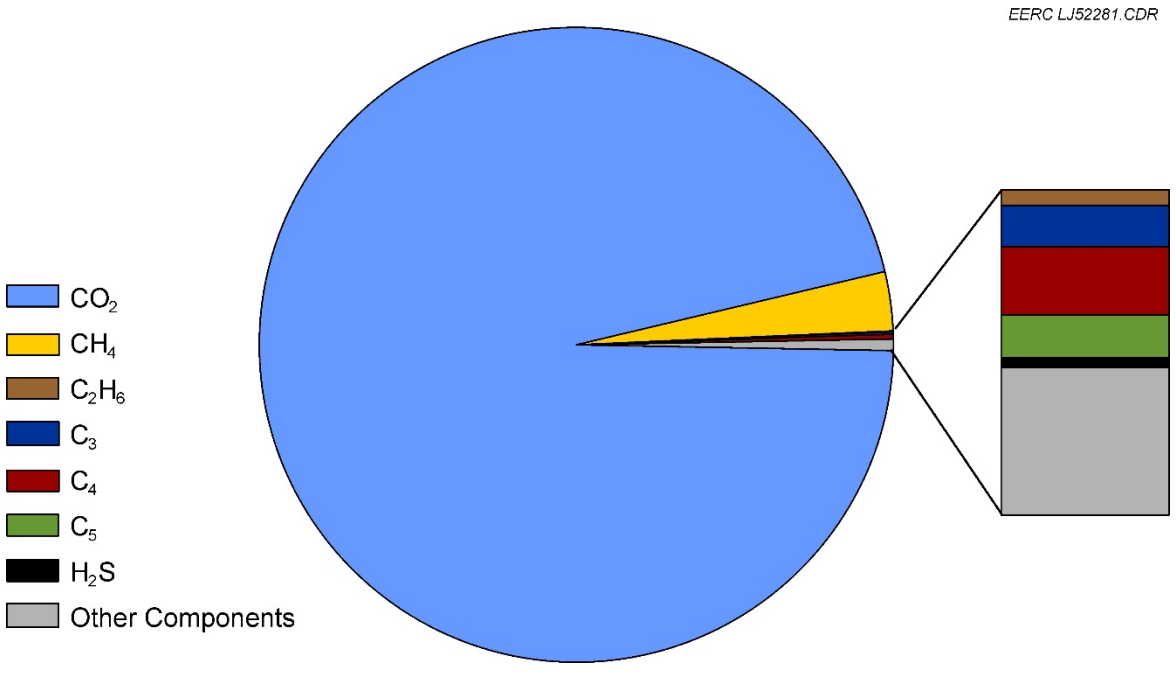

Figure 24. Recycled gas composition on October 29, 2014.

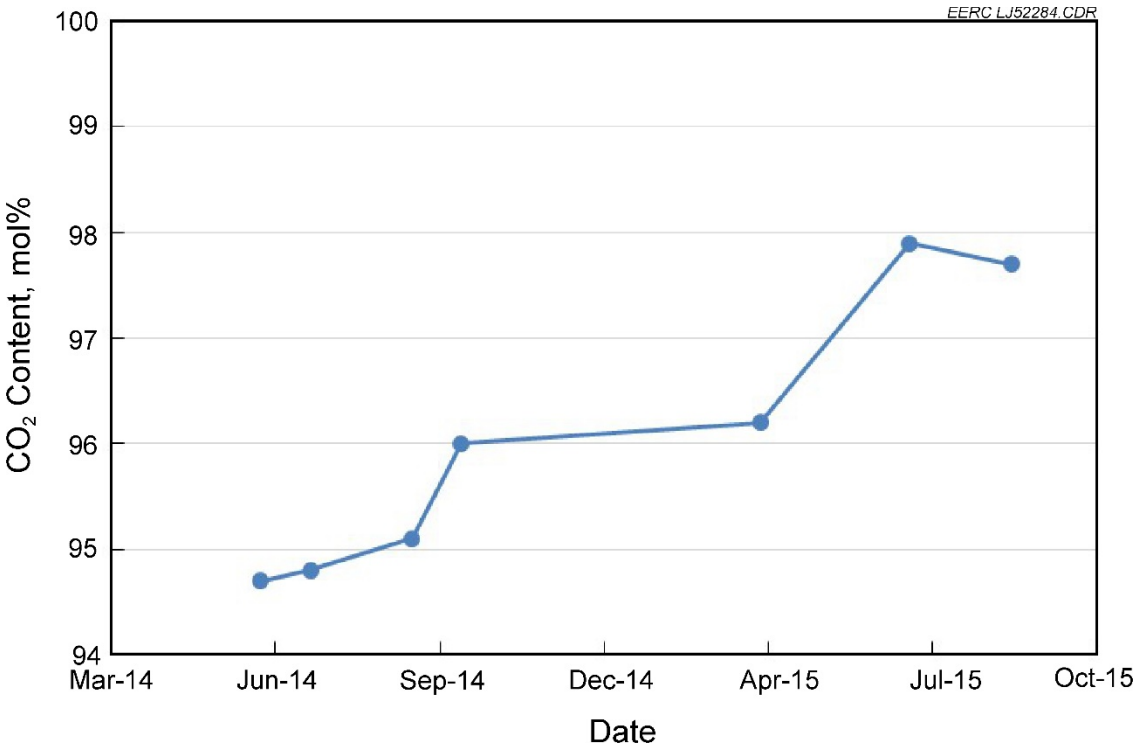

Figure 25. Recycled gas CO_2 content change with time.

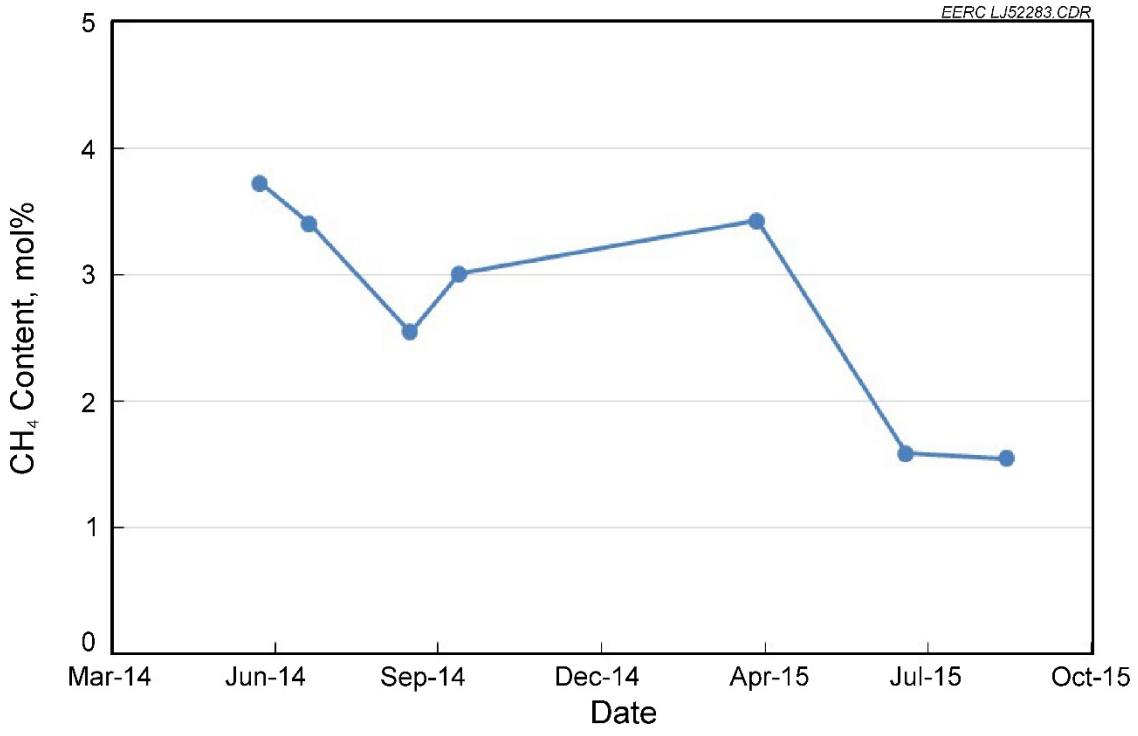

Figure 26. Recycled gas CH_4 content change with time.

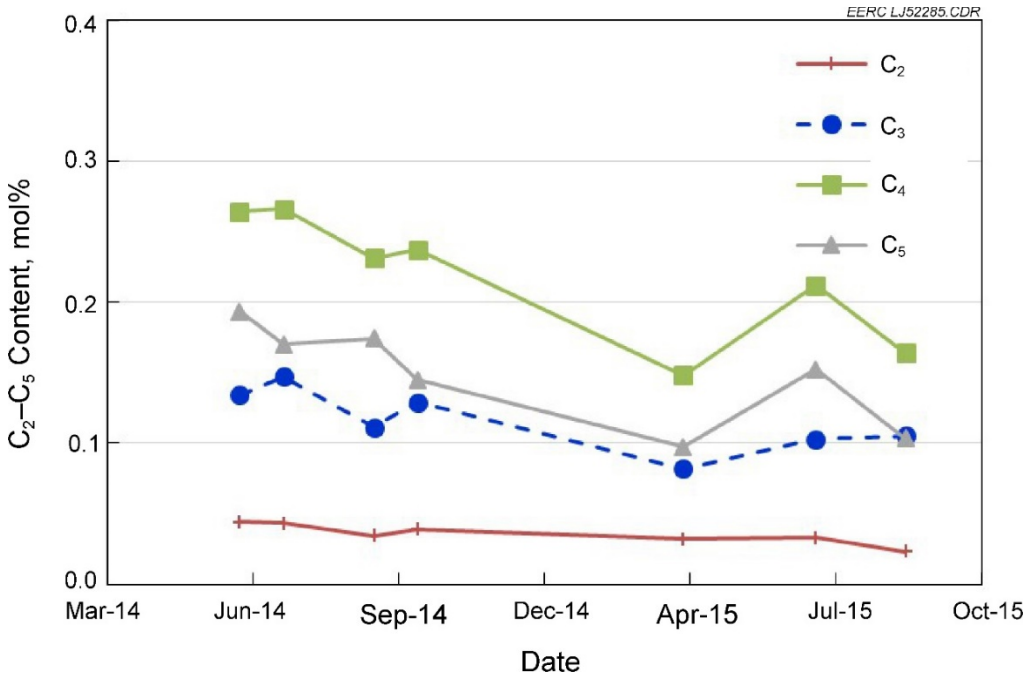

Figure 27. Recycled gas C_2–C_5 content change with time.

Effect of CH_4 on Bulk (Injection) Gas Physical Properties

Since CH_4 is the main impurity in the produced CO_2 stream which is recycled for injection, it is important to know the effect of CH_4 on bulk (injection) gas properties. A range of CH_4 fractions in the CO_2 stream were investigated, varying from 0 to 100 mol%. Key gas properties, including density, viscosity, and Z factor, were investigated at reservoir temperature and a wide range of pressure values to cover the range of possible operational conditions.

Figure 28 illustrates the change in gas density as a function of pressure (temperature is assumed to be a constant 108°F) for different CO_2–CH_4 gas stream compositions. The figure shows CH_4 has a significant impact on the gas density. For example, 10 mol% of CH_4 can reduce the gas density from 49.52 to 43.65 lb/ft^3 under reservoir conditions of 3000 psi and 108°F. The relationship between density of CO_2 and pressure acts in a nonlinear fashion when the critical pressure is exceeded (the phase changes from gas to supercritical fluid). However, CH_4 has a nearly linear relationship between density and pressure (for the pressure range investigated), as it is always in gas state. Gas viscosity exhibits similar relationships to pressure (Figure 29), behaving more linearly as the gas stream's CH_4 composition increases. Figure 30 shows that CH_4 also has evident effect on a gas mixture's Z factor (compressibility factor: the ratio of the molar volume of a gas to the molar volume of an ideal gas at the same temperature and pressure). In general, the differences in behavior and properties between pure and contaminated CO_2 become more obvious when pressure is greater than 1200 psi. Reservoir pressure during Bell Creek injection operations falls between 2000 and 3000 psi in the current CO_2 flooding area. The nonlinear curvature noted in the figures indicate that flow behavior of the recycled gas in the reservoir is a function of CH_4 fraction and pressure.

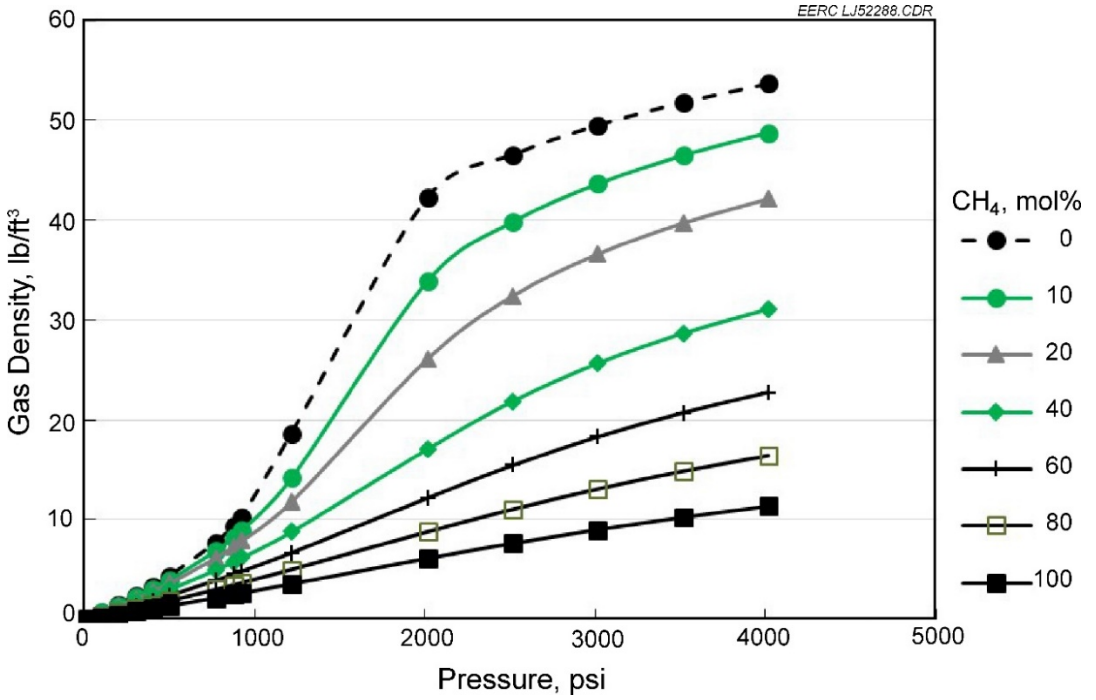

Figure 28. Effect of CH_4 on density of CO_2–CH_4 mixtures at 108°F.

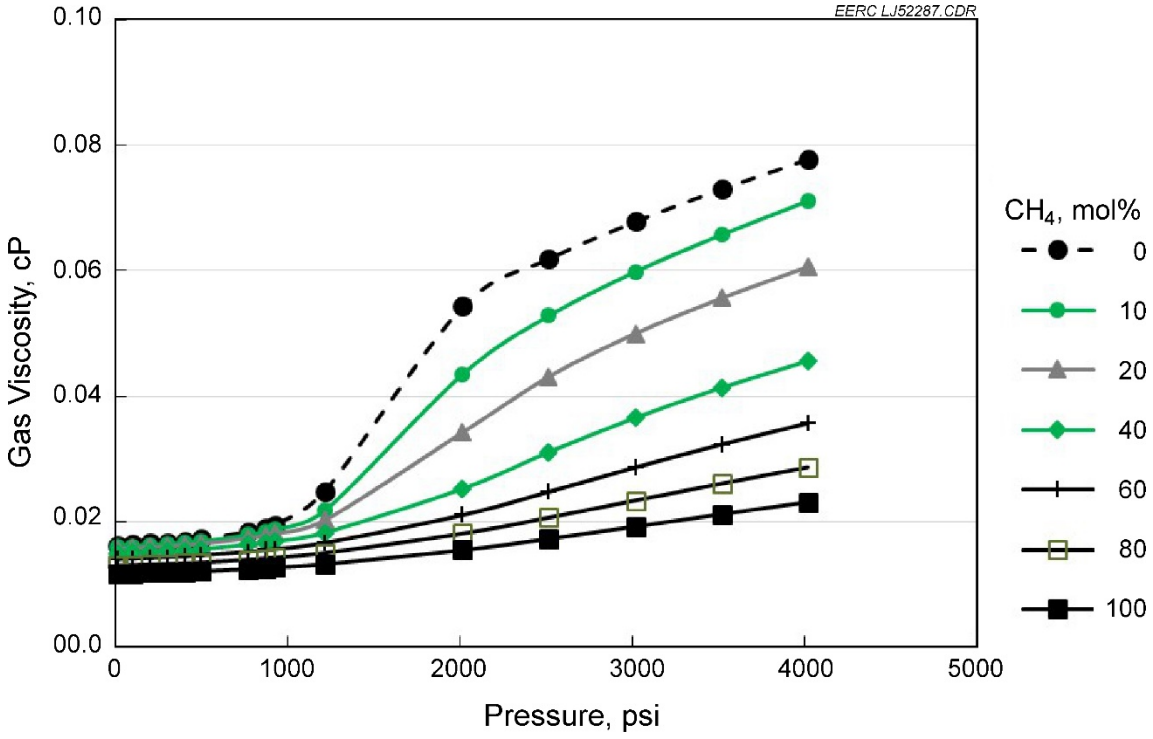

Figure 29. Effect of CH_4 viscosity of CO_2–CH_4 mixtures at 108°F.

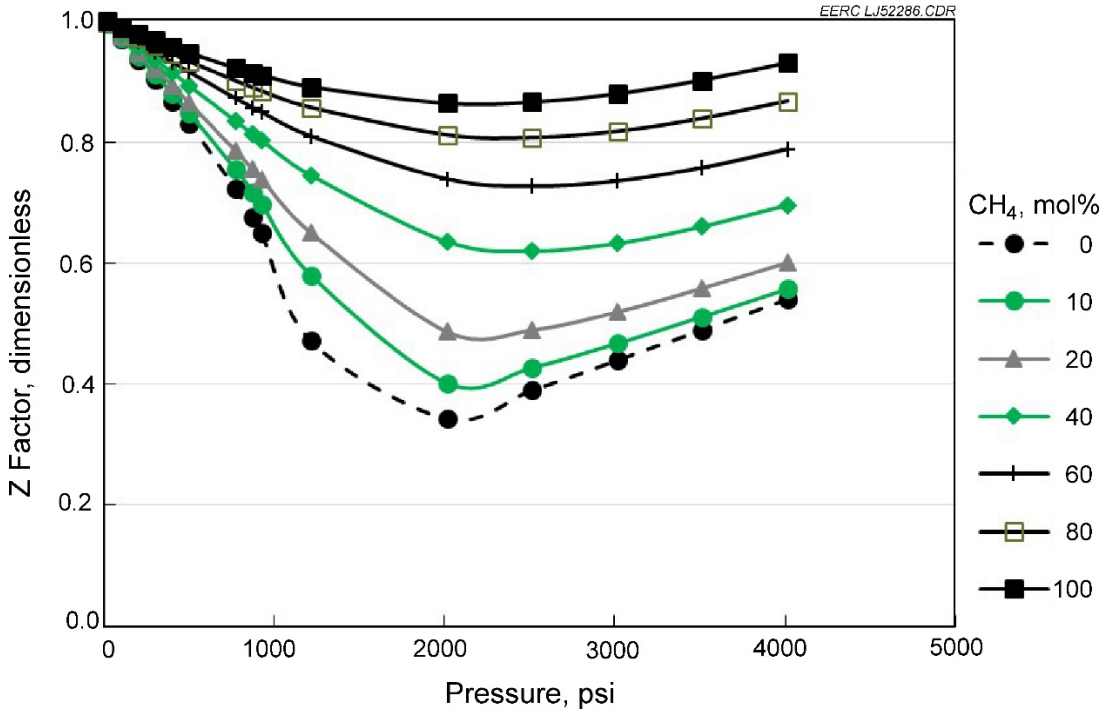

Figure 30. Effect of CH_4 on Z factor of CO_2–CH_4 mixtures at 108°F.

When gas flows through porous media, the flow behavior is governed by the physical properties of the formation, PVT properties of the gas–fluid system, flow geometry, and pressure distribution in the formation, as shown in Equation 2 (Al-Hussainy and others, 1966; Guo and Ghalambor, 2005):

$$\nabla \cdot \left[\frac{p}{\mu(p)z(p)}\nabla p\right] = \frac{\emptyset}{k}\frac{\partial}{\partial t}\left[\frac{p}{z(p)}\right] \qquad \text{[Eq. 2]}$$

Where, p is the reservoir pressure, *psi*; μ is the gas viscosity, *cP*; z is the gas Z factor, *dimensionless*; ϕ is the reservoir porosity, *fraction*; k is the reservoir permeability, *mD*; t is time, *day*. When gas flows to a vertical well, a general solution can be derived for Equation 2 assuming pseudo-steady-state flow in radial flow geometry:

$$q_g = \frac{kh\left[m(\bar{p}) - m(p_{wf})\right]}{1424T\left[ln\left(\frac{0.472r_e}{r_w}\right) + s + D\right]} \qquad \text{[Eq. 3]}$$

Where, q_g is the gas flow rate, *Mscf/d*; h is the thickness of pay zone, *ft*; m is the pseudopressure in the reservoir, psi^2/cP; $\bar{p}$ is the average reservoir pressure, *psi*; p_{wf} is the flowing BHP, *psi*; T is the reservoir temperature, *°F*; r_e is the radius of drainage area, *ft*; r_w is the wellbore radius, *ft*; s is the skin factor, *dimensionless*; D is the non-Darcy coefficient, *d/Mscf*. An observation of

Equation 3: *k*, *h*, *T*, r_e and r_w, are constants. If we ignore *s* and *D*, which is acceptable in many cases, then the gas flow is controlled by *m(p)*, which can be defined as:

$$m(p) = 2\int_{p_b}^{p} \frac{p}{\mu(p)z(p)}dp \qquad \text{[Eq. 4]}$$

Where, p_b is the base pressure, *psi*. Combining Equations 3 and 4, we can easily see that gas flow rate is a function of the combination of pressure, viscosity, and Z factor:

$$q_g = f\left[\frac{p}{\mu(p)z(p)}\right] \qquad \text{[Eq. 5]}$$

Figure 31 shows the change of parameter combination *[p/(μ*z)]* with pressure, where higher pressure does not always yield higher value for the combination when the CH_4 content is less than 60 mol% in the CO_2 stream. It indicates that there might be an optimum pressure existing for each CH_4–CO_2 mixture when the CH_4 mol% is less than 60%.

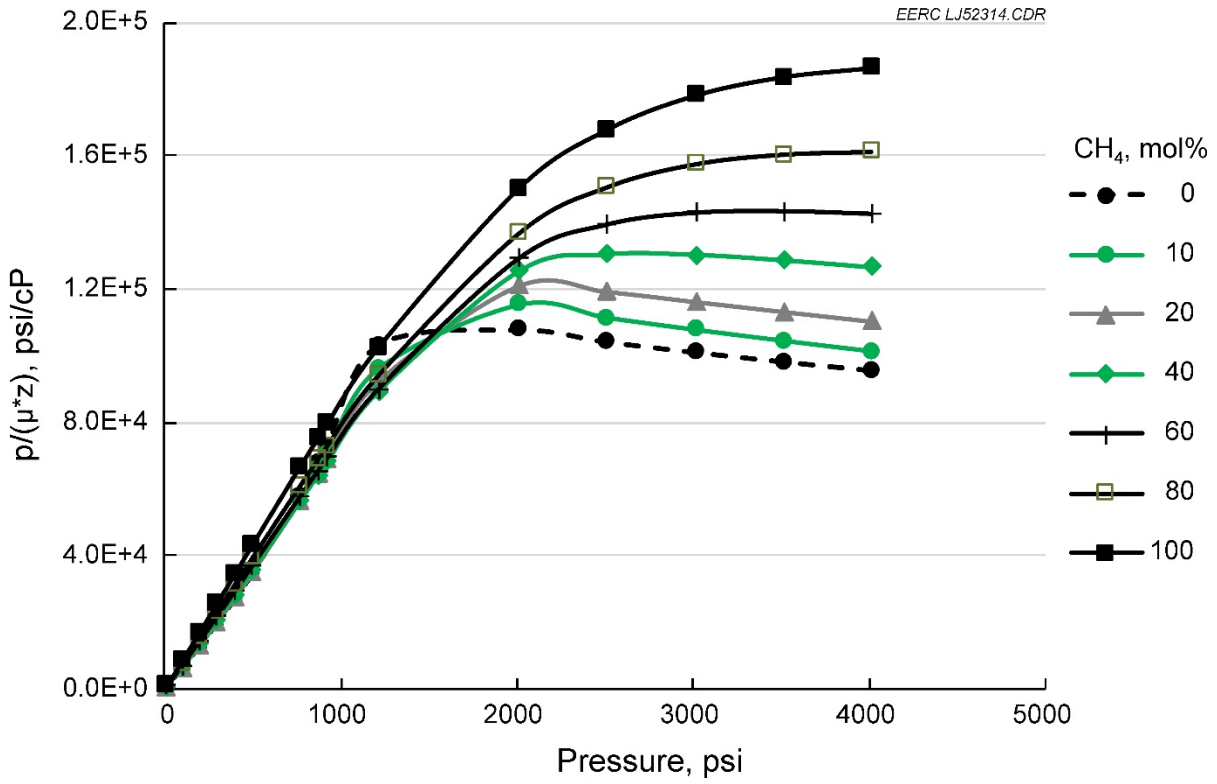

Figure 31. Effect of CH_4 on bulk gas flow parameter combination [p/(μ*z)] at 108°F.

MMP of Oil with CH_4–CO_2 Mixtures

When CO_2 is injected into a reservoir to remove oil from the porous matrix, it may involve one or several mechanisms such as solution gas drive, immiscible CO_2 drive, first-contact miscible drive, and/or multicontact (dynamic) miscible drive, etc. (Holm and Josendal, 1974). Generally, multicontact miscible drive is used more often than other processes as it is more effective than

immiscible CO_2 drive when a high pressure is not required to achieve first-contact miscibility. Based upon the reservoir and fluid properties, multicontact miscible flooding is used in the Bell Creek Field. In the miscible flooding process, CO_2 reduces oil viscosity, swells oil volume, vaporizes and extracts hydrocarbons from oil, and develops miscibility under certain reservoir pressures and temperatures (Hamouda and Tabrizy, 2013). A critical parameter in this process is the MMP, which is the pressure required to eliminate the interfacial tension (IFT) between the fluids (when the reservoir pressure is greater than MMP, there is no IFT existing between CO_2- and oil-dominated phases). The efficiency of oil displacement by CO_2 in porous media is related to the mass transfer between the oil and CO_2 phases, which is governed by IFT. The transfer of molecules to the CO_2 phase (across the oil/gas interface) occurs more readily when IFT approaches zero, which triggers dynamic miscibility conditions between the two interacting phases. As the amount of hydrocarbons moving into the CO_2 phase increases, so does the recovery potential for those hydrocarbon components.

MMP Measuring Methods

Studies have shown that different impurities have different effects on the CO_2–oil MMP: N_2, O_2, and CH_4 will increase MMP, while H_2S and light hydrocarbons such as C_2–C_5 will reduce it (Wilkinson and others, 2010; Jiang and others, 2012; Yin and others, 2014). The majority of the impurity in the Bell Creek recycled gas is CH_4; therefore, the focus of this investigation is related to better understanding how CH_4 impacts the MMP under reservoir conditions. Several methods have been used for MMP determination including the slim-tube test, rising bubble method, vanishing interfacial tension (VIT) test, and so on (Yellig and Metcalfe, 1980; Elsharkawy and others, 1996; Dong and others, 2001; Ayirala and Rao, 2011; Zhang and Gu, 2015). The slim-tube test has been used for MMP determination for decades and may be the most widely used technique among those mentioned above. However, the method has also received criticism from many investigators for being slow and expensive, having no consistent or widely accepted operating parameters, and lacking a fundamental physio-chemical definition of MMP (Zhang and Gu, 2015; Ahmad and others, 2016; Hawthorne and others, 2016). The rising bubble method can be used to estimate MMP efficiently, but the value of MMP is subject to the operator's interpretation, as it is determined by visual operation (Elsharkawy and others, 1996). The VIT method is a relatively new technique compared to the others. It was developed based on a rigid definition of MMP as the pressure at which the IFT between two phases reaches zero (Ayirala and Rao, 2011; Ahmad and others, 2016; Hawthorne and others, 2016). As IFT is strongly related to the composition of the injected solvent, oil properties, injection pressure, and reservoir temperature, the VIT technique may also be used to determine the minimum miscibility enrichment (MME: the solvent composition capable of complete miscibility with the displaced oil in the reservoir). The VIT test is also more efficient and less expensive than the slim-tube test, and the results of VIT tests are more repeatable than those from other methods (Ahmad and others, 2016; Hawthorne and others, 2016). Therefore, the VIT test was used in this study to determine MMP with various CH_4 fractions in the recycled gas. More detail on the VIT method is included in Appendix B of this report, as well as in Hawthorne and others (2016).

MMP Measuring Results

The VIT-measured MMP of Bell Creek oil is around 1410 psi for pure CO_2 at reservoir temperature (108°F). For comparison, the slim-tube test yields a MMP of 1430 psi. The difference between two measurements is less than 1.5%, indicating the result from VIT is very close to that of the slim-tube test, encouraging procedural validation.

By adding CH_4 to the CO_2 stream and repeating the VIT test procedure, the variation of Bell Creek oil MMPs for different CO_2/CH_4 mixtures may be measured (Figure 32). The figure demonstrates that MMP values increase linearly with increase in the CH_4 fraction of the CO_2/CH_4 mixture. The MMP values vary from approximately 1400 psi for 0 mol% CH_4 to about 4000 psi for 100 mol% CH_4 in the mixture. The results indicate miscible gas flooding may still be attainable with up to 30 mol% CH_4 in the recycled gas stream if the reservoir pressure is maintained at or above 2500 psi (Figure 32).

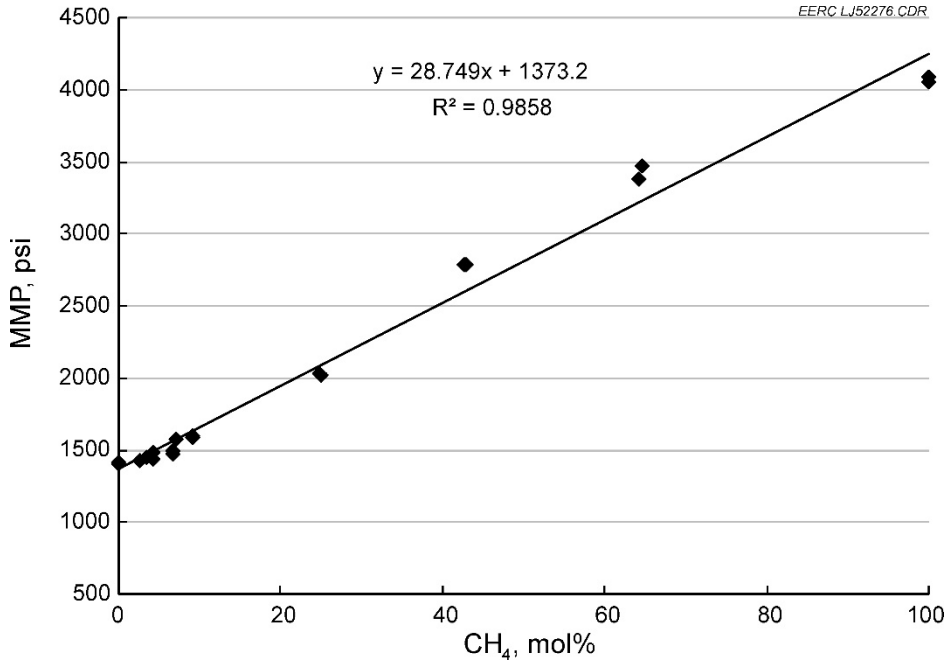

Figure 32. MMP for Bell Creek oil with CO_2–CH_4 mixtures at 108°F.

The VIT process also gives insight as to how CO_2 recovers the oil remaining in the pore space after waterflooding. The oil is in a residual condition relative to water and does not move if the IFT is not reduced. Miscible CO_2 injection mobilizes some of this oil (based on the various mechanisms mentioned above) and drives the hydrocarbons into the CO_2 phase. The mobilized oil is then produced (with or without CO_2). Because water has higher density and viscosity than CO_2 (and CO_2 is highly soluble in water), in some scenarios it may be helpful to inject a slug of water to displace the hydrocarbon-saturated CO_2, potentially improving sweep efficiency and oil recovery. This process is referred to as WAG injection, which has been widely used in CO_2 EOR operations (Rogers and Grigg, 2000; Manrique and others, 2007; Chen and others, 2010; Uj and Fekete, 2011).

Simulation of Produced Gas Recycle Injection

Considerable work has been done in geologic modeling construction and numerical simulation for the Bell Creek Field in the past several years. A detailed 3-D static geocellular model of the Bell Creek Field area (V2 model) was constructed using pertinent reservoir characterization data (geologic core samples and well logs) from 748 wells in the field and its surrounding area, to represent geologic stratigraphy, facies, and petrophysical properties necessary for simulation activities. A series of simulation models were developed based on the static model, including a quarter five-spot model, a five-spot model, a Phase 1-localized model, a Phase 2-localized model, a combined model for the Phase 1 and 2 areas, and a model of the Phase 3–7 areas (Pu and others, 2011; Saini and others, 2012; Braunberger and others, 2013; Liu and others, 2014). A systematic simulation approach was developed for effective history matching and production performance prediction based on analysis of core data, production history, and dimensionless groups (Bosshart and others, 2015). These studies greatly enhanced our ability to understand the reservoir dynamics and enable prediction of reservoir performance under various operational conditions. All of these previously developed simulation models were available for simulating the reservoir performance of produced gas recycle injection.

PVT Model Analysis

Because of strong heterogeneity and complex reservoir properties in the Bell Creek Field, a seven-component PVT model was developed previously and applied in the above-mentioned simulation models. The model included CO_2 as a single component and six lumped components (N_2–C_2, C_3–C_4, C_5–C_7, C_8–C_{13}, C_{14}–C_{24}, and C_{25}–C_{36}) to capture the phase behavior of the reservoir fluids. The model was tuned and able to match all of the experimental testing results (Pu and others, 2011). This model worked well for primary depletion, waterflooding, and pure CO_2 flooding (Liu and others, 2014); however, it did not consider the effects of each individual impurity, such as N_2 or CH_4, as they were lumped together in one pseudo component (N_2–C_2). An analysis of oil composition used for the PVT model tuning is required to evaluate the feasibility of using the lumped components for predictions of impurity effects. Figure 33 shows the detailed oil composition used for tuning the PVT model. Table 1 illustrates the key components in the oil and injection gas used in various PVT tests, which included saturation pressure, separator, constant composition expansion, differential liberation, and swelling tests. The C_{7+} components are briefly divided into several pseudo components in the table, because heavier components can exist in multiple orientations, and their properties are generally determined by correlations based on oil properties (Ahmed, 2007).

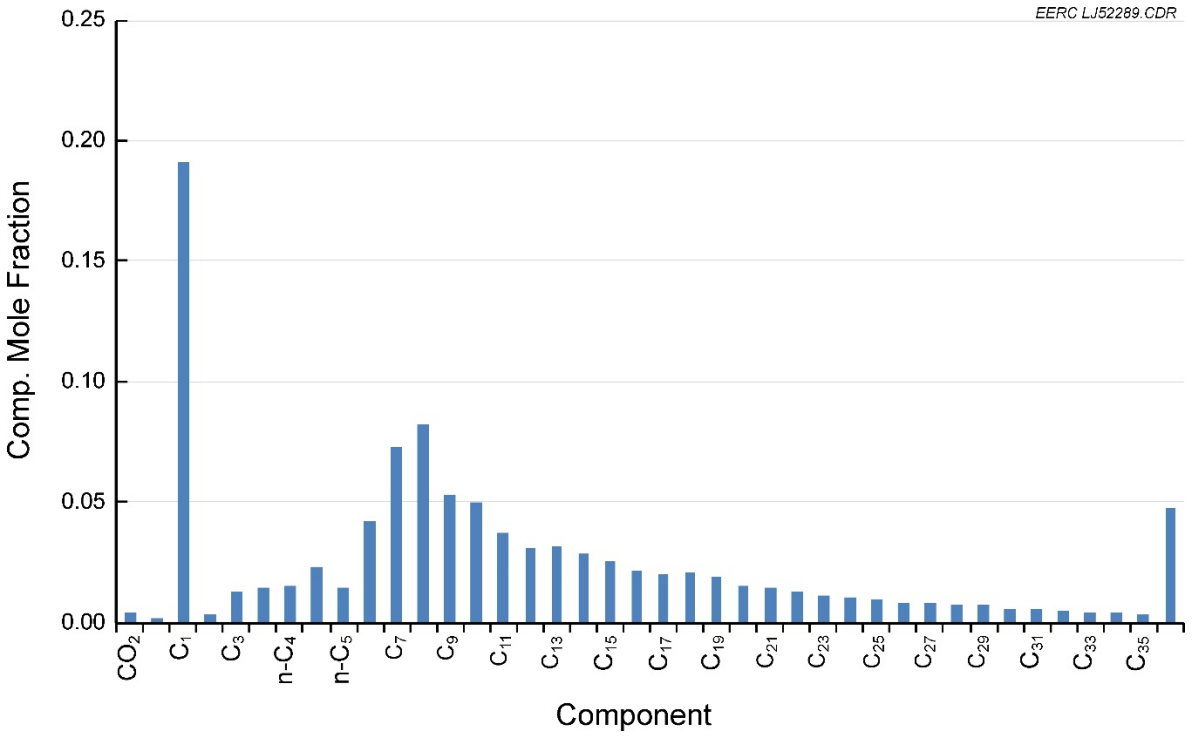

Figure 33. Composition of Bell Creek oil used for PVT tuning.

Table 1. Main Components in Bell Creek Oil and Injection Gas Used for PVT Tuning

Oil Composition	
Component	**Mole Fraction**
CO_2	0.0042
N_2	0.0019
C_1	0.1909
C_2	0.0033
C_3	0.0132
C_4	0.0297
C_5	0.0382
C_6	0.0420

Oil Composition	
Component	**Mole Fraction**
C_7	0.0724
C_8–C_{13}	0.2860
C_{14}–C_{24}	0.1997
C_{25}–C_{36+}	0.1184
Injection Gas Composition	
Component	**Mole Fraction**
CO_2	0.9987
N_2	0.0013

The data in the table show that CH_4 made up 97.31 mol% in the N_2–C_2 group when it was lumped. The produced gas CH_4 content of the N_2–C_2 group varied in a comparable range, from approximately 84 to 99 mol%. This observation indicated the N_2–C_2 group may be used to evaluate the impact of impurities when the produced gas is used for recycle injection. Thus, the previously history-matched reservoir models could be used for large-scale performance prediction without going through further history-matching efforts. However, a new nine-component PVT model was also developed (with N_2, CH_4, and C_2H_6 separated) to compare with the results of the lumped N_2–C_2 components.

Phase-Scale Prediction

A large-scale simulation model covering the Bell Creek Field Phase 1 and 2 areas has been developed with a total of 859,362 cells and 102 wells: 26 producing wells and 27 injection wells in the Phase 1 area; 17 producing wells and 18 injection wells in the Phase 2 area; and ten producing wells and four injection wells in the areas beyond these phases. History-matching results of primary production, waterflooding, and CO_2 flooding indicated the model could capture the overall flow behavior in the area. The CO_2 EOR activities were effective for oil production in this area; however, the gas production rate increased rapidly as the flooding went on. Figure 34 shows the gas production rate exceeded 45 million scf/day in April 2015. Based on the test results from Figures 24–27, a considerable amount of impurities were injected into the reservoir. To evaluate the impact of this recycle gas injection, a set of predictive runs were carried out using the history-matched model. The pseudo component N_2–C_2 was used to represent the impurities, and the main component in the injected solvent was CO_2.

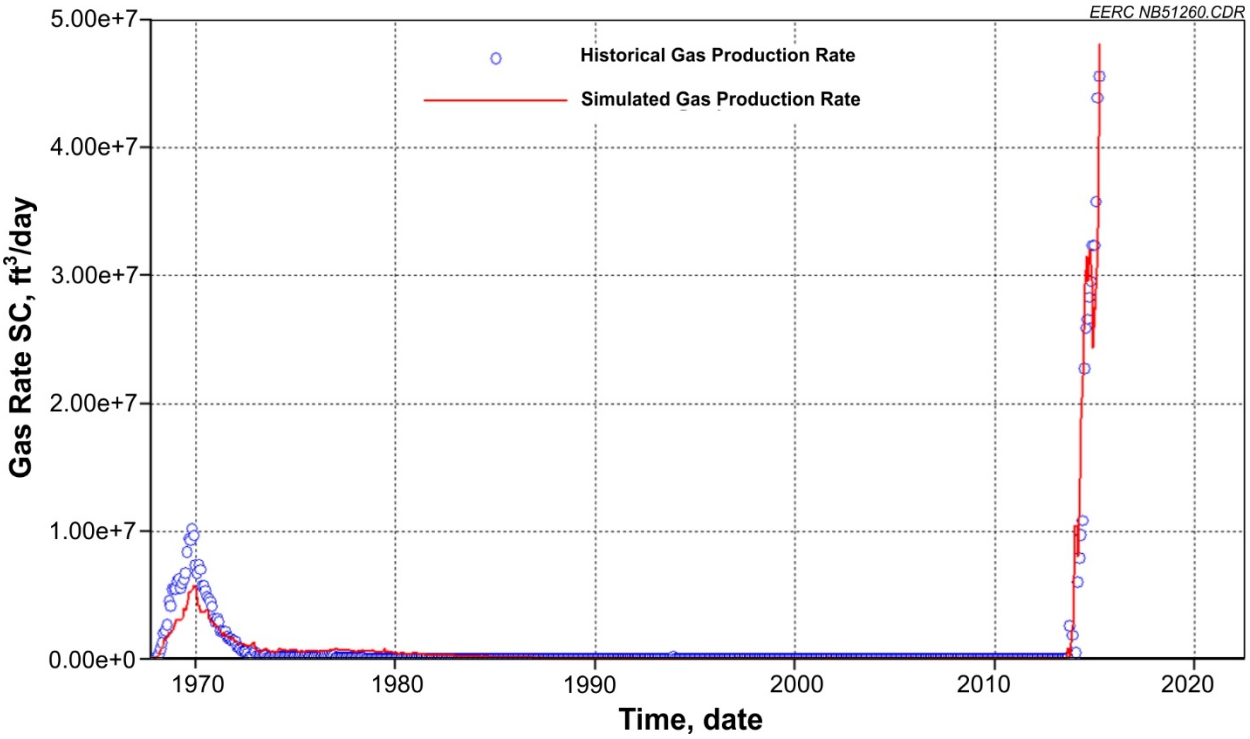

Figure 34. Gas production rate in the Bell Creek Phase 1 and 2 areas (SC refers to standard conditions).

Table 2 shows the values of injection gas impurities used in the simulations, where the content of N_2–C_2 was varied from 0 to 99.6 mol% to cover the full range of the major impurity. WAG operations were simulated in all cases to conform with the actual field operation. To make the results realistic, the pressure constraints in the injection and production wells were set at 2800 and 2300 psi, respectively, and the predictive simulation duration was set to 45 years (2015–2060) for all simulation runs.

Table 2. Impurities in the Recycled Gas for Simulation

Impurity	mol%
N_2–C_2	0–99.6
C_3–C_4	0.3
C_5–C_7	0.1
C_8–C_{13}	0
C_{14}–C_{24}	0
C_{25}–C_{36}	0

The oil recovery factor for different cases is shown in Figure 35. An interesting point to note: the purest CO_2 does not lead to the best oil recovery in the same period of time. Recycled gas with 20 mol% impurities seems to be better for EOR in this reservoir. Although the volume of fluids injected to the reservoir is identical in the standard conditions for all cases, the hydrocarbon pore volume injected (HCPVI) in reservoir conditions is quite different, as shown in Figure 36. Referring back to Figure 30, which showed that impurities like CH_4 have a strong effect on the Z factor (compressibility) of the recycled gas, as the impurity content in the gas increases, the more incompressible it becomes. Therefore, significantly more hydrocarbon pore volumes (HCPV) may be injected into the reservoir when there are more impurities in the recycled gas. Also, CO_2 is at its most compressible when the reservoir pressure is between 1500 and 3000 psi, which spans the operational pressure range for CO_2 EOR in the Bell Creek Field, suggesting this reservoir is likely to be sensitive to impurities in the EOR process.

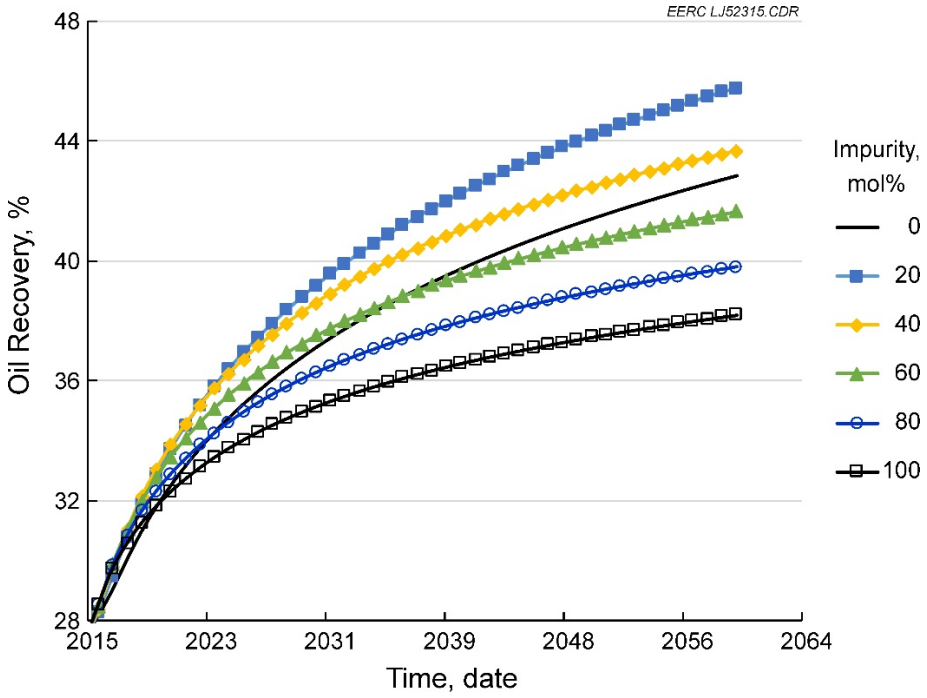

Figure 35. Oil recovery factor for WAG scenarios using recycled gas injection and varying injection gas impurity content in Bell Creek Field Phases 1 and 2.

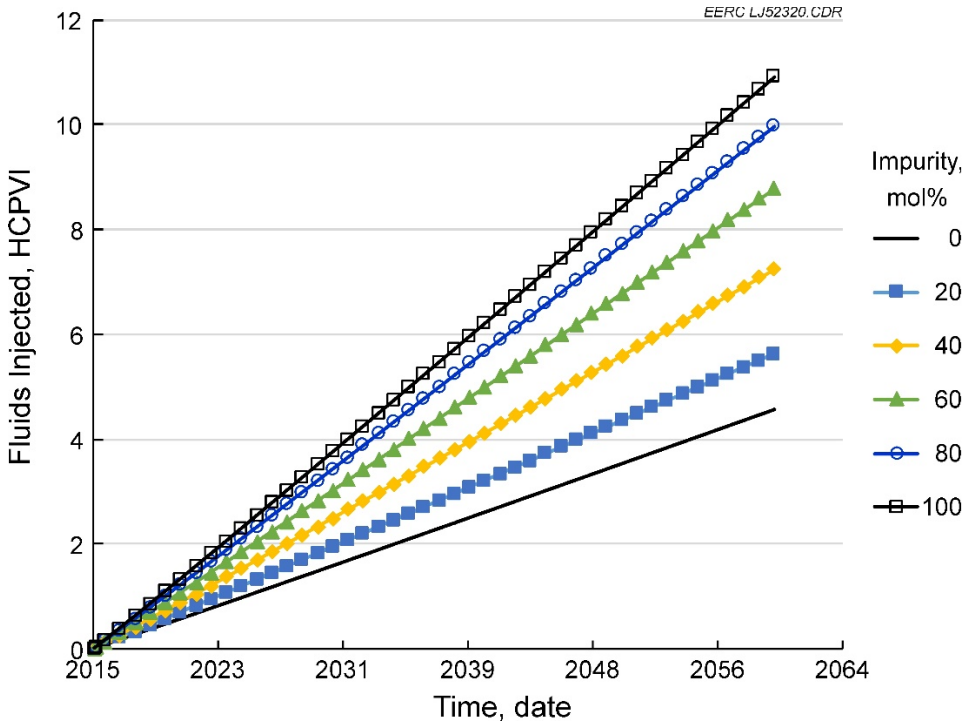

Figure 36. Cumulative fluid injection for WAG scenarios using recycled gas injection and varying injection gas impurity content in the Bell Creek Field Phase 1 and 2 model.

Figures 37 to 39 show the oil recovery factor performance for gases with different levels of impurities based on the HCPVI. Figure 37 shows that WAG with pure CO_2 has the least HCPVI. Gas injection with 20 mol% of impurities yields better oil recovery than pure CO_2 flooding with the same HCPVI. Oil recovery drops drastically when the impurity level exceeds 40 mol% regardless of the fact that more pore volume can be flooded by the mixtures. Figure 38 compares the EOR performance after four HCPVs of recycled gas injection with impurity contents ranging from 0 to 40 mol%. It is clear that there is an optimum composition range for the injected gas to achieve maximum oil recovery. In comparing the WAG oil recovery factor after four HCPV of recycled gas injection with varying impurity levels, the optimum composition range is apparent (Figure 39). Oil recovery appears to be maximized when the injection gas contains between 10 to 20 mol% of impurities. Oil recovery appears to decline significantly after exceeding 30 mol% of impurities in the injection gas. When the impurity level exceeds 40 mol% in the injection gas, the flooding changes from miscible to immiscible (refer back to Figure 32), which leads to significant reduction of flood efficiency.

The impact of impurities on CO_2 storage can be seen in Figure 40, which shows pure CO_2 flooding results in the greatest amount of stored CO_2. As the impurities occupy more pore volume than CO_2 in the reservoir conditions (the impurities are less compressible than CO_2), the performance of CO_2 storage is more sensitive to impurities than that of oil recovery. However, based on the actual content of impurities in the recycled gas analyzed in this study (Figures 26 and 27), CO_2 will still be stored in the reservoir effectively.

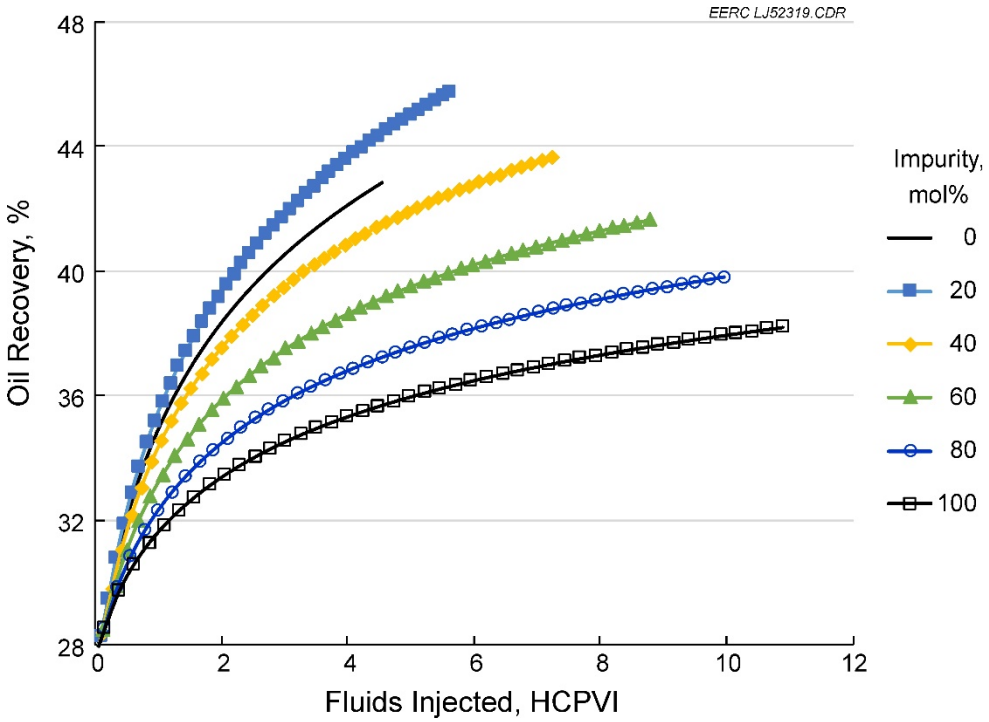

Figure 37. Oil recovery efficiency factor (by HCPVI) for WAG scenarios using recycled gas injection and varying gas impurity content in the Bell Creek Field Phase 1 and 2 model.

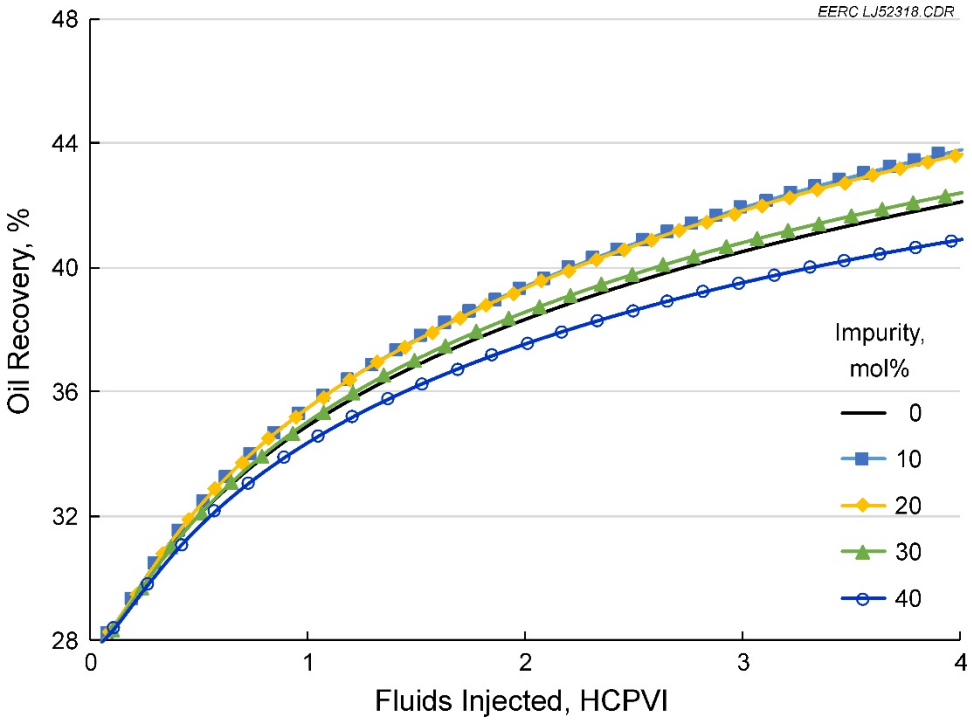

Figure 38. Oil recovery factor resulting from WAG scenarios with four HCPVI of recycled gas injection and varying gas impurity content from 0 to 0.4 in the Bell Creek Field Phase 1 and 2 model.

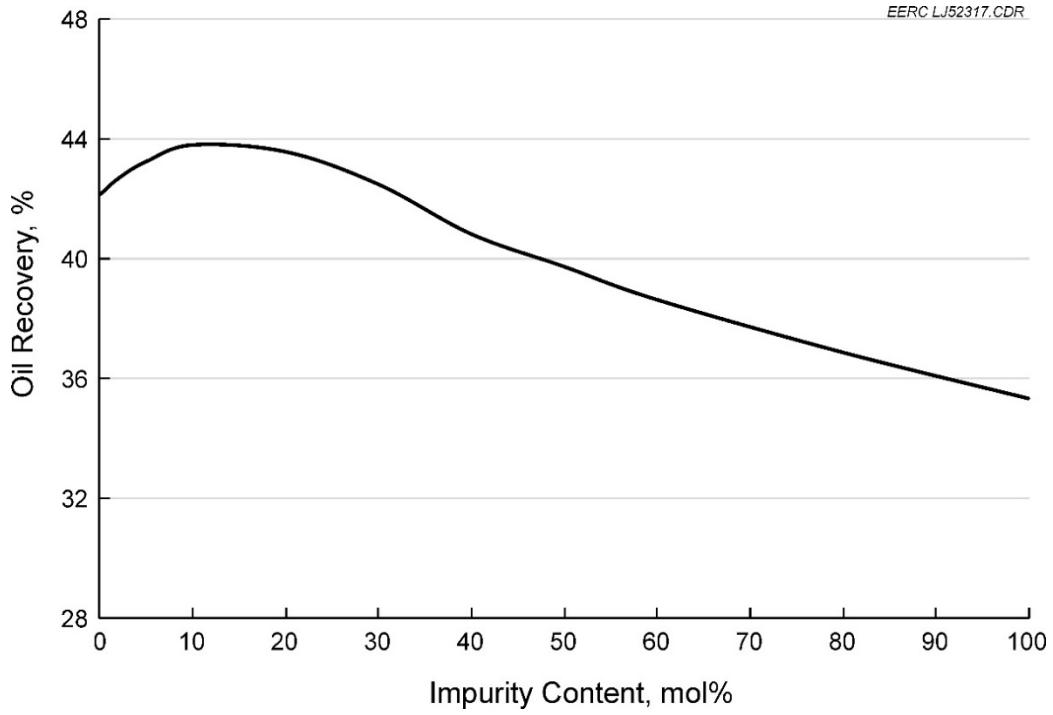

Figure 39. Oil recovery factor as a result of varying WAG injection gas impurity content after four HCPVI in the Bell Creek Field Phase 1 and 2 model.

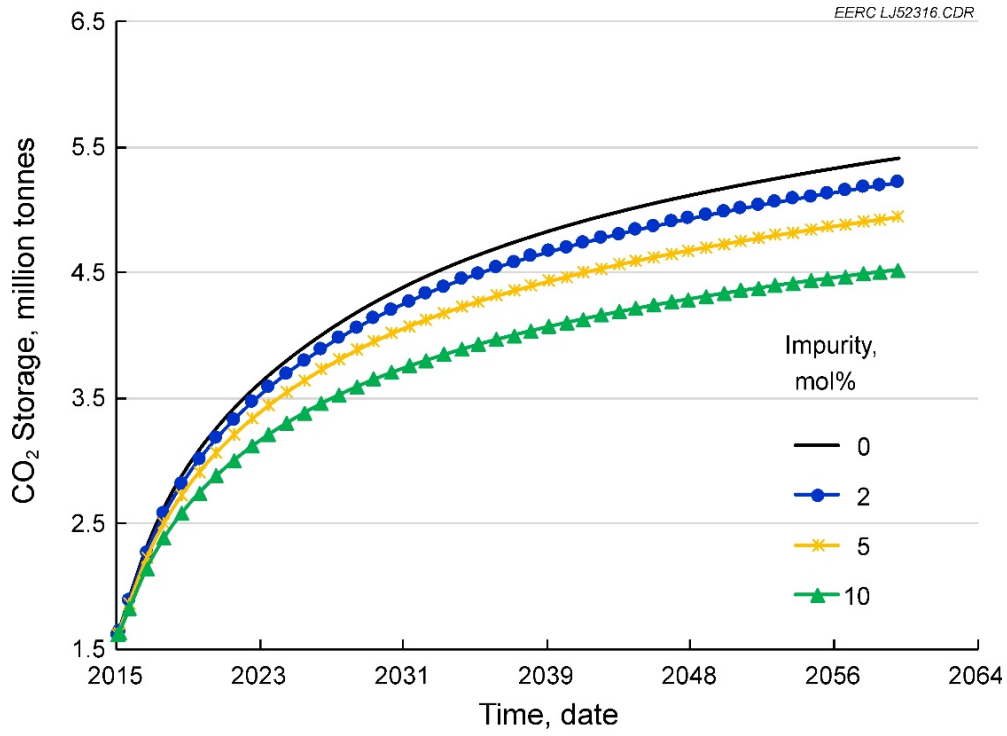

Figure 40. Stored CO_2 resulting from WAG recycled gas injection with varying impurity content in the Bell Creek Field Phase 1 and 2 model.

Subphase-Scale Prediction

The discussion above of phase-scale simulation with a seven-component PVT model shows that a limited amount of impurities in the recycled CO_2 stream would not reduce the oil recovery factor and CO_2 that could also be stored effectively. Previous studies showed that different impurities have different effects on CO_2–oil MMP and oil recovery. For example, N_2 and CH_4 reduce the gas–oil miscibility by increasing the MMP, while ethane (C_2H_6) and propane (C_3H_8) promote miscibility and make the extraction process easier (Metcalfe, 1982; Shyeh-Yung and Stadler, 1995; Wilkinson and others, 2010; Jiang and others, 2012; Hamouda and Tabrizy, 2013; Yin and others, 2014; Hawthorne and others, 2016). Therefore, a nine-component PVT model (with the main impurities separated) was developed to clarify the effects of different impurities on CO_2 flooding in the Bell Creek Field. The new PVT model includes four individual components: CO_2, N_2, CH_4, and C_2H_6, and five lumped components: C_3–C_4, C_5–C_7, C_8–C_{13}, C_{14}–C_{24} and C_{25}–C_{36}. Similar to the seven-component model, the nine-component model is tuned with experimental PVT tests, including saturation pressure, constant composition expansion (CCE), differential liberation and swelling experiments.

Since the new PVT model required significantly more computational resources to predict the flood performance, a sub-Phase 2 simulation model was cut from the phase-scale model to make the simulation more efficient. The sub-Phase 2 model covered most of the Phase 2 area (Figure 41). This model included the structural complexity and heterogeneity of the reservoir, as well as the prolonged production history with ten injection wells and 11 production wells. Coupled with the nine-component PVT model the sub-Phase 2 model was used to predict the impact of impurities on recycled gas injection performance.

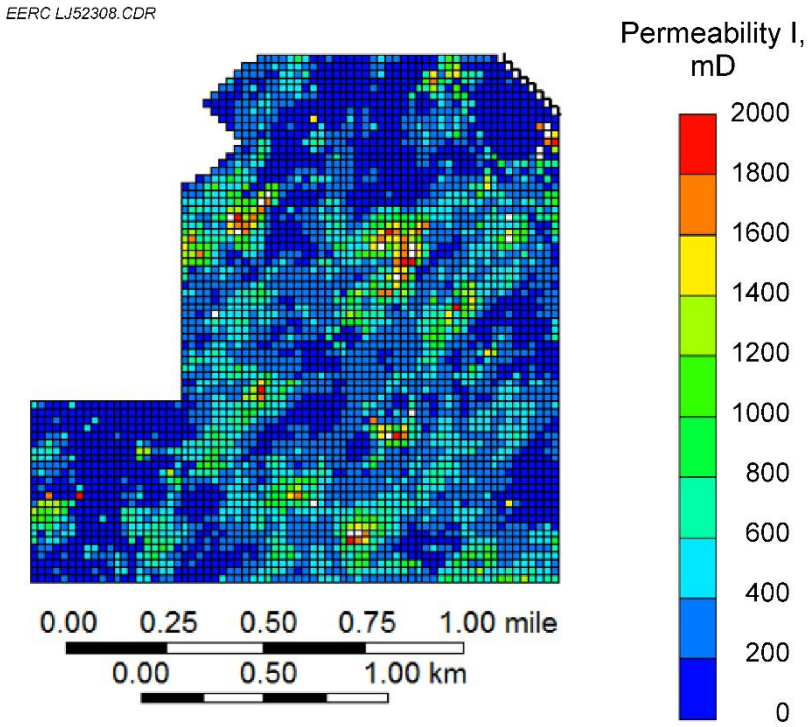

Figure 41. Schematic of the sub-Phase 2 model.

To investigate a broader spectrum of scenarios, CGI operations were simulated with injection and producing pressures fixed at 3000 and 2500 psi, respectively. The oil recovery and CO_2 storage performance at various CH_4 contamination levels is shown in Figures 42–44. The figures show similar results to those of the phase-scale model. Figures 42 and 43 suggest maximum oil recovery may be achieved when there is 20 mol% CH_4 in the recycled gas. Recycled injection gas with 30 mol% CH_4 appears to show results similar to the oil recovery exhibited from pure CO_2 flooding. Recycled gas with 5 mol% CH_4 would have no significant impact on CO_2 storage performance (Figure 44). Based on the similarity of results, the seven-component PVT model appears capable of accurately simulating the effects of recycled gas injection in the Bell Creek Field.

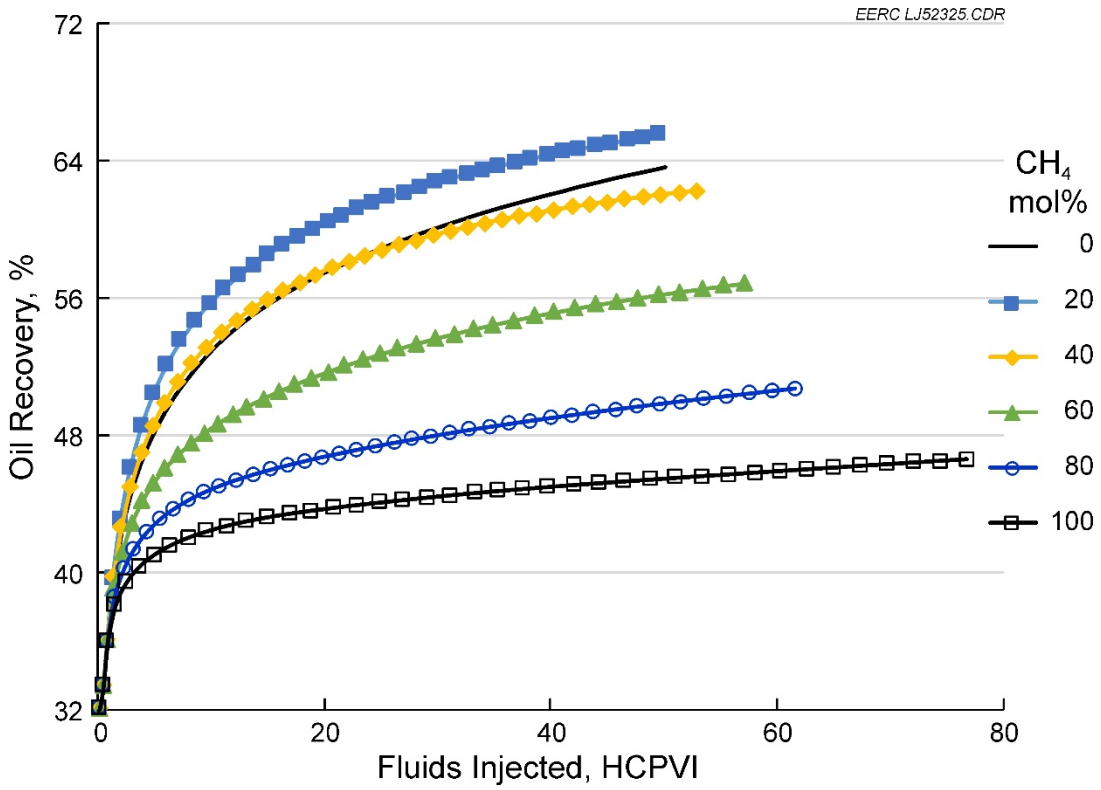

Figure 42. Oil recovery factor with varying CH_4 content in the Bell Creek sub-Phase 2 area using recycled gas CGI operations; nine-pseudo component PVT model.

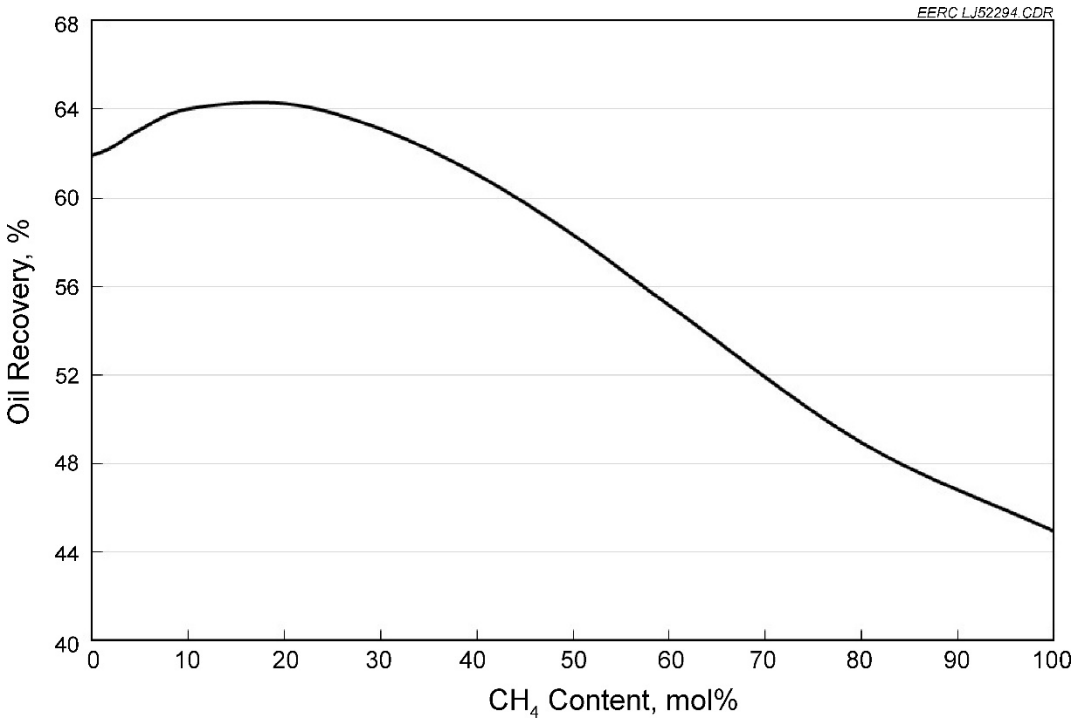

Figure 43. Oil recovery factor comparison for varying CH_4 content in the Bell Creek sub-Phase 2 area at four HCPVI using recycled gas CGI operations; nine-pseudo component PVT model.

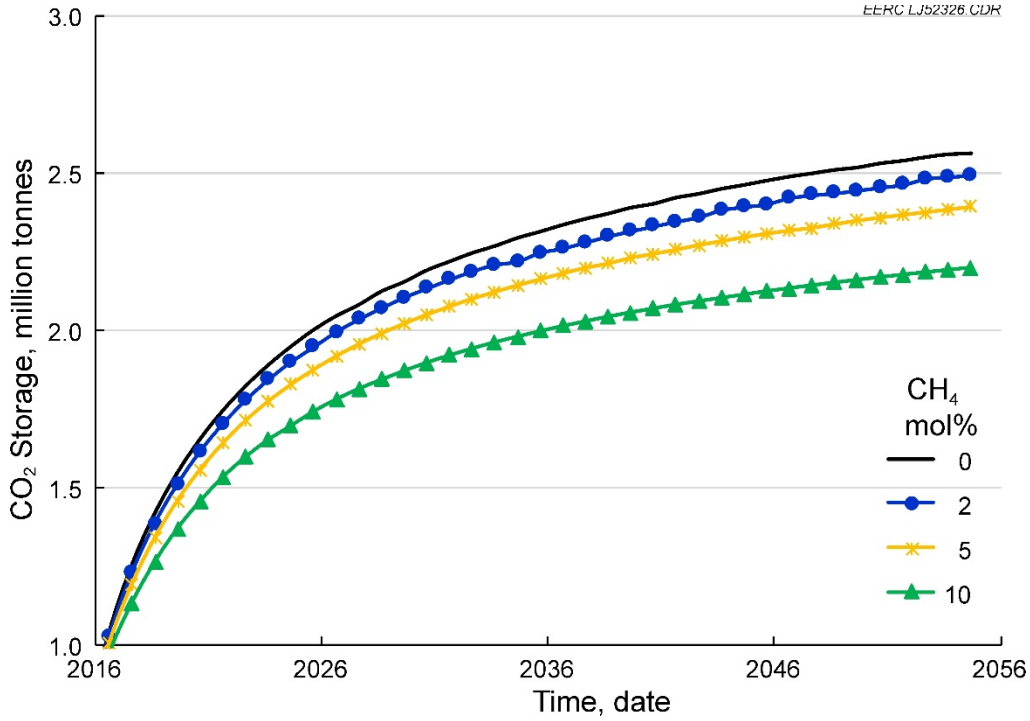

Figure 44. Stored CO_2 resulting from varying CH_4 content in recycled gas CGI within the Bell Creek sub-Phase 2 area; nine-pseudo component PVT model.

Impact of Geology and Pressure

Although miscible flooding has been applied successfully around the world in the past decades, some turned out to be "miserable flooding" in the postmortem evaluations (Thomas and others, 1994). The reason for some floods being successful and others less so might be closely related to the parameters of gas injection and the nature of the process itself, where the geology plays a critical role in the flooding processes (Gardner and Ypma, 1984; Thomas and others, 1994).

Geologic conditions are important factors when studying CO_2 flooding performance. Two groups of geologic parameters have been divided: macroscale parameters such as heterogeneity and reservoir structure, and microscale parameters such as pore-size distribution. Usually, there are different flow units in a reservoir because of the macroscale heterogeneities such as impermeable barriers, high-conductivity fractures and high-permeability channels, etc., which significantly impact the way fluids flow (Pande, 1992). The pore-size distribution may also impact the optimal design significantly, as it directly relates to the fundamental fluid parameters such as IFT and viscosity ratio. The microscale effects become more important when the reservoirs are tight (Jin and others, 2015, 2016a, 2016b). Therefore, a successful operation may be difficult to achieve when the geology is inconsistent.

Pressure is another important parameter in the gas flooding process, as it determines whether "miscible flooding" is achievable in a reservoir. However, there is still ongoing debate as to whether one needs to achieve miscibility to optimize the oil recovery, or whether the "near-miscible flooding" is equally adequate for field implementation of EOR processes (Thomas and others, 1994; Sohrabi and others, 2008; Fatemi and Sohrabi, 2013; Aryana and others, 2014; Khosravi and others, 2015).

Because of the complexity of reservoir conditions in the Bell Creek Field, a basic quarter five-spot model was used to evaluate the impact of geology and pressure on EOR performance (Figure 45), to enable clear analysis. Poston and Gross (1986) systematically studied sandstone reservoir rocks and identified four basic types based on depositional environments (Figure 46). These sandstone sequences included homogeneous, regressive, transgressive, and alternating. These geologic configurations have been observed in well logs and core analysis data and provide insight into the major flow paths within the reservoir. These four geologic settings were integrated in the quarter five-spot model by varying permeability in each layer, as shown in Figure 47. Cross sections of the original (heterogeneous) and four hypothetical simulation models are illustrated in Figure 48, demonstrating the notable differences in permeability distributions. Injection pressure was varied from 2000 to 4000 psi, and the producing pressure was varied from 1500 to 3500 psi. The pressure difference between injection and production wells was fixed at 500 psi. CO_2 and CH_4 were used as the flooding gas, and CH_4 content was varied from 0 to 100 mol%. The nine-component PVT model was used in these simulations. These efforts in varying geologic conditions were designed to capture the different potential flow behaviors in the reservoir.

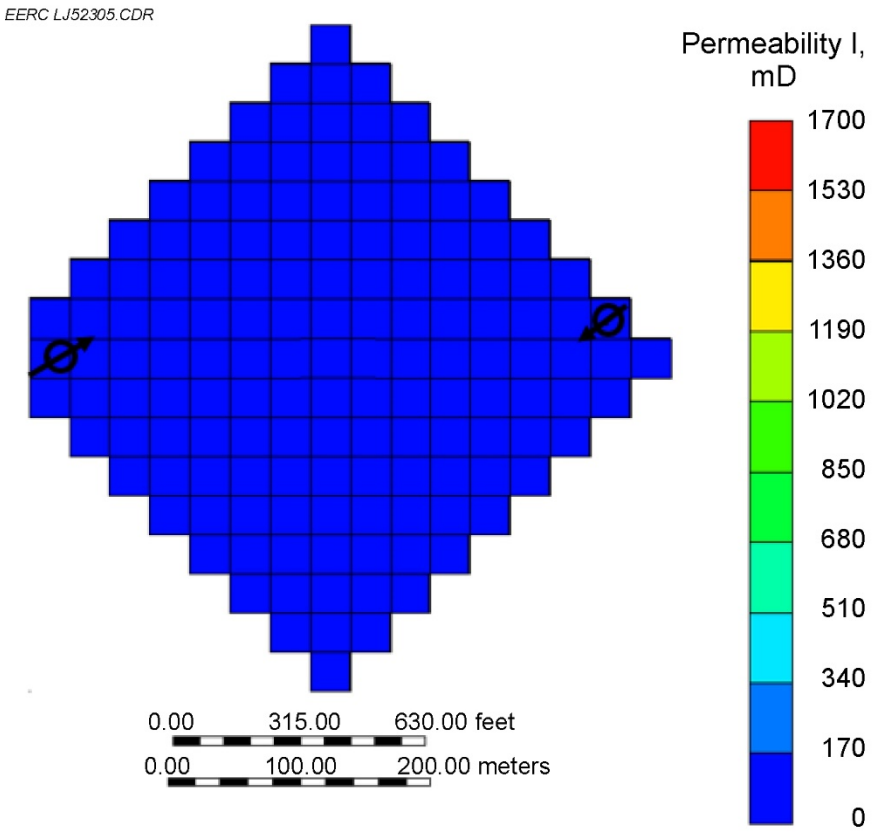

Figure 45. Schematic of the Bell Creek quarter five-spot model.

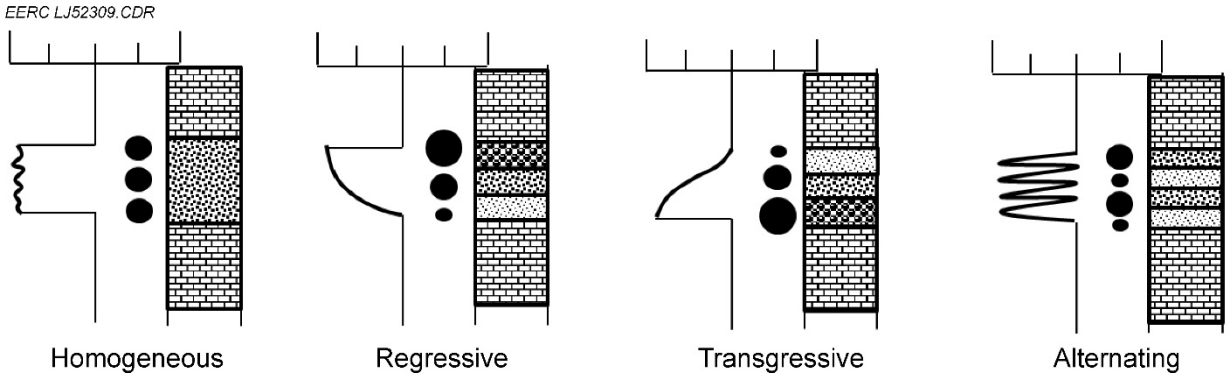

Figure 46. Four basic sandstone sequences described by Poston and Gross (1986).

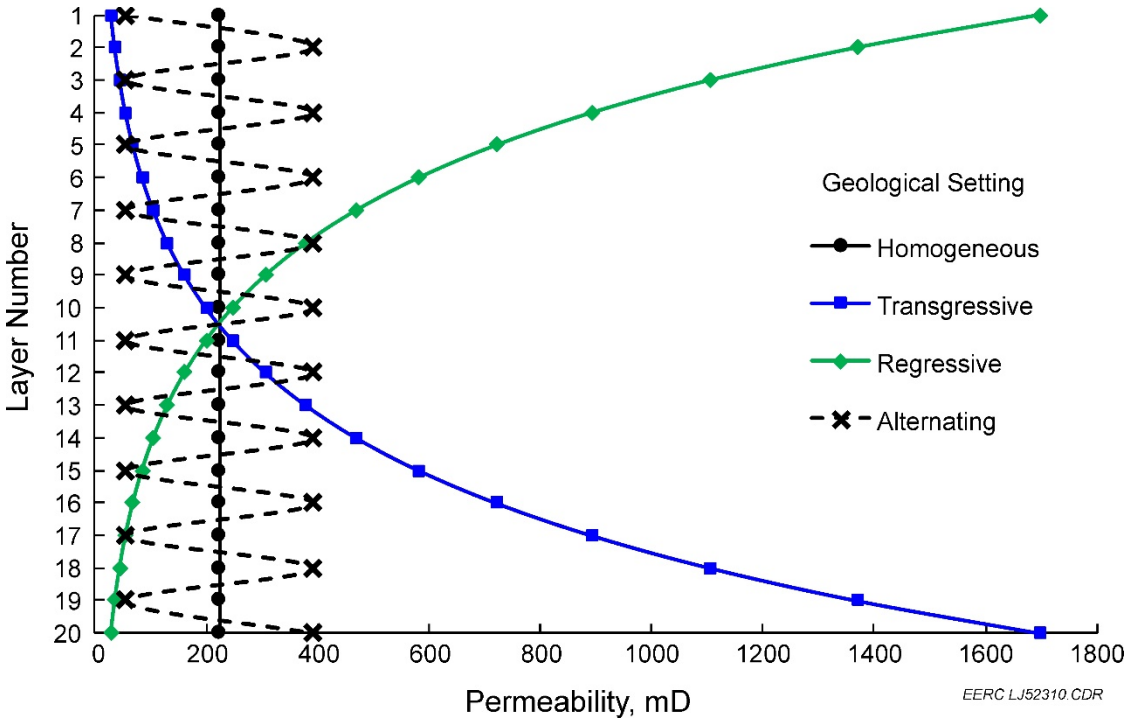

Figure 47. Illustration of the different quarter five-spot models' permeability distributions by layer.

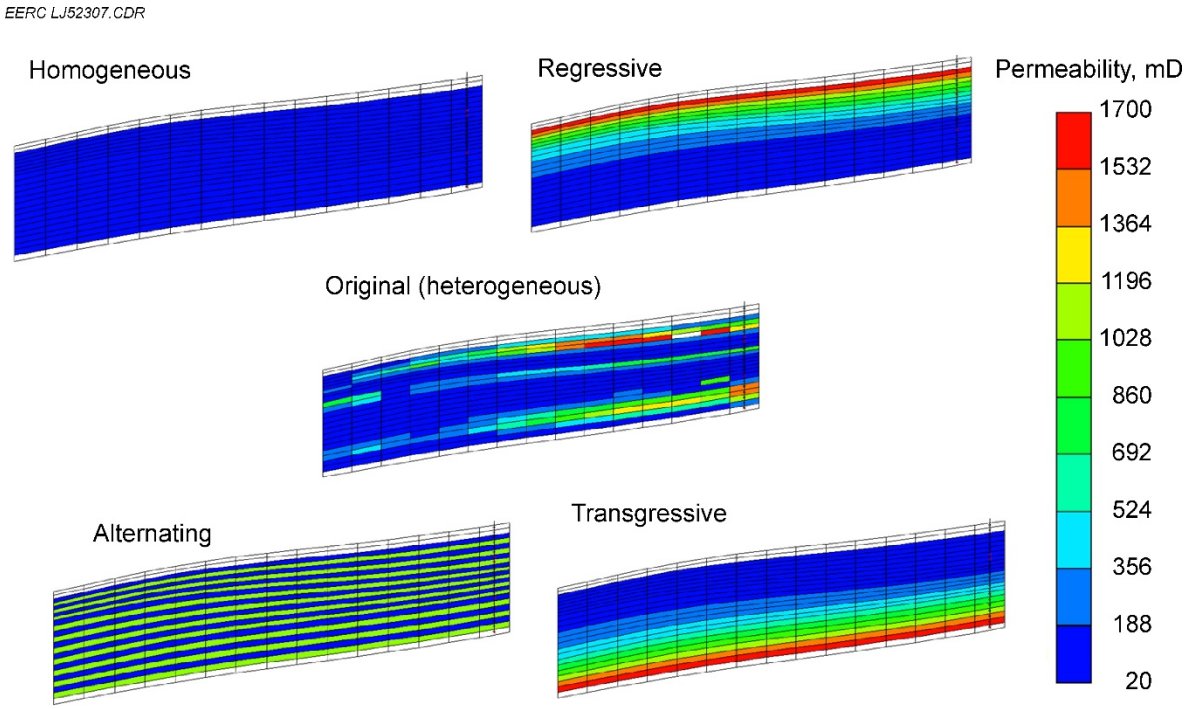

Figure 48. Permeability cross sections of the different Bell Creek quarter five-spot simulation models.

Similar to the sub-Phase-scale cases, 40 years of CGI was simulated for each quarter five-spot case. Figure 49 shows the oil recovery of the various geology, pressure, and impurity combinations. It is clear that all three parameters have significant effects on oil recovery. As the injection–production pressure is increased, more CH_4 can be tolerated in the injection gas. The simulations indicated an ability to achieve significant oil recovery when the reservoir pressure was above but not significantly exceeding the MMP. This observation is similar to some near-miscible flooding studies (Thomas and others, 1994), where flooding pressure conforming to the reservoir and fluid properties is effective. This suggests that high pressure may not be necessary to yield the best oil recovery. It is evident that heterogeneity is always detrimental to the flood performance. Regressive geological sequences are also challenging for good oil recovery. Alternating, homogeneous, and transgressive geologic settings are favorable for gas flooding in most cases. This may be attributed, in part, to the geologic heterogeneity's effects on EOR fluid density and sweep efficiency. Gas, being lighter than oil, tends to flow in the upper part of the reservoir. These buoyancy effects are obvious in the regressive geology where oil in the lower part of the reservoir is difficult to sweep. The transgressive geology seemed to mitigate this effect and showed resilience when injecting light gas (i.e., increased CH_4 content in the injection gas).

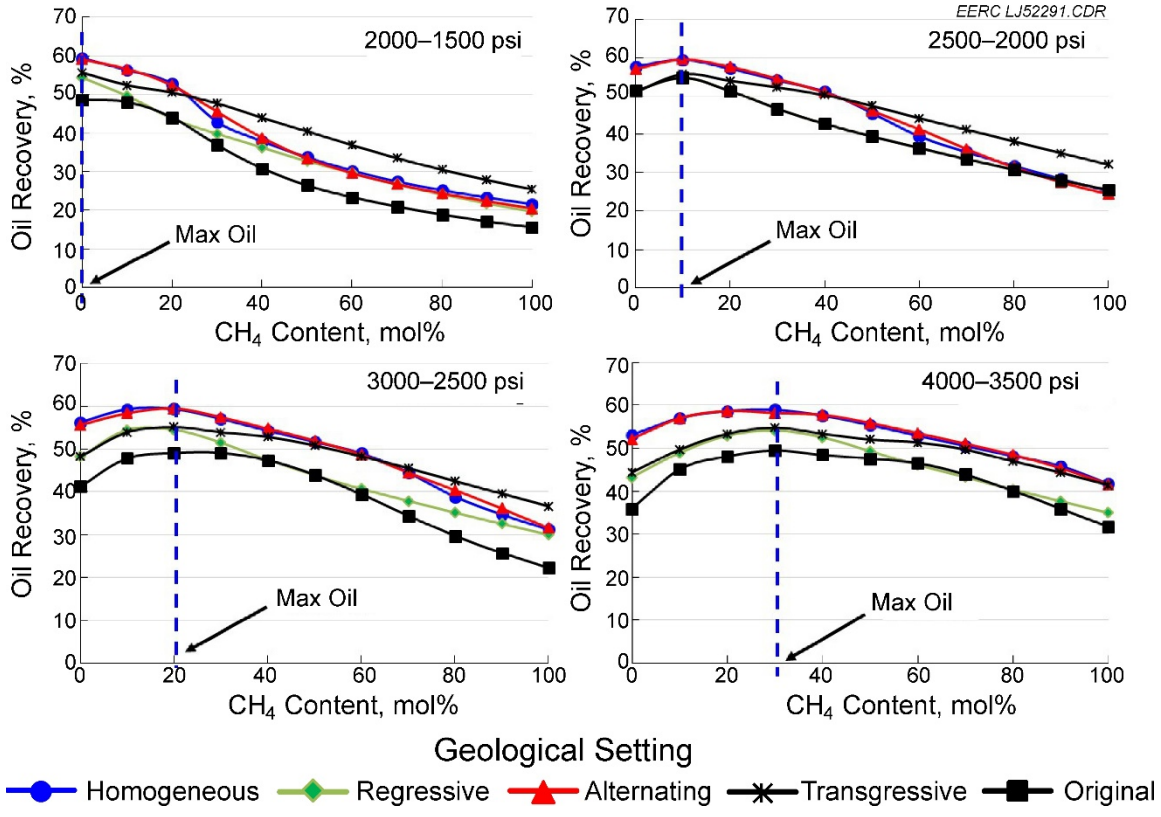

Figure 49. Oil recovery factor for different pressures and geologic conditions with varying CH_4 content after 40 years of recycled gas CGI.

History Match for the Bell Creek Phase 3 Area

Figure 50 shows the general profile of the Bell Creek Phase 3 simulation model which was clipped from the full-field (V2) geologic model. Based on sensitivity analyses of previous simulation models in Phases 1 and 2, a cell size of 100 feet × 100 feet and average thickness of 1 foot was selected. The model dimensions were 180 × 240 × 26 cells, resulting in just over 800,000 cells. There were 42 active wells in the Phase 3 model, including 21 production wells, 19 WAG injection wells, and two water injection wells. The detailed well distribution is shown in Figure 51.

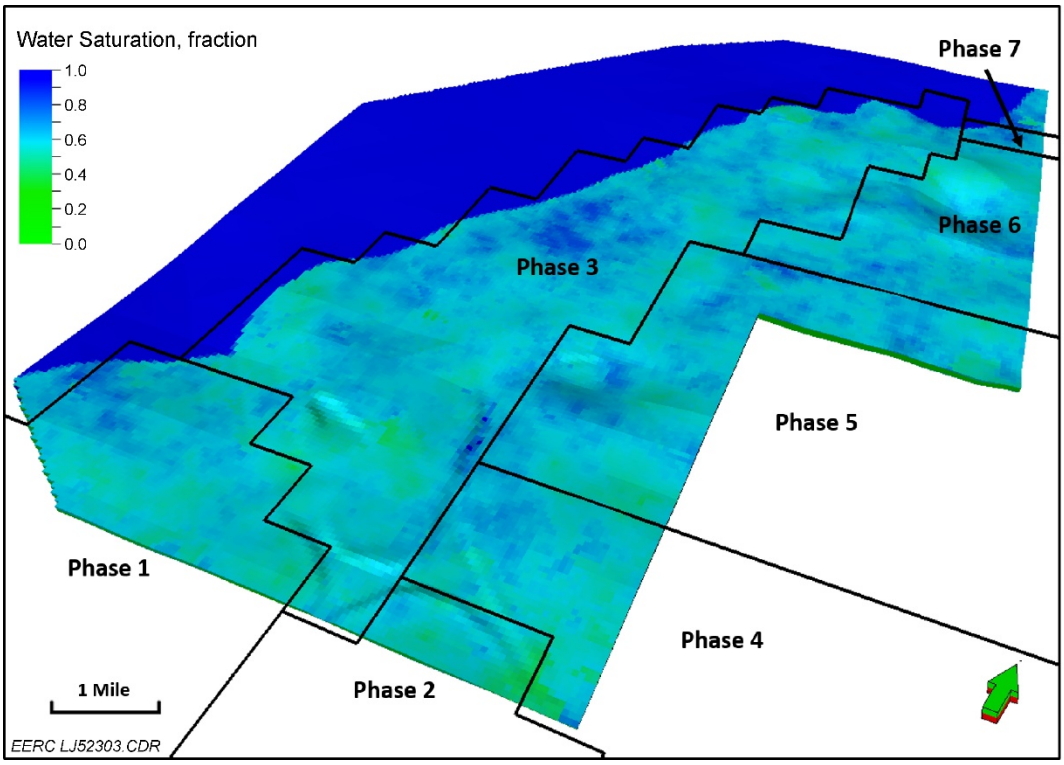

Figure 50. Schematic of the Bell Creek Phase 3 simulation area.

The Phase 3 area is located in the northwest region of the field, where there is considerable edge water (aquifer support) connecting to the pay zone (Figure 50). This has been confirmed by the behavior of production wells in this region. Figure 52 shows the early water breakthrough to wells along the western boundary of Phase 3 during the primary production stage. The rapid increase of water cut in these wells indicates good connectivity between the edge aquifer and the main reservoir.

EERC LJ52293.CDR

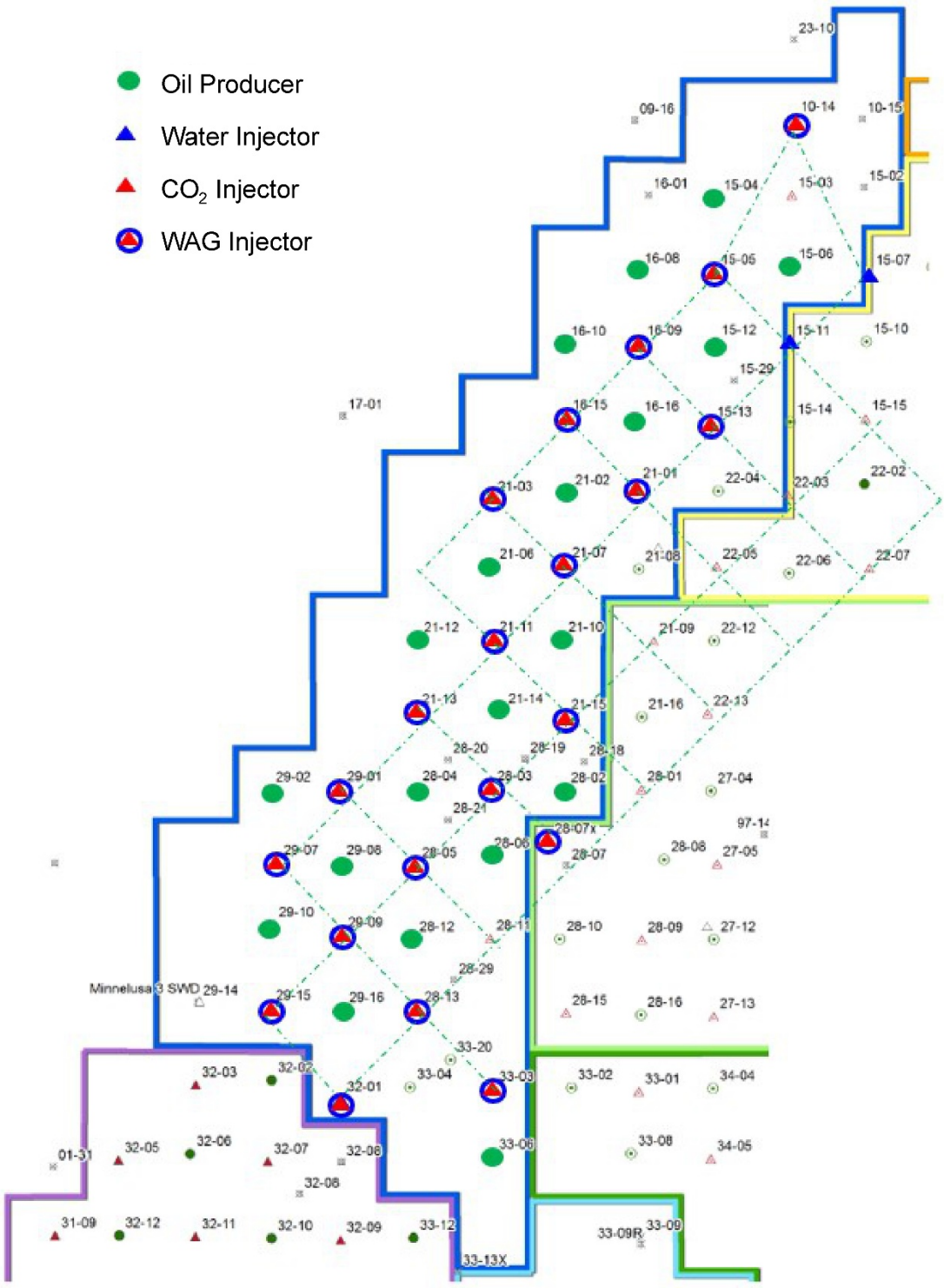

Figure 51. Well distribution in the Bell Creek Phase 3 and surrounding area.

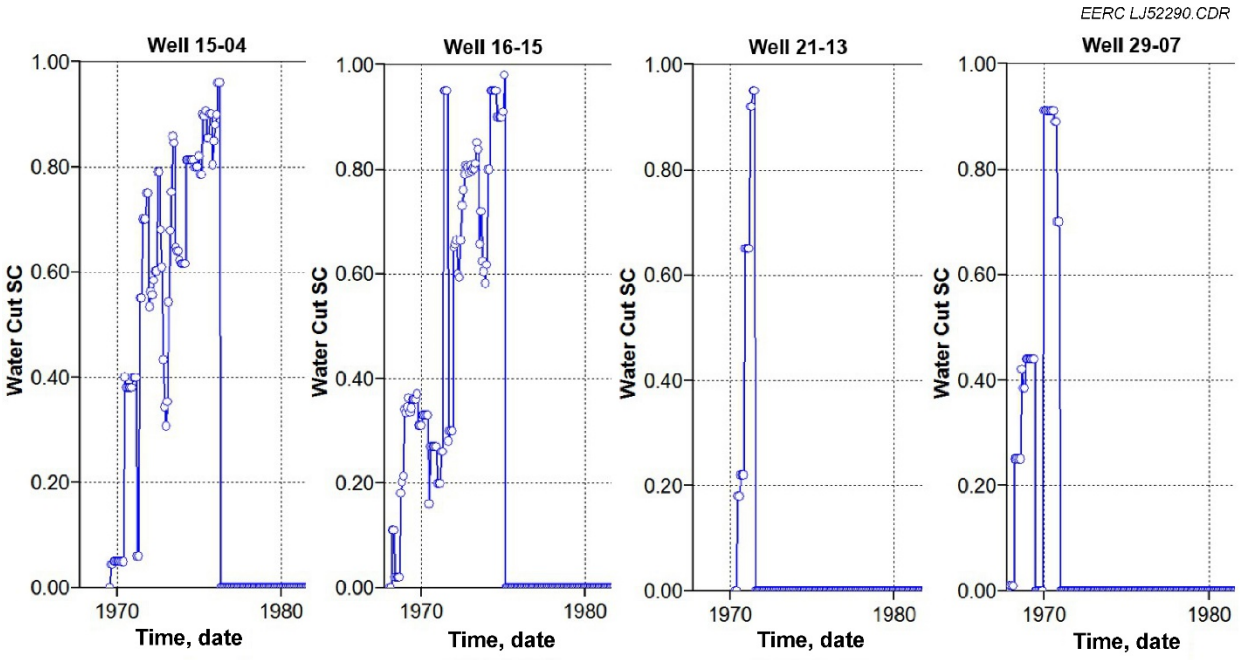

Figure 52. Early water breakthrough to wells along the western boundary of Phase 3.

The field has been divided into nine developmental phases, and the placement of these phase boundaries was informed by reservoir compartmentalization, as understood during earlier field development. There is some interphase fluid communication. The earliest CO_2 injection in Phase 3 began in December 2014 in Wells 28-05, 28-13, 29-15, and 33-03; however, CO_2 breakthrough was observed in Well 29-16 near the southern boundary of Phase 3 in June 2014 (approximately 6 months earlier than the beginning of injection in Phase 3). Phase 1 CO_2 injection began in May 2013, and it appears part of the injected CO_2 in Phase 1 migrated across the boundary and flowed into Well 29-16 in Phase 3.

There also appears to be some hydraulic communication between Phases 3 and 6. During previous waterflooding operations (early 1970s) in Phase 3, there were several water injection wells located along the boundary between these two phases, including Wells 15-07, 15-11, 15-14 and 22-03 (Figure 51). The water cut increased substantially in some of the nearby production wells in Phase 6, indicating water injected into Phase 3 was migrating into in Phase 6. Figure 53 shows the correlation between water injection in Phase 3 Well 15-14 and water cut in the nearby Phase 6 production Well 15-15. The water cut in Well 15-15 mimics the water injection in Well 15-14, and there were no water injection wells close to Well 15-15 in Phase 6 during the same period shown in the figure. Similar phenomena were observed in well pairs 15-07 and 15-08, and 15-10 and 15-11. Both of these pieces of evidence (early Phase 3 CO_2 breakthrough and Phase 6 water cut increase) suggest Phase 3 is at least partially open to Phases 1 and 6.

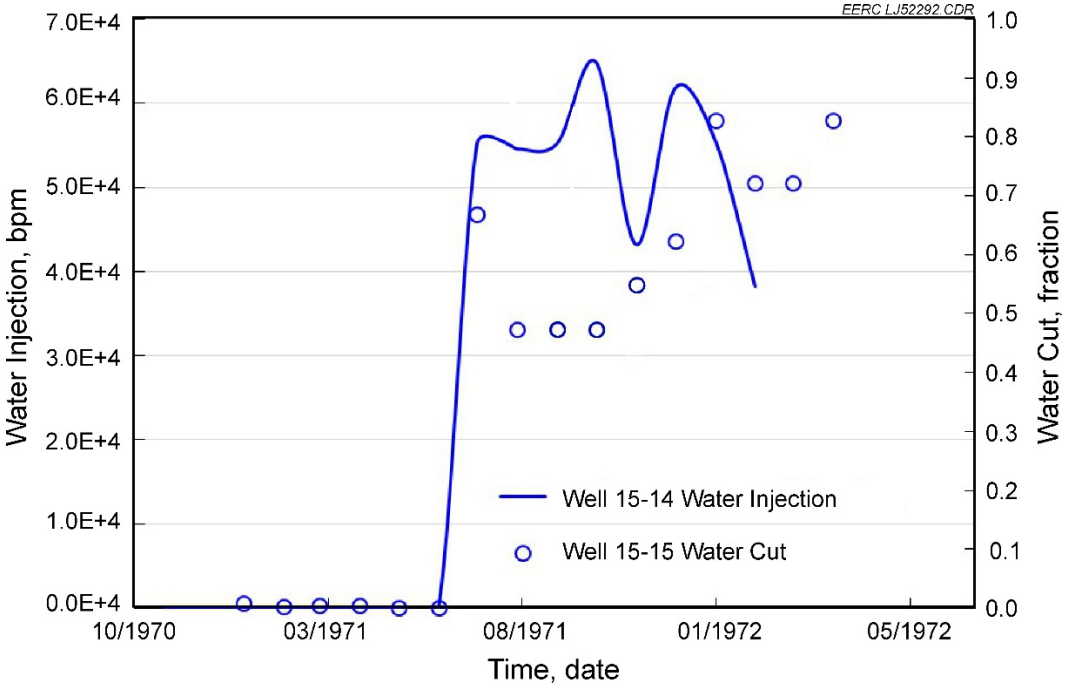

Figure 53. Correlation between water injection in Well 15-14 (Phase 3) and water cut in Well 15-15 (Phase 6).

The EERC has developed an effective methodology to conduct history matching of the production data in the Bell Creek Field (Braunberger and others, 2013; Liu and others, 2014; Bosshart and others, 2015). The production history has been divided into three clear stages: primary production, waterflooding, and CO_2 flooding. Ten dimensionless groups with clear physical meanings were used to analyze the simulation results and guide parameter tuning. Five sets of relative permeability curves (oil–water and liquid–gas) reported by Bosshart and others (2015) were used to represent the different lithologies in the reservoir. The EERC's high-performance computing cluster was used to conduct history matching, as the parallel simulation characteristics of the cluster greatly improved the simulation efficiency. Similar to the previously reported studies, liquid production and injection rates were used as primary constraints. Oil, water, and gas production rates, as well as water cut and GOR, were used in comparison to the simulated results. In the primary production stage, local water saturation was adjusted to match the water breakthrough time. In the waterflooding stage, high-permeability channels, permeability barriers, and out-boundary flow were adjusted. In the CO_2 flooding stage, relative permeability curves and endpoint saturations were tuned, as they related to the EOR fundamentals.

Figure 54 shows the historical data of liquid production rate, which was used as the primary control constraint. Figures 55–59 show a reasonably good match of the production history after systematic parameter tuning and production/injection analysis. Figure 60 shows the simulated average reservoir pressure for all production stages. Although there are no field data available for comparison, the shape and range of the curve is very similar to the ones observed in other phases (Braunberger and others, 2013; Liu and others, 2014; Bosshart and others, 2015). The results show that the simulation is able to capture the overall reservoir performance, but some local points cannot be matched exactly.

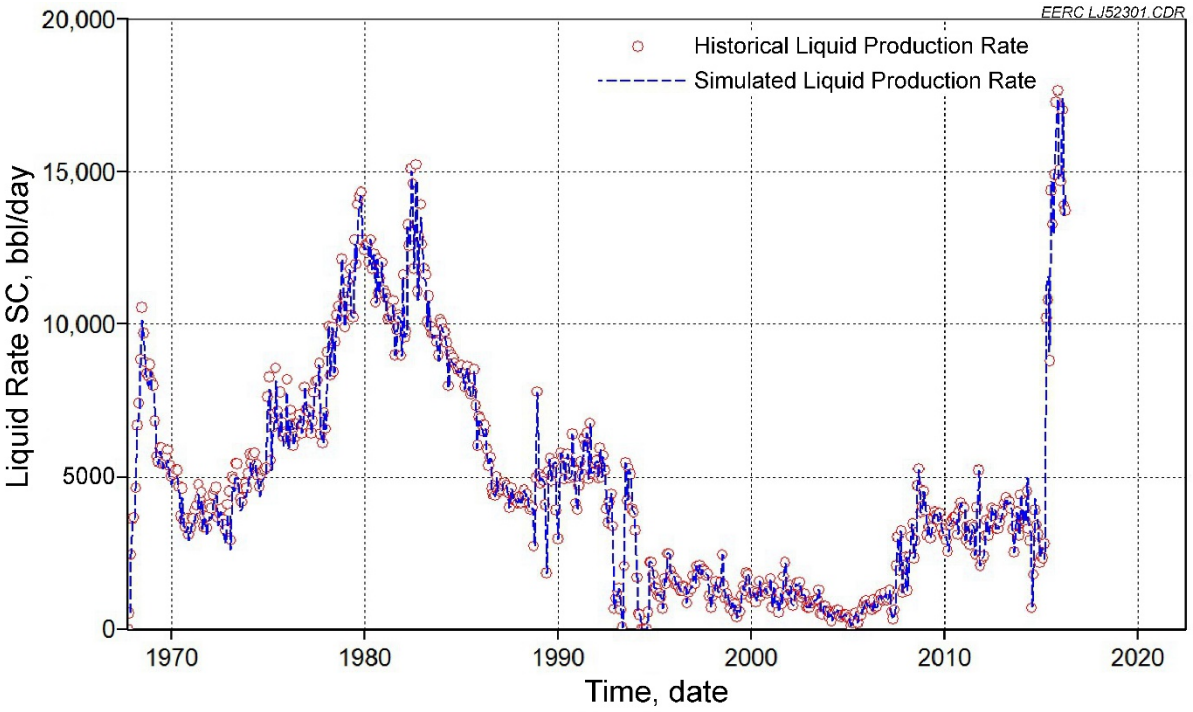

Figure 54. Bell Creek Phase 3 liquid production rate history match results.

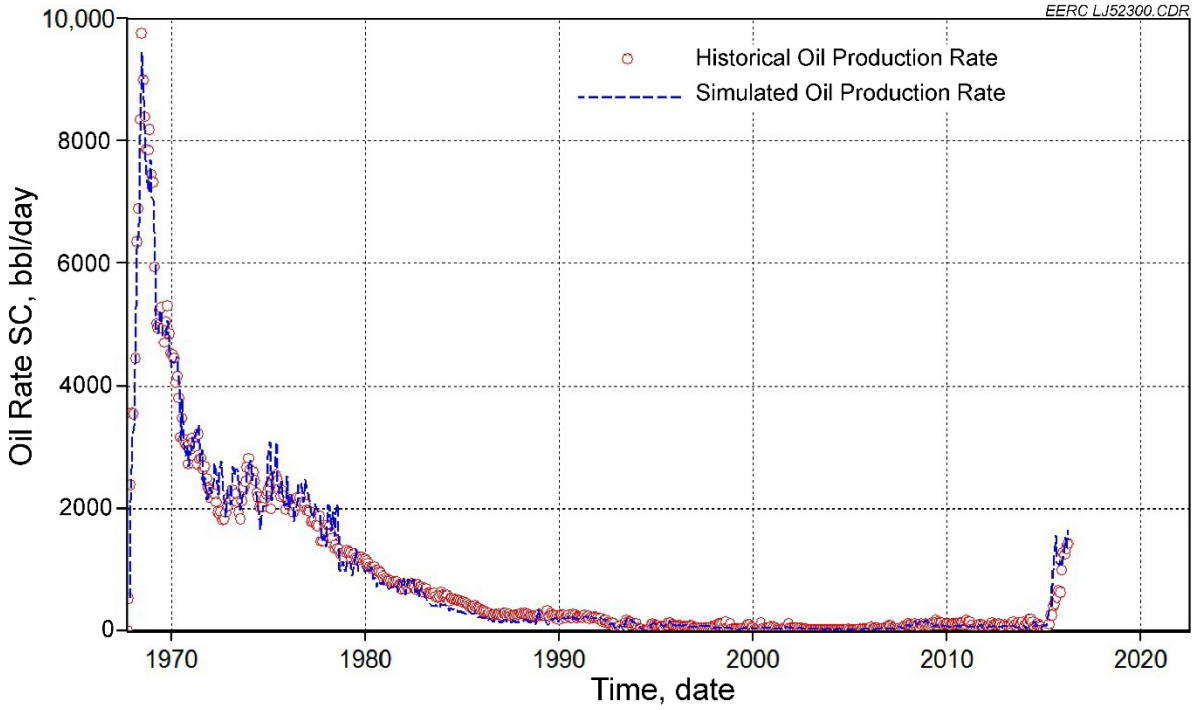

Figure 55. Bell Creek Phase 3 oil production rate history match results.

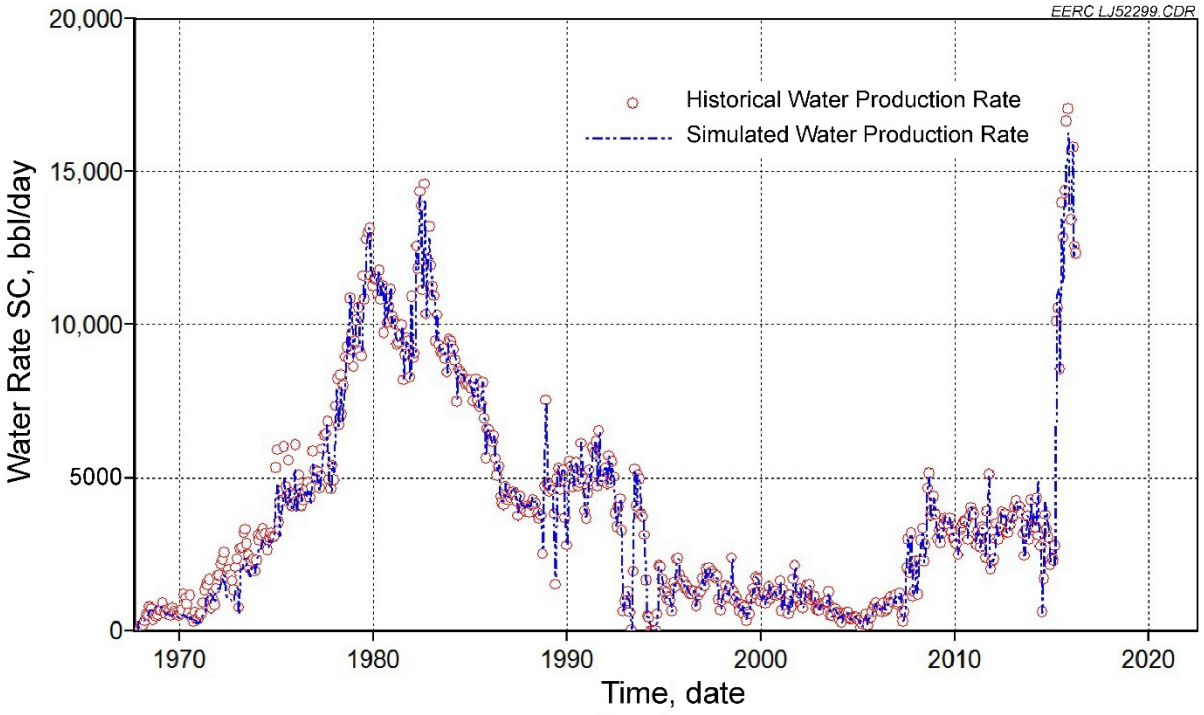

Figure 56. Bell Creek Phase 3 water production rate history match results.

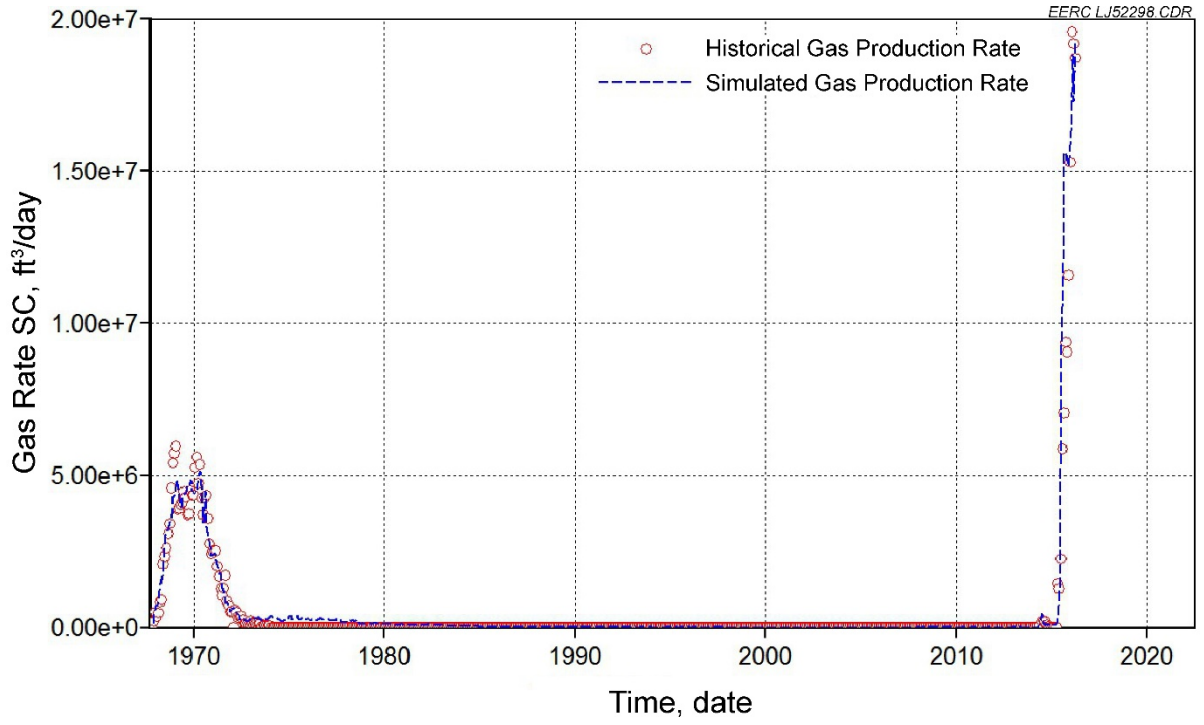

Figure 57. Bell Creek Phase 3 gas production rate history match results.

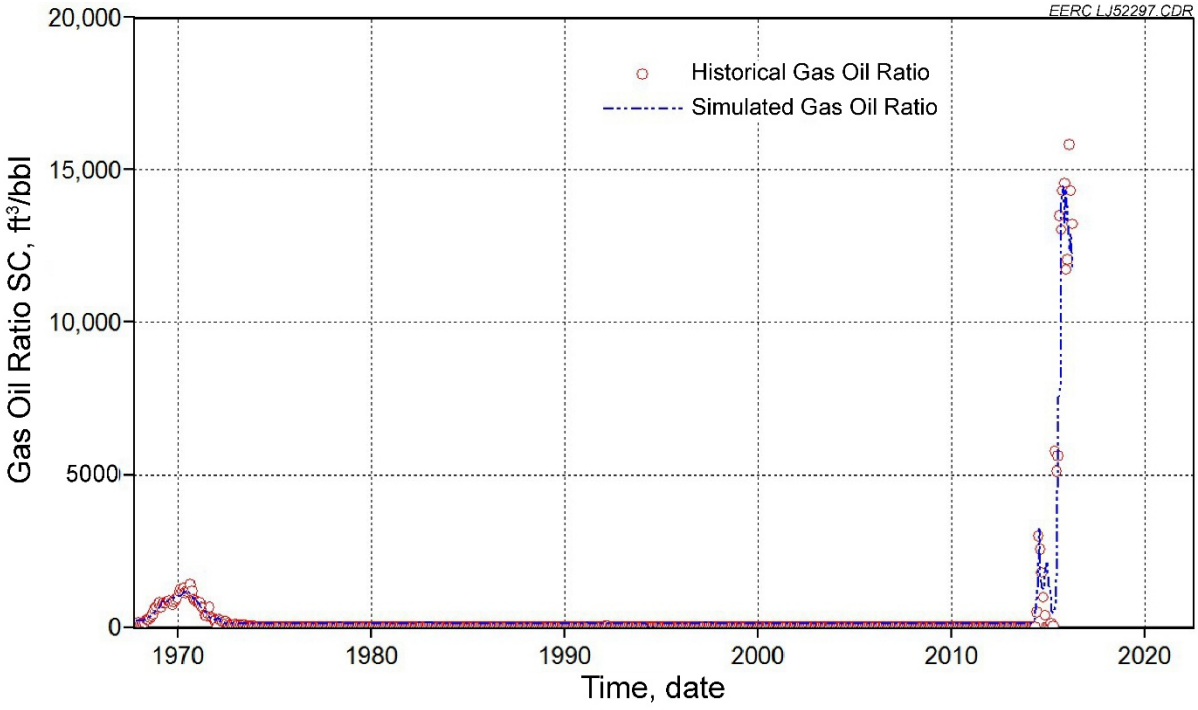

Figure 58. Bell Creek Phase 3 GOR history match results.

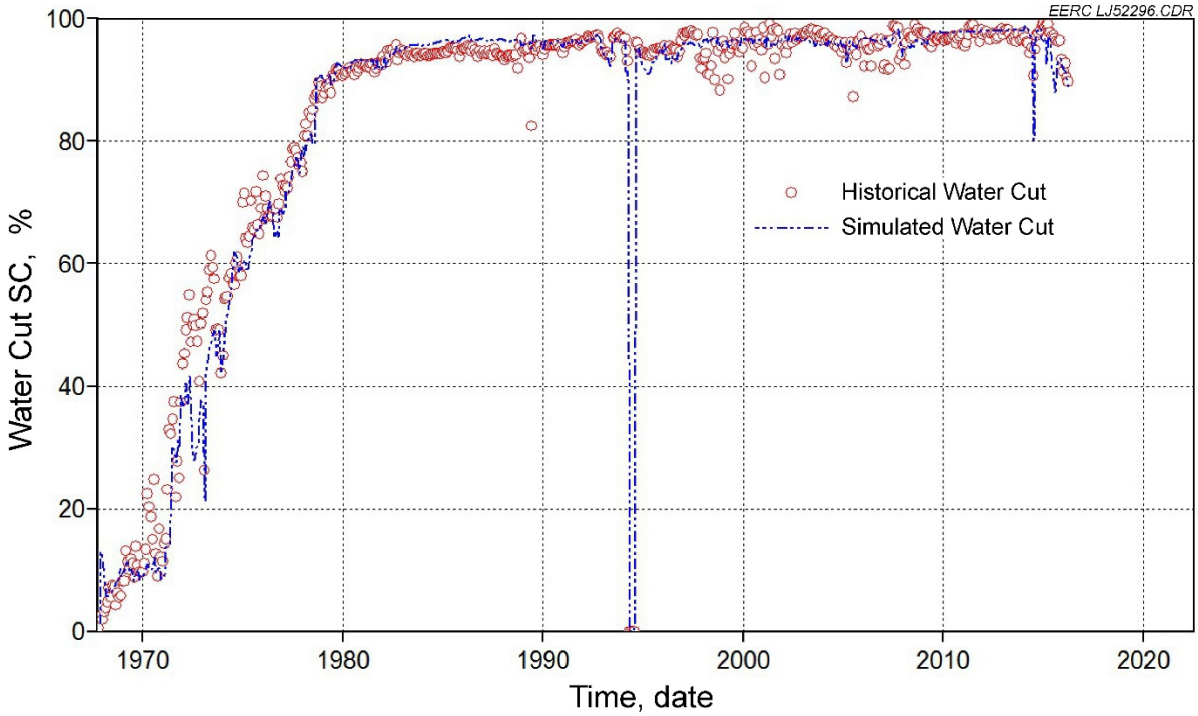

Figure 59. Bell Creek Phase 3 water cut history match results.

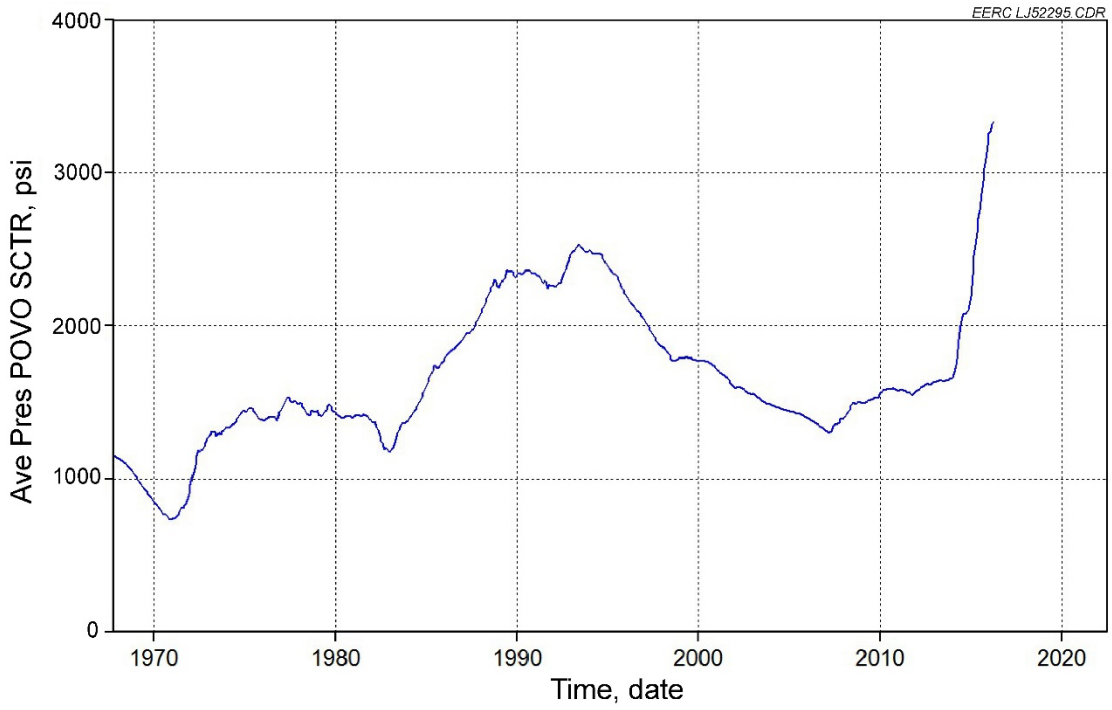

Figure 60. Bell Creek Phase 3 simulated average reservoir pressure.

Long-term CO_2 Migration Prediction

Referring back to Figure 22, over 5 million tonnes of CO_2 have been injected into the Muddy reservoir in Phases 1 through 4 as of April 2016. Approximately 60% of the injected gas has been stored in the formation. Larger injection and storage quantities are expected as the flooding operation continues and expands to the remaining phases. Monitoring and predicting the long-term migration potential of such a large quantity of CO_2 are important steps to assure the overall success of the project.

The monitoring and modeling technologies used for CO_2 EOR operations have been well proven by various CO_2 flooding projects (Grigg and Schechter, 1997; Christensen and others, 1998; Terrell and others, 2002; Gozalpour and others, 2005; Shelton and others, 2016). Parameters such as reservoir pressure, gas injection rate, fluid production rate, etc., may be adjusted to ensure operational safety during the EOR process (the wells are actively managed and controlled by operators). However, the situation is substantially different when the operational phase ends and the site closure/postclosure phase is initiated (wells are plugged and abandoned, and natural hydrodynamic conditions return). As this occurs, the CO_2 present in the subsurface has potential to migrate in an unintended manner (including the potential for CO_2 release at the surface), and there is currently no clear understanding of options which may be employed for corrective action. Accurate forecasting and prediction of the long-term fate of injected CO_2 seem the feasible courses of action in avoidance of such unintended consequences. To that end, efforts have been made in determining the long-term fate of CO_2 injected into the reservoir of Bell Creek Field. Prediction of CO_2 movement involves an evaluation of the potential for CO_2 to migrate through both natural and

man-made pathways (wellbores). This requires technical input from many disciplines, including geology and hydrogeology, geochemistry, geomechanics, reservoir simulation, geophysics, and wellbore technology (Weir and others, 1995; Lindeberg and Bergmo, 2003; Zhou and others, 2004; Martin and Ringrose, 2009; Green and Ennis-King, 2010).

Other studies have shown that CO_2 may be stored in deep geologic formations for a very long time (on the order of millions of years) in some situations, and this conclusion was supported by the existence of natural CO_2 reservoirs (Allis and others, 2001; White and others, 2005). Three trapping mechanisms were identified to retain supercritical CO_2 in deep burial formations: 1) stratigraphic trapping by low-permeability capping units; 2) hydrodynamic trapping by interaction between supercritical CO_2 and the reservoir fluid; and 3) mineral trapping where CO_2 within the system combines with other elements (such as Fe, Ca, Mg, etc.) in the precipitation of carbonate minerals (Bachu and others, 1994; Hitchon, 1996; Li and others, 2005; Moore and others, 2005; Martin and Ringrose, 2009). More recent studies have shown that hydrodynamic trapping plays an important role in long-term CO_2 migration and plume distribution in formations saturated with liquids (Lindeberg and Bergmo, 2003; Green and Ennis-King, 2010; Pau and others, 2010; Karsten and Nordbotten, 2011).

Assuming there was no leak in the cap rock and ignoring the slower progression of mineral trapping in the formation, a preliminary study was conducted to predict the CO_2 plume distribution in the Bell Creek Phase 3–7 area over a 5000-year period. Figure 61 shows a schematic of the simulation model, which was also clipped from the V2 geologic model. Because of the large areal coverage of the model, a cell size of 300 feet × 300 feet and average thickness of 1 foot was selected for dynamic simulation. The cell dimensions were 131 × 134 × 26, which enabled the simulation to be completed in a reasonable time.

Initial reservoir pressure and temperature conditions were 2000 psi and 108°F, respectively and represent abandonment conditions of the project that are effective in keeping CO_2 in the supercritical state. The reservoir properties, including porosity and permeability distributions, were upscaled to maintain the heterogeneity and enable a more accurate prediction. All wells were assumed to be abandoned (the simulation was designed to begin after the completion of injection operations).

CO_2 saturation was set at 90% in certain blocks to represent an injected mass of CO_2 and no CO_2 saturation was given to the remaining cells. Figure 62 shows a case assuming 8 million tonnes of CO_2 in the middle of the field. Even when there is no pressure differential induced within the reservoir (e.g., no injection or production), CO_2 will still migrate through porous media as a result of the effects of buoyancy between CO_2 and the native formation fluids. In the case of Bell Creek, structural dip is to the west/northwest (dip angle of 1°–2°), so we would expect buoyancy-driven migration to occur in the opposite direction. Figure 63 shows the CO_2 migration process and plume development over a simulated 5000-year interval. The shape of the plume indicates that the migration process is slow. After 2000 years, the CO_2 has still not reached the eastern boundary of the field. The average migration velocity is less than 3 ft/year. After 5000 years of migration, the CO_2 plume appears to have reached the eastern field boundary, as indicated in the last image in Figure 63; however, the majority of the CO_2 is still contained well within the field bounds. It is

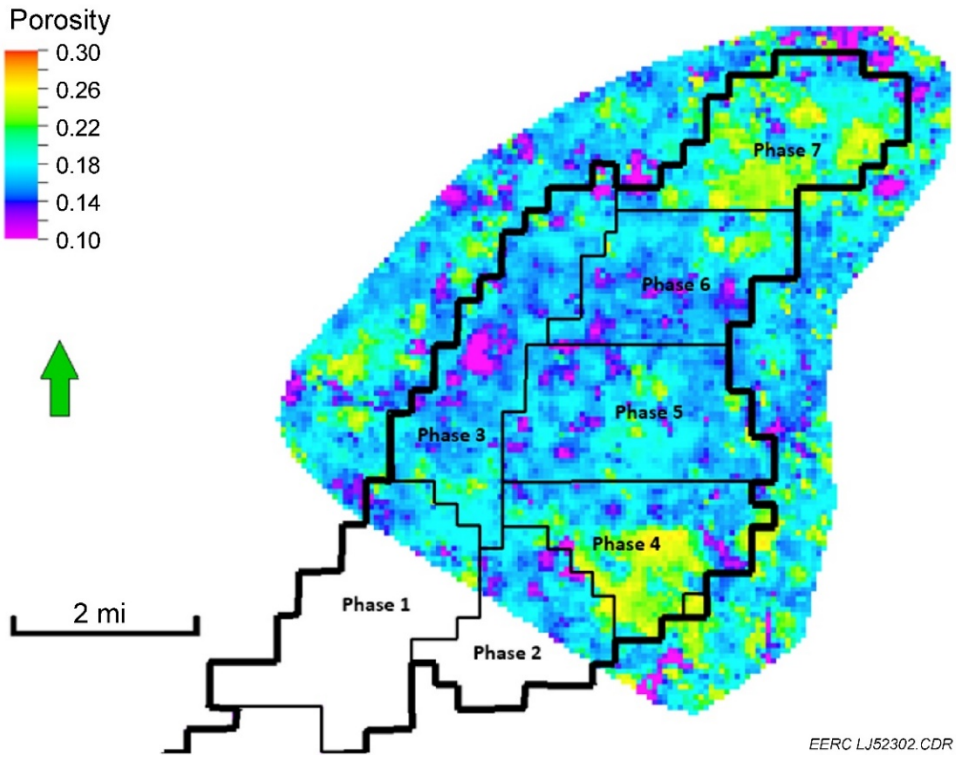

Figure 61. Schematic of the Bell Creek Phase 3–7 simulation model with Phase boundaries overlain.

clear that reservoir heterogeneity plays a rather large role in determining the shape of the plume front because of the small driving force (CO_2 tends to migrate through the reservoir in a channelized manner). Figures 64 and 65 show a different simulation case with 15 million tonnes of CO_2 in the reservoir where the CO_2 was located in the western region of the model. After 5000 years, the CO_2 had nearly reached the eastern field boundary. The maximum migration velocity was also found to be about 3 feet/year.

Based upon these observations, CO_2 may be stored in the Bell Creek reservoir for thousands of years without significant migration beyond the field boundaries. However, as mentioned above, these simulations were only designed to investigate the long-term migration potential due to fluid density differences. Other factors not taken into account which would likely further inhibit CO_2 migration would include 1) CO_2 mineralization (removal of dissolved CO_2 from the system through conversion to carbonate minerals); 2) the presence of an updip pinchout of reservoir-quality sandstone (which has been interpreted as the underlying reason as to why hydrocarbons were trapped in the Bell Creek Field area in the first place); and 3) even if reservoir-quality sandstone persisted uninterrupted to Muddy Formation outcrops in the northwestern region of the Black Hills Uplift, this area serves as an aquifer recharge zone and the hydrodynamic flow is oriented in the opposite direction and would oppose CO_2 migration. In summary, this particular investigation suggests the updip migration potential of CO_2 injected within the Bell Creek Field is limited, and the likelihood of CO_2 ever reaching outcrops near the Black Hills Uplift and being released to the atmosphere appears negligible.

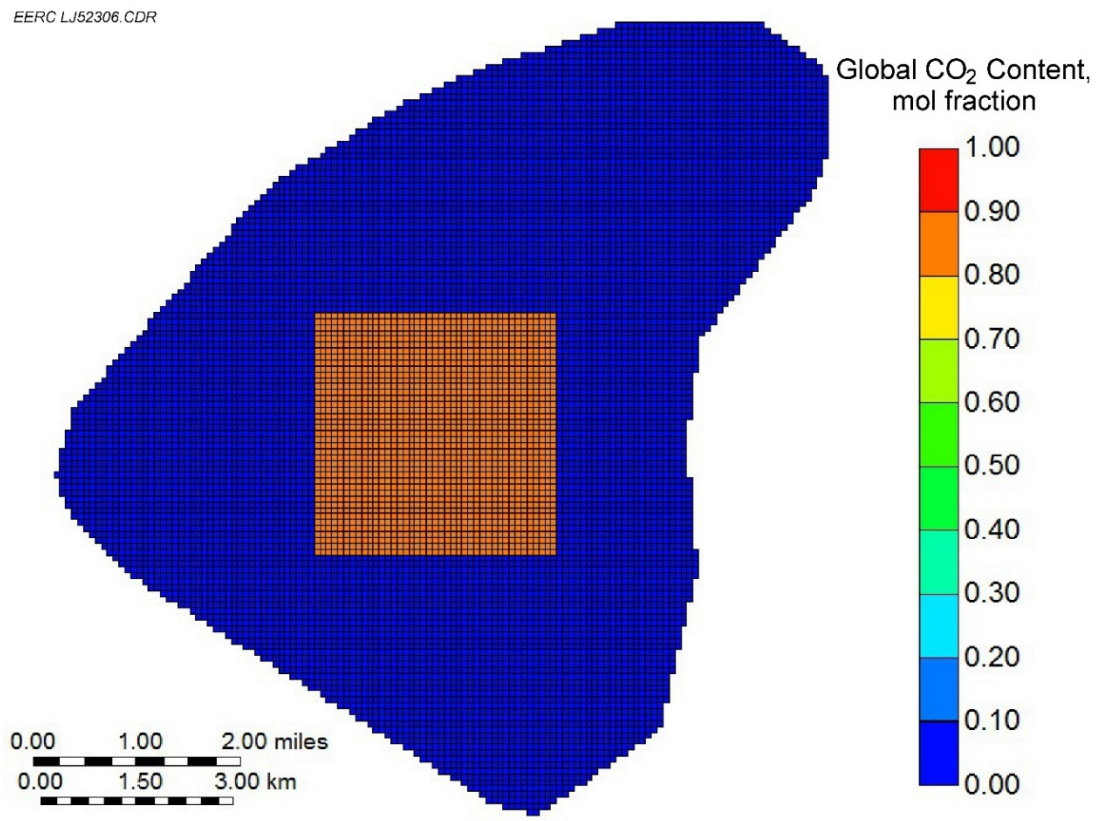

Figure 62. Schematic of a long-term CO_2 migration simulation model (8-million-tonne case).

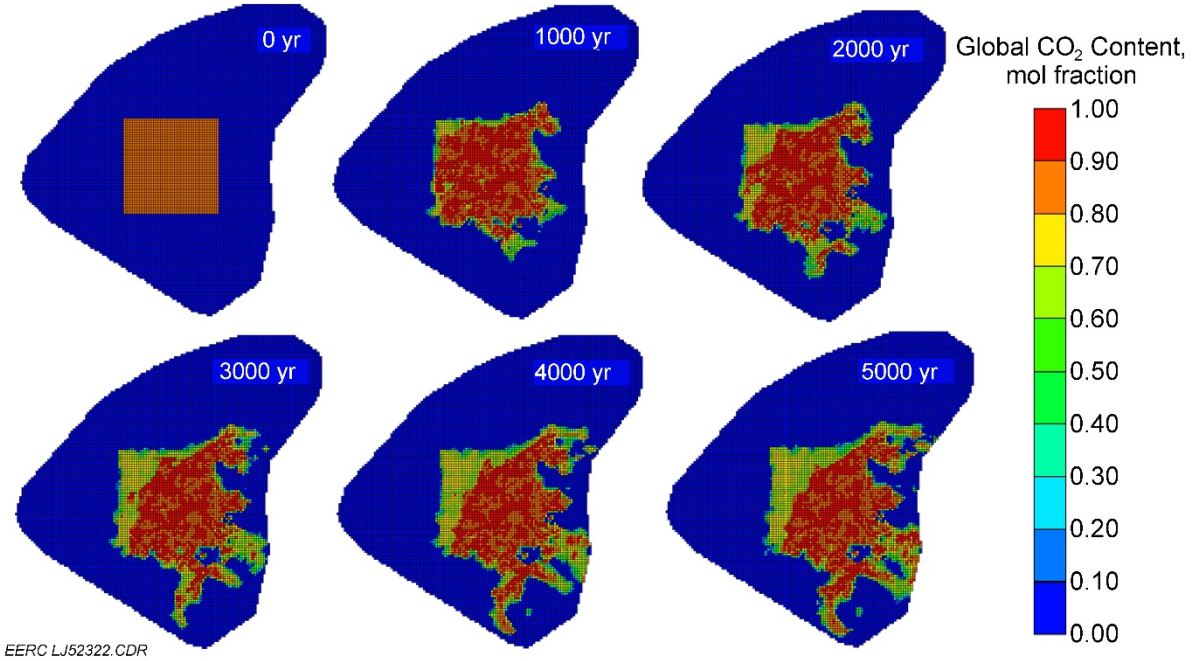

Figure 63. CO_2 plume progress over the course of 5000 years (8-million-tonne case).

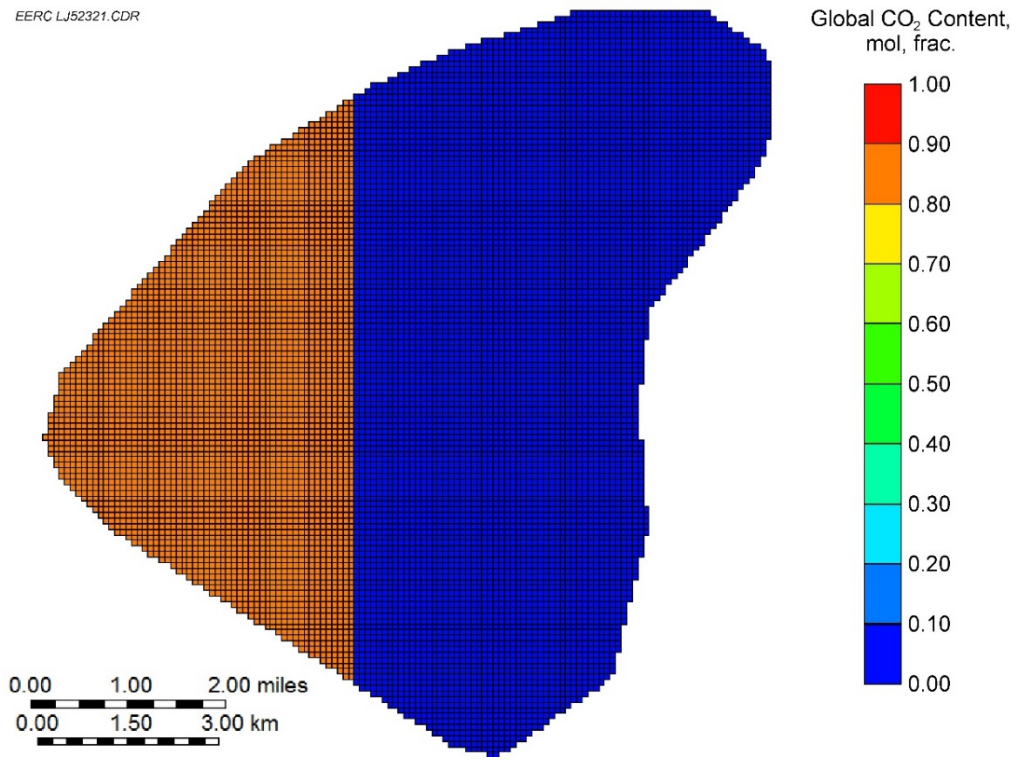

Figure 64. Schematic of a long-term CO_2 migration simulation model (15-million-tonne case).

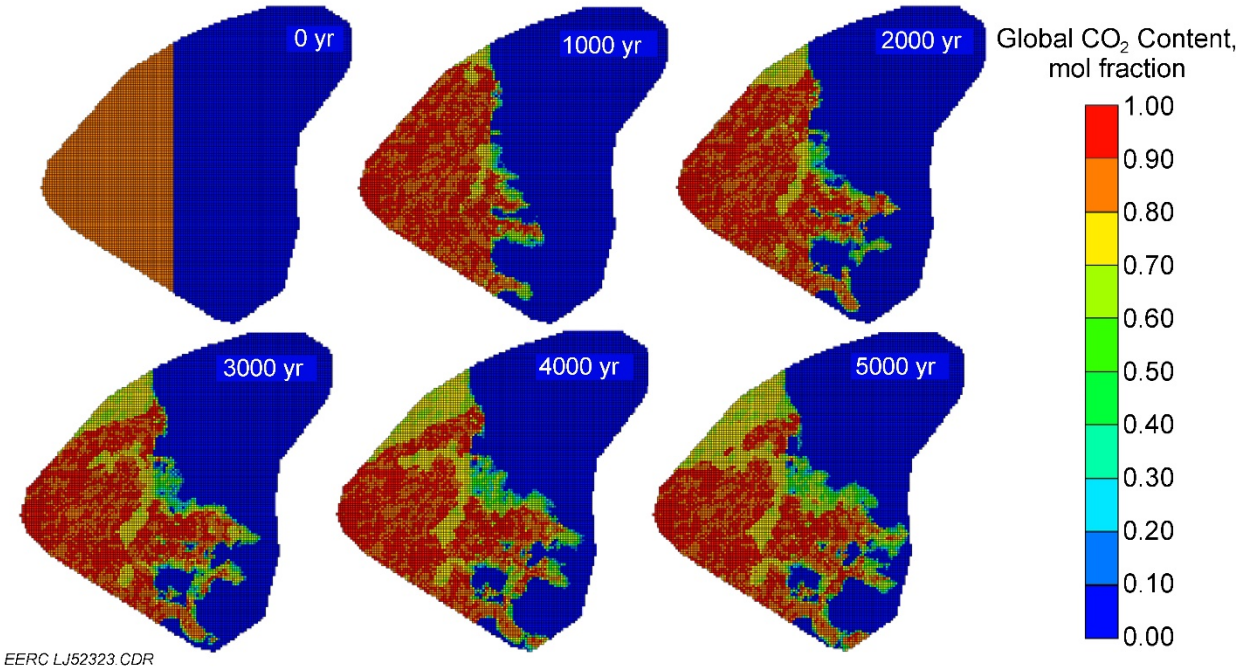

Figure 65. CO_2 plume progress over the course of 5000 years (15-million-tonne case).

Summary and Conclusions

Bell Creek Field modeling, reservoir engineering, and simulation activities from August 2015 to August 2016 have been discussed, including updates to the PNL program; recently acquired seismic data and its interpretation; efforts pertaining to the V3 geologic model; completion of regional- and basin-scale geologic models; determination of the effects of impurities on bulk gas properties and the effects of recycled gas injection on EOR and storage performance; determination of the effects of different geologic conditions and pressure constraints on EOR performance; history-matching efforts on a Phase 3 simulation model, and the execution of long-term (thousands of years) simulations to examine the migration potential and long-term fate of injected CO_2. The results of these efforts will assist with risk assessment, risk management, and MVA plan implementation (and possibly adaptation/modification) necessary for safe and secure, long-term CO_2 storage. Key results and conclusions from this report include the following:

- Twelve new baseline PNLs and five repeat PNLs were acquired. A total of 45 wells with PNLs, of which 20 contain at least one repeat PNL, have provided confidence in updating the local stratigraphic column and unit thicknesses in the area of investigation from reservoir to ground surface. Repeat PNLs in injection and production wells have identified the fluid saturation changes (CO_2, water, and oil). The results of these logging activities have been integrated into the ongoing modeling and simulation activities.

- Newly acquired seismic data have enabled further geologic interpretation and reservoir characterization within the field. Seismic analyses have enabled the creation of time-lapse images of CO_2 distribution in the Muddy Formation reservoir.

- The incorporation of new 3-D seismic data has provided further validation of the new geologic interpretation that supports a shoreline trending from the northwest to the southeast during deposition. This understanding, and further interpretations, are being integrated within the V3 model construction efforts.

- Permeability barriers noted and discussed in previous studies (Bosshart and others, 2015) continue to be detected in time-lapse images of seismic difference volumes. The morphology of these features, as seen in baseline (3-D) and repeat/monitor (4-D) investigations, substantiate the new interpretation of the erosional/depositional processes through which they were created. The main north–south permeability barrier noted along the eastern margin of Phase 3 is due to fluvial erosion of regressive sands during subaerial exposure before transgression and infill with fine-grained deposits. The main permeability barrier along the northern boundary of Phases 1 and 2 is attributed to lagoonal deposits on the landward (northern) side of an east–west trending local barrier bar trending through the center of these phases.

- As noted in Bosshart and others (2015), a limited area of hydraulic connectivity appears to exist between the Phase 1 and 2 areas (across the north–south incised channel permeability barrier) in 4-D seismic analyses. These analyses also suggest the presence of hydraulic connectivity between the Phase 1 and 3 areas.

- Current V3 modeling efforts are focused on integrating newly acquired seismic data to create more accurate facies and petrophysical property distributions for the Phase 3–7 areas. A full-field V3 model will be complete after this integration.

- Regional- and basin-scale models were constructed to help determine the potential long-term fate of injected CO_2. These models have not yet been subjected to simulation efforts.

- The near-surface model that was previously under construction has been completed. It will be used to determine (potential) migration patterns of CO_2 in shallow aquifers. To reiterate, there is no evidence of unintended CO_2 saturation in shallow aquifer units nor any reason to believe this will ever be the case. This investigation aims to inform where MVA efforts may be best implemented for rapid detection and response.

- Impurities in Bell Creek produced gas samples were analyzed. Results showed CH_4 was the main impurity which varied from 1 to 4 mol%. The quantity of impurities appears to be decreasing as the CO_2 flood continues.

- A series of MMP measurements were conducted for CH_4–CO_2 mixtures under reservoir conditions using the VIT method. Results showed that the VIT method of determining MMP produced similar results to the slim-tube method, but the testing was faster and more cost-effective. The measured MMPs of the Bell Creek oil increased from 1403 to 4085 psi as the CH_4 mol% increased from 0% to 100% in the solvent phase.

- Three simulation models of different sizes and a PVT model with nine pseudo components were developed to investigate the impact of impurities on recycled gas EOR and storage performance. Results indicated that the previously used PVT model with seven pseudo components may continue to be used with the history-matched simulation models to capture the effects of impurities on EOR performance in the field. A range of impurities can be tolerated in the recycled gas injection without impairing the EOR efficiency or CO_2 storage performance.

- A dynamic simulation model was built for the Phase 3 area and a reasonable history match was achieved.

- A simulation model was developed to span the area of Phases 3–7 to simulate long-term (thousands of years) CO_2 migration behavior (excluding the effects of mineral trapping, the pinchout of reservoir-quality sand updip of the field, and natural hydrodynamics operating in the direction opposite to the CO_2 migration vector). Two case studies simulated for 5000 years showed that CO_2 migration, under the effects of buoyancy only, would be a slow process in the Bell Creek Field (around 3 feet/year to the east/southeast). Migration would likely be much slower with the added effects discussed above. This indicates that injected CO_2 is likely to remain contained within the field for thousands of years.

Limitations

Geologic Model of the Reservoir

Simulation results presented in this update are based on the V2 geologic model. While these results are meaningful and useful, they do not contain some important learnings presented in Bosshart and others (2015) and additional learnings from data acquired over the past year. The V3 model (currently in development) will incorporate all available data to increase the accuracy of the resulting facies and corresponding petrophysical property distributions. Simulation of the V3 model should yield more accurate predictive results with a reduction in uncertainty.

Regional- and Basin-Scale Models

The large extents of the regional- and basin-scale models require large cell sizes to keep the cell count at a reasonable number for simulation. The large cell size reduced the ability to capture realistic geologic heterogeneity in the Muddy Formation. Because of this, the lateral extrapolation of the Bell Creek sand interval in the models may not necessarily be representative of the formation.

Near-Surface Model

Because of the shallow nature of the Fox Hills and Hell Creek Formations within the model extent, most well logs lack readings for this interval. The most consistent log available across the model area is the ILD collected during PNL acquisition. Few wells within the area had other available logs (such as GR), and of the wells with other logs available very few had corresponding ILDs. This made more detailed facies modeling (beyond identification of sand-rich [aquifer] and sand-deficient [aquitard] intervals) very challenging.

Additionally, the lack of locally derived porosity and permeability measurements provided a challenge in modeling petrophysical properties. A sparse assortment of porosity and permeability data was found for equivalent units in the Williston Basin and used as the basis for property distributions. This (forced) assumption introduced greater uncertainty into the accuracy of the model; however, it is still believed the model will provide benefit in understanding the (potential) effects of unintended CO_2 saturation in the shallow aquifer units.

ONGOING AND FUTURE WORK

Reference Model

The Bell Creek reference model provides a consolidated data source for future geologic modeling efforts. Created and intended as such, the model will be updated continually with various pertinent data sets as they become available in the future.

V3 Geologic Model

Seismic coverage is now available for nearly all of the Bell Creek Field. Results from PNLs, baseline seismic surveys (from 2012 and 2015), and repeat/monitor seismic surveys (from 2014 and 2015) are being investigated to enhance structural, lithological, and petrophysical interpretations. Petrophysical properties will be more accurately determined and distributed within the full-field V3 model based on this enhanced resolution. Identification of structural features will reduce uncertainty in thickness. Seismic-assisted lithologic determination will allow for increased accuracy in predicting the flow of CO_2 in the reservoir. Additionally, the 4-D seismic data analyses provide a tool for identifying out-of-zone CO_2 migration (along wellbores or through vertical fractures).

Extended seismic data in the field have strengthened and expanded the new understanding of the deposition of the Muddy Formation at Bell Creek. V3 model facies distributions are currently under way, integrating facies modeling efforts discussed in Bosshart and others (2015) within areas covered by the most recently acquired seismic data. These facies distributions are being conducted using advanced geostatistical methods, including MPS, to enhance geologic understanding throughout the field and expanded area of review. A petrophysical model will be conditioned to the resulting facies model using variogram-based geostatistical methods. Petrophysical properties are being calculated, compiled, and binned (by new facies interpretations) using results from legacy core analyses, as well as log-derived porosity and permeability characteristics (from both PNLs and legacy well logs). Other key rock properties, such as fluid saturations, will be populated based on field tests and PNLs (to be fine-tuned later through history matching). An upscaling process will follow the conclusion of property modeling to prepare an appropriate simulation model.

History Matching of CO_2 Flooding

CO_2 flooding has been initiated in the Phase 1 through 4 areas of Bell Creek Field since May 2013. Simulation models have been developed and used in the history matching of injection and production characteristics of the Phase 1, 2, and 3 areas to better understand the reservoir characteristics, production dynamics, and CO_2 EOR and storage performance. New simulation models will be built and used in future history-matching efforts of the other phases to follow the field's development.

Predictive Simulations

History matching has been done for the Phase 3 area with all three production stages (primary, secondary, and now tertiary/EOR stages), and predictive simulations are ongoing for both WAG and CGI operations. In this study, recycled gas EOR in quarter five-spot models with various geologic settings were investigated. Results showed that chosen operational pressure constraints play a significant role in the EOR process in all different geologic conditions. Therefore, different injection-producing pressure combinations will be simulated in the new rounds of simulation work.

Relative Permeability Hysteresis Measurement and Incorporation

Three sets of oil–water and five sets of gas–liquid relative permeability curves have been experimentally measured from core samples taken from two wells (BC 22-03 and 05-06 OW) by Core Laboratories. These curves greatly increased the history-matching efficiency and enhanced our understanding of the rock–fluid properties. However, gas–liquid hysteresis curves were not measured in the previous experiments. Since hysteresis is irreversible (or path-dependent) in the CO_2 flooding process, it closely relates to the trapping of CO_2 in the pore space (Juanes and others, 2006; Spiteri and others, 2008). Core and fluid samples have been prepared in the EERC laboratories to measure the gas–liquid hysteresis curves, which will then be incorporated in the simulation models to make predictive simulations more accurate.

Integrating Seismic Data into Simulation Models

Seismic surveys have been acquired to serve several purposes for characterization and MVA activities of the Bell Creek project. These data have aided in 1) the structural interpretation of the field, 2) identifying and mapping the distribution of lateral heterogeneity and flow boundaries within the field, and 3) the ability to track the distribution and movement of CO_2 in the reservoir (Burnison and others, 2014). Reservoir simulation and history matching of production rates and pressure may produce nonunique solutions for reservoir descriptions. Uncertainty can be significant in some instances. Seismic surveys provide additional information to reduce such uncertainty and make the models more reliable (Terrell and others, 2002; Gosselin and others, 2003). Therefore, data extracted from seismic surveys can be used to improve the simulation models, optimize production and improve estimates of ultimate oil recovery and CO_2 storage.

REFERENCES

Afonja, G., Hughes, R.G., Nagineni, V., and Jin, L., 2012, Simulation study for optimizing injected surfactant volume in a miscible carbon dioxide flood, *in* Proceedings of SPETT Energy Conference and Exhibition, SPE 158220: Port-of-Spain, Trinidad, June 11–13.

Ahmad, W., Vakili-Nezhaad, G., Al-Bemani, A.S., and Al-Wahaibi, Y., 2016, Uniqueness, repeatability analysis and comparative evaluation of experimentally determined MMPs: Journal of Petroleum Science and Engineering, v. 147, November.

Ahmed, T., 2007, Equations of state and PVT analysis—applications for improved reservoir modeling: Houston, Texas, Gulf Publishing Company.

Al-Hussainy, R., Ramey Jr., H.J., and Crawford, P.B., 1966, The flow of real gases through porous media: Journal of Petroleum Technology, v. 18, no. 05.

Allis, R., Chidsey, T., Gwynn, W., Morgan, C., White, S., Adams, M., and Moore, J., 2001, Natural CO_2 reservoirs on the Colorado Plateau and southern Rocky Mountains—candidates for CO_2 sequestration, *in* Proceedings of the First National Conference on Carbon Sequestration.

Aryana, S.A., Barclay, C., and Liu, S., 2014, North Cross Devonian unit—a mature continuous CO_2 flood beyond 200% HCPV injection, *in* Proceedings of the SPE Annual Technical Conference and Exhibition, SPE 170653: Amsterdam, the Netherlands, October.

Ayirala, S.C., and Rao, D.N., 2011, Comparative evaluation of a new gas/oil miscibility-determination technique: Journal of Canadian Petroleum Technology, v. 50, no. 9/10.

Bachu, S., Gunter, W.D., and Perkins, E.H., 1994, Aquifer disposal of CO_2—hydrodynamic and mineral trapping: Energy Conversion and Management, v. 35, no. 4.

Bosshart, N.W., Jin, L., Dotzenrod, N.W., Burnison, S.A., Ge, J., He, J., Burton-Kelly, M.E., Ayash, S.C., Gorecki, C.D., Hamling, J.A., Steadman, E.N., and Harju, J.A., 2015, Bell Creek test site – simulation report: Plains CO_2 Reduction (PCOR) Partnership Phase III Task 9 Deliverable D66 Update 5 for U.S. Department of Energy National Energy Technology Laboratory Cooperative Agreement No. DE-FC26-05NT42592, August.

Braunberger, J.R., Pu, H., Gorecki, C.D., Bailey, T.P., Bremer, J.M., Peck, W.D., Gao, P., Ayash, S.C., Liu, G., Hamling, J.A., Steadman, E.N., and Harju, J.A., 2013, Bell Creek test site – simulation report: Plains CO_2 Reduction (PCOR) Partnership Phase III Task 9 Deliverable D66 Update 2 for U.S. Department of Energy National Energy Technology Laboratory Cooperative Agreement No. DE-FC26-05NT42592, August.

Burnison, S.A., Burton-Kelly, M.E., Zhang, X., Gorecki, C.D., Steadman, E.N., and Harju, J.A., 2014, Bell Creek test site – 3-D seismic and characterization report: Plains CO_2 Reduction (PCOR) Partnership Phase III Task 4 Deliverable D96 for U.S. Department of Energy National Technology Laboratory Cooperative Agreement No. DE-FC26-05NT42592, March.

Chen, S., Li, H., Yang, D., and Tontiwachwuthikul, P., 2010, Optimal parametric design for water-alternating-gas (WAG) process in a CO_2-miscible flooding reservoir: Journal of Canadian Petroleum Technology, v. 49, no. 10.

Christensen, J.R., Stenby, E.H., and Skauge, A., 1998, Review of WAG field experience, *in* Proceedings of the international petroleum conference and exhibition of Mexico, SPE-39883: Villahermosa, Mexico, March 3–5.

Dong, M., Huang, S., Dyer, S.B., and Mourits, F., 2001, A comparison of CO_2 minimum miscibility pressure determinations for Weyburn crude oil: Journal of Petroleum Science and Engineering, v. 31, no. 1.

Elsharkawy, A.M., Poettmann, F.H., and Christiansen, R.L., 1996, Measuring CO_2 minimum miscibility pressures—slim-tube or rising-bubble method? Energy & Fuels, v. 10.

Farnham, F.E., and Haddenhorst, F.A., 1972, Four and one-half years—discovery to unitized operation of the major, multi-reservoir Bell Creek Field: Society of Petroleum Engineers, doi:10.2118/3834-MS.

Fatemi, S.M., and Sohrabi, M., 2013, Recovery mechanisms and relative permeability for gas/oil systems at near-miscible conditions—effects of immobile water saturation, wettability, hysteresis, and permeability: Energy & Fuels, v. 27.

Gardner, J.W., and Ypma, J.G.J., 1984, An investigation of phase behavior-macroscopic bypassing interaction in CO_2 flooding: Society of Petroleum Engineers Journal, v. 24, no. 05.

Gorecki, C.D., 2016, Bell Creek CO_2 storage reporting – April 2016: Prepared for the U.S. Department of Energy National Energy Technology Laboratory, Grand Forks, North Dakota, Energy & Environmental Research Center.

Gorecki, C., Hamling, J., Klapperich, R., Steadman, E., and Harju, J., 2012, Integrating CO_2 EOR and CO_2 storage in the Bell Creek oil field: Presented at Carbon Management Technology Conference, Paper 151476.

Gosselin, O., Aanonsen, S.I., Aavatsmark, I., Cominelli, A., Gonard, R., Kolasinski, M., Ferdinandi, F., Kovacic, L., and Neylon, K., 2003, History matching using time-lapse seismic (HUTS), *in* Proceedings of the SPE Annual Technical Conference and Exhibition, SPE-84464: Denver, Colorado, October 5–8.

Gozalpour, F., Ren, S.R., and Tohidi, B., 2005, CO_2 EOR and storage in oil reservoirs: Oil & Gas Science and Technology—Rev. IFP, v. 60, no. 3.

Green, C.P., and Ennis-King, J., 2010, Effect of vertical heterogeneity on long-term migration of CO_2 in saline formations: Transport in Porous Media, v. 82, no. 1.

Grigg, R.B., and Schechter, D.S., 1997, State of the industry in CO_2 floods, *in* Proceedings of the SPE Annual Technical Conference and Exhibition, SPE-38849: San Antonio, Texas, October 5–8.

Guo, B., and Ghalambor, A., 2005, Natural gas engineering handbook: Gulf Publishing Company, Houston, Texas.

Hamling, J.A., Gorecki, C.D., Klapperich, R.J., Saini, D., and Steadman, E.N., 2013, Overview of the Bell Creek combined CO_2 storage and CO_2 enhanced oil recovery project: Energy Procedia, v. 37, p. 6402–6411.

Hamouda, A.A., and Tabrizy, V.A., 2013, The effect of light gas on miscible CO_2 flooding to enhance oil recovery from sandstone and chalk reservoirs. Journal of Petroleum Science and Engineering, v. 108.

Hawthorne, S.B., Miller, D.J., Jin, L., and Gorecki, C.D., 2016, Rapid and simple capillary-rise/vanishing interfacial tension method to determine crude oil minimum miscibility pressure – Pure and mixed CO_2, methane, and ethane: Energy & Fuels, v. 30, p. 6365–6372; DOI: 10.1021/acs.energyfuels.6b01151.

Hitchon, B., 1996, Aquifer disposal of carbon dioxide: hydrodynamic and mineral trapping—proof of concept: Sherwood Park, AB, Canada, Geoscience Publishing Ltd.

Holm, L.W., and Josendal, V.A., 1974, Mechanisms of oil displacement by carbon dioxide: Journal of Petroleum Technology, v. 26, no. 12.

Jiang, H., Nuryaningsih, L., and Adidharma, H., 2012, The influence of O_2 contamination on MMP and core flood performance in miscible and immiscible CO_2 WAG, *in* Proceedings of the SPE Improved Oil Recovery Symposium, SPE 154252: Tulsa, Oklahoma, April 14–18.

Jin, L., Wang, Y., and Li, Y., 2015, The consideration of pore size distribution in organic-rich unconventional formations may increase oil production and reserve by 25%, Eagle Ford case study, *in* Proceedings of the Unconventional Resources Technology Conference, URTeC-2148314: San Antonio, Texas, July 20–22.

Jin, L., Sorensen, J.A., Hawthorne, S.B., Smith, S.A., Bosshart, N.W., Burton-Kelly, M.E., Miller, D.J., Grabanski, C.B., and Harju, J.A., 2016a, Improving oil transportability using CO_2 in the Bakken System – a laboratorial investigation, *in* Proceedings of the SPE International

Conference & Exhibition on Formation Damage Control, SPE-178948: Lafayette, Louisiana, February 24–26.

Jin, L., Hawthorne, S.B., Sorensen, J.A., Kurz, B., Pekot, L.J., Smith, S.A., Bosshart, N.B., Azenkeng, A., Gorecki, C.D., and Harju, J.A., 2016b, A systematic investigation of gas-based improved oil recovery technologies for the Bakken tight oil formation, *in* Proceedings of the Unconventional Resources Technology Conference, URTeC-2433692: San Antonio, Texas, August 1–3.

Juanes, R., Spiteri, E.J., Orr Jr., F.M., and Blunt, M.J., 2006, Impact of relative permeability hysteresis on geological CO_2 storage: Water Resources Research, v. 42, no. 12.

Karsten, P., and Nordbotten, J., 2011, Numerical simulation studies of the long-term evolution of a CO_2 plume in a saline aquifer with a sloping caprock: Transport in Porous Media, v. 90, no. 1.

Khosravi, M., Rostami, B., Emadi, M., and Roagaie, R., 2015, Marangoni flow—an unknown mechanism for oil recovery during near-miscible CO_2 injection: Journal of Petroleum Science and Engineering, v. 125, p. 263–268.

Li, S., Dong, M., Li, Z., Qing, H., and Nickel, E., 2005, Gas breakthrough pressure for hydrocarbon reservoir seal rocks—implications for the security of long-term CO_2 storage in the Weyburn Field: Geofluids, v. 5, no. 4.

Lindeberg, E., and Bergmo, P., 2003, The long-term fate of CO_2 injected into an aquifer: Greenhouse Gas Control Technologies, v. 1.

Liu, G., Braunberger, J.R., Pu, H., Gao, P., Gorecki, C.D., Ge, J., Klenner, R.C.L., Bailey, T.P., Dotzenrod, N.W., Bosshart, N.W., Ayash, S.C., Hamling, J.A., Steadman, E.N., and Harju, J.A., 2014, Bell Creek test site – simulation report: Plains CO_2 Reduction (PCOR) Partnership Phase III Task 9 Deliverable D66 Update 3 for U.S. Department of Energy National Energy Technology Laboratory Cooperative Agreement No. DE-FC26-05NT42592, August.

Manrique, E.J., Muci, V.E., and Gurfinkel, M.E., 2007, EOR field experiences in carbonate reservoirs in the United States: SPE Reservoir Evaluation & Engineering. v. 10.

Martin, I., and Ringrose, P., 2009, Evaluating the impact of fractures on the long-term performance of the In Salah CO_2 storage site: Energy Procedia, v. 1, no. 1.

Metcalfe, R.S., 1982, Effects of impurities on minimum miscibility pressures and minimum enrichment levels for CO_2 and rich-gas displacements: Society of Petroleum Engineers Journal, v. 22, no. 02.

Molnar, P.S., 1990, Geologic reservoir study of the Bell Creek Field, Carter and Powder River Counties, Montana: Midland, Texas, Exxon Company.

Moore, J., Adams, M., Allis, R., Lutz, S., and Rauzi, S., 2005, Mineralogical and geochemical consequences of the long-term presence of CO_2 in natural reservoirs: an example from the Springerville—St. Johns Field, Arizona, and New Mexico, USA: Chemical Geology, v. 217, no. 3.

Pande, K.K., 1992, Effects of gravity and viscous crossflow on hydrocarbon miscible flood performance in heterogeneous reservoirs, in Proceedings of the SPE Annual Technical Conference and Exhibition, SPE 24935: Washington, D.C., October 4–7.

Pau, G.S.H., Bell, J.B., Pruess, K., Almgren, A.S., Lijewski, M.J., and Zhang, K., 2010, High-resolution simulation and characterization of density-driven flow in CO_2 storage in saline aquifers: Advances in Water Resources, v. 33, no. 4.

Poston, S.W., and Gross, S.J., 1986, Numerical simulation of sandstone reservoir models: SPE Reservoir Engineering, v. 1, no. 04.

Pu, H., Hamling, J.A., Bremer, J.M., Bailey, T.P., Braunberger, J.R., Ge, J., Saini, D., Sorensen, J.A., Gorecki, C.D., Steadman, E.N., and Harju, J.A., 2011, Bell Creek test site – simulation report: Plains CO_2 Reduction (PCOR) Partnership Phase III Task 9 Deliverable D66 for U.S. Department of Energy National Energy Technology Laboratory Cooperative Agreement No. DE-FC26-05NT42592, August.

Rogers, J.D., and Grigg, R.B., 2000, A literature analysis of the WAG injectivity abnormalities in the CO_2 process, in Proceedings of the SPE/DOE Improved Oil Recovery Symposium, SPE-59329: Tulsa, Oklahoma, April 3–5.

Saini, D., Braunberger, J.R., Pu, H., Bailey, T.P., Ge, J., Crotty, C.M., Liu, G., Hamling, J.A., Gorecki, C.D., Steadman, E.N., and Harju, J.A., 2012, Bell Creek test site – simulation report: Plains CO_2 Reduction (PCOR) Partnership Phase III Task 9 Deliverable D66 Update 1 for U.S. Department of Energy National Energy Technology Laboratory Cooperative Agreement No. DE-FC26-05NT42592, August.

Shelton, J.L., Mcintosh, J.C., Hunt, A.G., Beebe, T.L., Parker, A.D., Warwick, P., Drake, R.M., and McCray, J.E., 2016, Determining CO_2 storage potential during miscible CO_2 enhanced oil recovery—noble gas and stable isotope tracers: International Journal of Greenhouse Gas Control, v. 51, p. 239–253.

Shyeh-Yung, J.J., and Stadler, M.P., 1995, Effect of injectant composition and pressure on displacement of oil by enriched hydrocarbon gases. SPE Reservoir Engineering, v. 10, no. 02.

Sohrabi, M., Danesh, A., Tehrani, D.H., and Jamiolahmady, M., 2008, Microscopic mechanisms of oil recovery by near-miscible gas injection: Transport of Porous Media, v. 72, no. 3, p. 351–367.

Spiteri, E.J., Juanes, R., Blunt, M.J., and Orr, Jr., F.M., 2008, A new model of trapping and relative permeability hysteresis for all wettability characteristics: SPE Journal, v. 13, no. 3.

Steadman, E.N., Anagnost, K.K., Botnen, B.W., Botnen, L.S., Daly, D.J., Gorecki, C.D., Harju, J.A., Jensen, M.D., Peck, W.D., Romuld, L., Smith, S.A., Sorensen, J.A., and Votava, T.J., 2011, The Plains CO_2 Reduction (PCOR) Partnership – developing carbon management options for the central interior of North America: Energy Procedia, v. 4, p. 6061–6068.

Terrell, M.J., Davis, T.L., Brown, L., and Fuck, R., 2002, Seismic monitoring of a CO_2 flood at Weyburn Field, Saskatchewan, Canada—demonstrating the robustness of time-lapse seismology, *in* Proceedings of the SEG Annual Meeting, SEG-2002-1673: Salt Lake City, Utah, October 6–11.

Thanke, J.N., Lecain, G.D., Ryter, D.W., Sando, R. and Long, A.J., 2014, Hydrogeologic framework of the uppermost principal aquifer systems in the Williston and Powder River Structural Basins, United States and Canada: Scientific Investigations Report 2014–5047.

Thomas, F.B., Holowach, N., Zhou, X., Bennion, D.B., and Bennion, D.W., 1994, Miscible or near-miscible gas injection, which is better? *in* Proceedings of the SPE/DOE improved oil recovery symposium, SPE 27811: Tulsa, Oklahoma, April 17–20.

Uj, I., and Fekete, T., 2011, CO_2 Gas + WAG + water injection in the same oil reservoir—case study, *in* Proceedings of the SPE Enhanced Oil Recovery Conference, SPE-143833: Kuala Lumpur, Malaysia, July 19–21.

Wang, J., Ryan, D., Anthony, E.J., Wildgust, and Aiken, T., 2011, Effects of impurities on CO_2 transport, injection and storage: Energy Procedia, v. 4, 2011.

Weir, G.J., White, S.P., and Kissling, W.M., 1995, Reservoir storage and containment of greenhouse gases: Energy Conversion and Management, v. 36, no. 6.

White, S.P., Allis, R.G., Moore, J., Chidsey, T., Morgan, C., Gwynn, W., and Adams, M., 2005, Simulation of reactive transport of injected CO_2 on the Colorado Plateau, Utah, USA: Chemical Geology, v. 217, no. 3.

Wilkinson, J.R., Leahy-Dios, A., Teletzke, G.F., and Dickson, J.L., 2010, Use of CO_2 containing impurities for miscible enhanced oil recovery, *in* Proceedings of the CPS/SPE International Oil & Gas Conference and Exhibition in China, SPE 131003: Beijing, China, June 8–10.

Yellig, W.F., and Metcalfe, R.S., 1980, Determination and prediction of CO_2 minimum miscibility pressures: Journal of Petroleum Technology, v. 32, no. 1.

Yin, D.D., Li, Y.Q., and Zhao, D.F., 2014, Utilization of produced gas of CO_2 flooding to improve oil recovery: Journal of the Energy Institute, v. 87, no. 4.

Zhang, K., and Gu, Y., 2015, Two different technical criteria for determining the minimum miscibility pressures (MMPs) from the slim-tube and coreflood tests: Fuel, v. 161.

Zhou, W., Stenhouse, J.J., Arthur, R., Whittaker, S., Law, S., Chalaturnyk, R., and Jazrawi, W., 2004, The IEA Weyburn CO_2 monitoring and storage project—modeling of the long-term migration of CO_2 from Weyburn, *in* Proceedings of the 7th International Conference on Greenhouse Gas Control Technologies.

APPENDIX A

BELL CREEK NEAR-SURFACE MODEL PETROPHYSICAL PROPERTIES

BELL CREEK NEAR-SURFACE MODEL PETROPHYSICAL PROPERTIES

Petrophysical properties were geostatistically distributed in the model following the correlation of available well logs with core data collected from the North Dakota Geological Survey's Ground-Water Resource Bulletins Part II on Ground-Water Basic Data (Randich, 1975; Klausing, 1976; Ackerman, 1977; Anna, 1980; Croft, 1985). Core data from the bulletins were combined for a total of 101 data points.

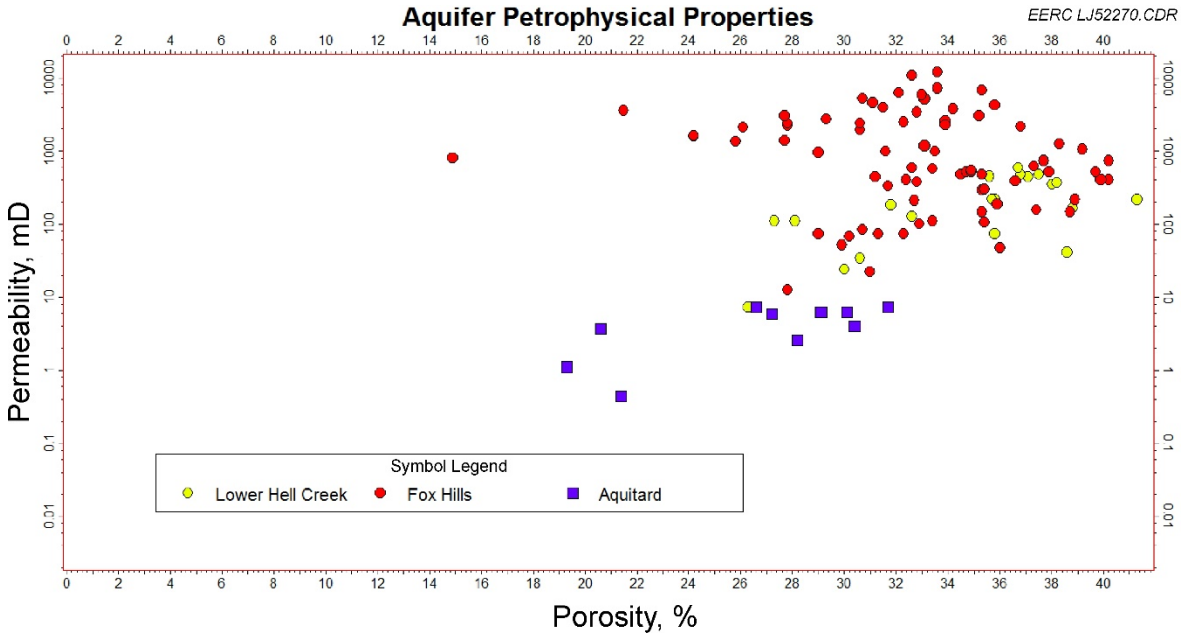

Figure A-1. Crossplot of the porosity vs. permeability of the Fox Hills and lower Hell Creek aquifers taken from the Williston Basin, North Dakota.

REFERENCES

Ackerman, D.J., 1977, Ground-water basic data for Morton County, North Dakota: U.S. Geological Survey for North Dakota State Water Commission County Ground-Water Studies 27, part II and North Dakota Geological Survey Bulletin 72, part II, 592 p.

Anna, L.O., 1980, Ground-water data for Billings, Golden Valley and Slope Counties, North Dakota: U.S. Geological Survey for North Dakota State Water Commission County Ground-Water Studies 29, part II and North Dakota Geological Survey Bulletin 76, part II, 241 p.

Croft, M.G., 1985, Ground-water basic data for McKenzie County, North Dakota: U.S. Geological Survey for the North Dakota State Water Commission County Ground-Water Studies 37, part II and North Dakota Geological Survey Bulletin 80, part II, 455 p.

Klausing, R.L., 1976, Ground-water basic data for Dunn County, North Dakota: U.S. Geological Survey for North Dakota State Water Commission County Ground-Water Studies 25, part II, and North Dakota Geological Survey Bulletin 68, part II, 501 p.

Randich, P.G., 1975, Ground-water basic data for Grant and Sioux Counties, North Dakota: U.S. Geological Survey for North Dakota State Water Commission County Ground-Water Studies 24, part II, and North Dakota Geological Survey Bulletin 67, part II, 303 p.

APPENDIX B

MEASURING MMP USING THE VANISHING INTERFACIAL TENSION (VIT) METHOD

MEASURING MMP USING THE VANISHING INTERFACIAL TENSION (VIT) METHOD

Figure B-1 shows the experimental setup of the capillary-rise vanishing interfacial tension (VIT) test for minimum miscibility pressure (MMP) measurement. The key components include a CO_2 supply tank with dip tube; an ISCO Model 260D syringe pump (ISCO-Teledyne, Lincoln, Nebraska, USA); two fluid control/shut-off valves; a digital pressure gauge calibrated to a deadweight tester; an Agilent Model 5890 gas chromatographic oven with the door modified to include a 1.3-cm-thick polycarbonate viewport (the oven provides fan-circulated heat within 0.1°C of the set point); a 1/16 inch stainless steel preheating coil; a high-pressure view cell (Inferno Manufacturing Corporation, Shreveport, Louisiana, USA) for pressures up to 6000 psi; a video camera; and a computer. The view cell contains a 1.0-cm-wide and 3.0-cm-long stainless steel rack holding three 15-mm-long glass capillary tubes labeled "A," "B," and "C," with their bottoms suspended in a pool of oil. The capillary tubes have inner diameters of 1.12, 0.84, and 0.68 mm, respectively (World Precision Instruments, Inc., Sarasota, Florida, USA). The oil heights in the capillary tubes are monitored with a video camera and recorded on a computer.

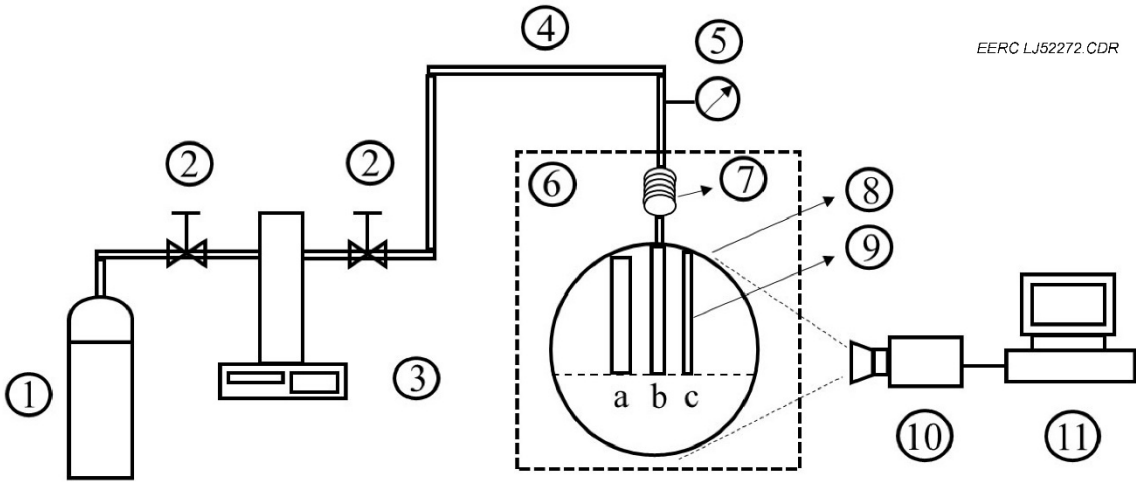

1: CO_2 tank; 2: Shut-off valves; 3: ISCO pump; 4: Connecting tubing;
5: Pressure gauge calibrated to a dead weight tester; 6: Gas chromatographic oven;
7: Preheating coil; 8: High-pressure view cell; 9: Capillary tubes;
10: Video camera; 11: Computer

Figure B-1. Schematic of VIT test experimental setup for MMP measurement (Hawthorne and Miller, 2014; Hawthorne and others, 2016).

The MMP measuring process using this setup is briefly described in the following steps:

1. Mount the capillary tubes and their rack into the high-pressure view cell.

2. Close the cell and sweep it several times with the test gas such as CO_2.

3. Inject the test oil into the view cell using a calibrated syringe. Immediately reattach the cell to the fluid inlet line. The volume of the injected oil is such that the top of the oil layer floods the capillary rack but leaves most of the capillary tubes' length exposed to the empty space.

4. Heat the view cell containing oil and test gas for 1 hour to the test temperature. The temperature for Bell Creek oil testing was 108°F. Record the pressure in the cell, and begin the video monitoring.

5. Increase the gas pressure in the cell by 40 to 100 psi per step by opening the control valve which is closer to the gas chromatographic oven. Shut this control valve after brief gas injection to eliminate backflow of the injectant. After allowing a suitable time for the fluids to equilibrate, record the cell pressure along with a time signature to correspond with the video recording that occurs throughout the procedure.

6. Record video of the oil height in the three capillary tubes at each test pressure. From the video displayed on a computer screen, record the height from the top of the bulk oil phase to the oil/CO_2 meniscus in each capillary tube by counting video pixels, yielding a capillary height resolution of <0.1 mm.

More in-depth experimental details have been described by Hawthorne and others (2016; Hawthorne and Miller, 2014).

MMP MEASURING RESULTS

Figure B-2 shows the oil–CO_2 dynamic miscibility developing process during a typical VIT test at a low-CO_2 pressure (left), pressure approximately ½ of the MMP (middle), and as the pressure approaches MMP (right). This clearly illustrates how two important processes occur (as temperature remains constant): 1) the interfacial tension (IFT) decreases (lowering of the oil/CO_2 meniscus), and 2) the hydrocarbons vaporize into the CO_2 with increasing injection pressure. When the injection pressure reaches MMP, the height of the oil in each capillary goes to zero (as the IFT between the two fluids goes to zero). This observation enables determination of MMP conveniently using a simple plot, such as is shown in Figure B-3, where the measured meniscus heights for the three different diameter capillary tubes are plotted together. The MMP is where the three extrapolated lines merge into a point on the pressure axis. The VIT-measured MMP of Bell Creek oil is around 1410 psi for pure CO_2 at reservoir temperature (108°F). For comparison, the slim-tube test yields an MMP of 1430 psi (Figure B-4). The difference between the two measurements is less than 1.5%, indicating the result from VIT is very close to that of the slim-tube test, encouraging procedural validation.

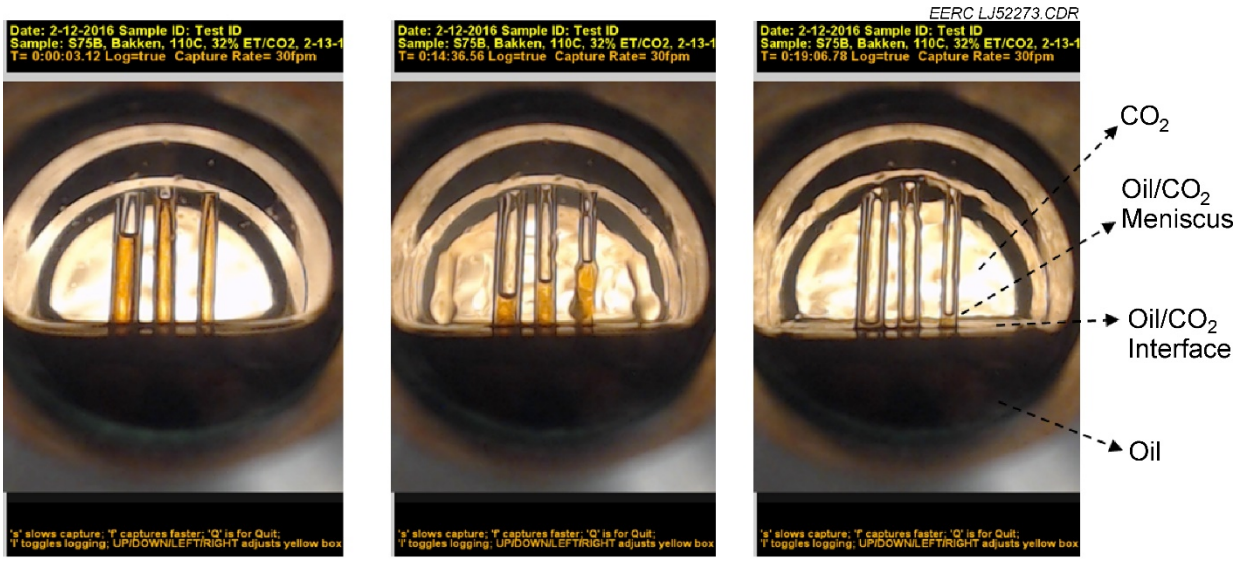

Figure B-2. Development of oil/CO_2 miscibility using the VIT method at different pressures (Hawthorne and Miller, 2014; Hawthorne and others, 2016).

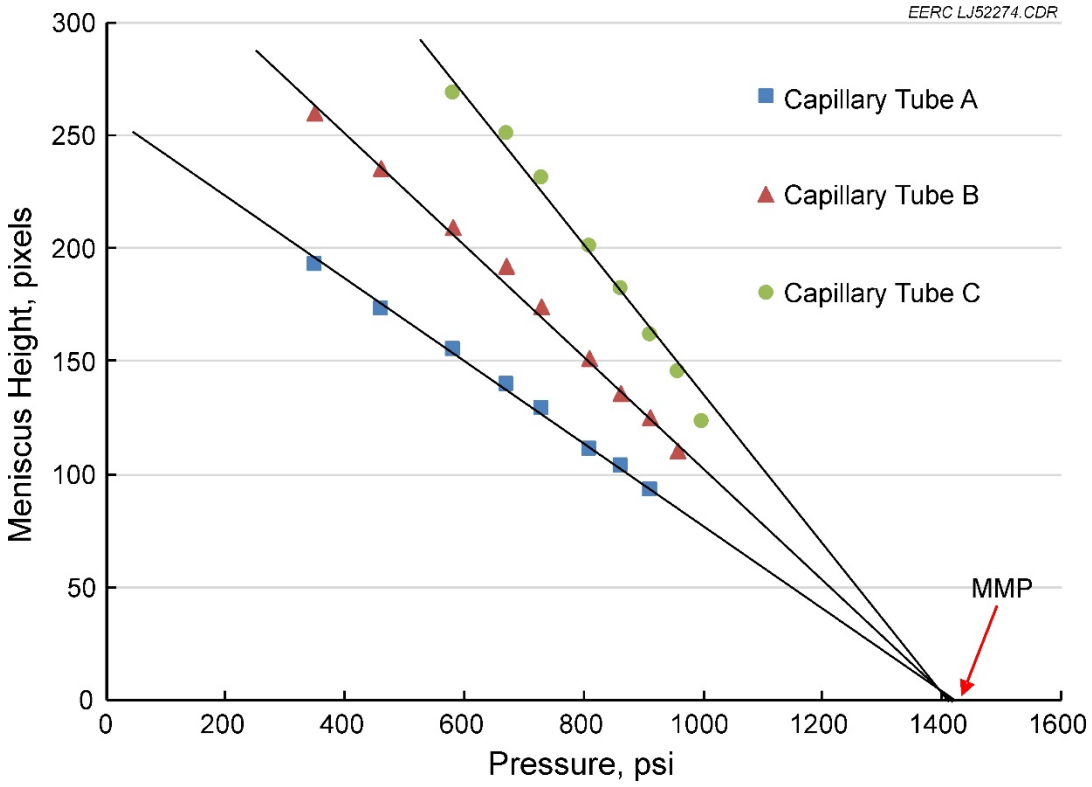

Figure B-3. VIT test for Bell Creek oil–CO_2 MMP measurement at 108°F.

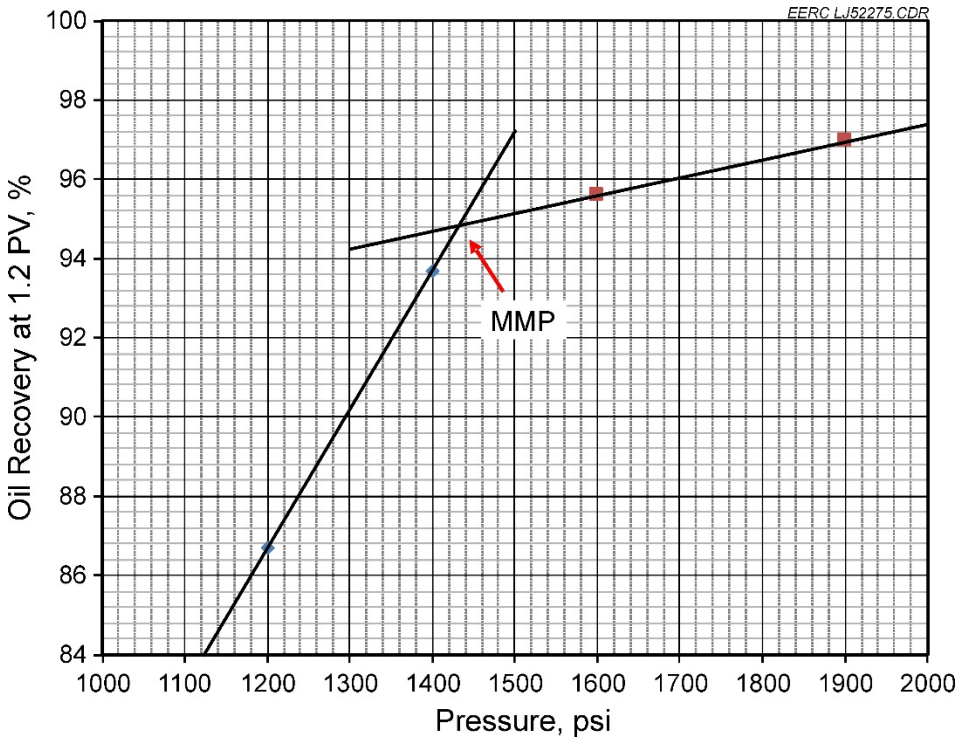

Figure B-4. Slim-tube test for Bell Creek oil–CO_2 MMP measurement at 108°F.

By adding CH_4 to the CO_2 stream and repeating the VIT test procedure discussed above (steps 1–6), the variation of Bell Creek oil MMPs for different CO_2/CH_4 mixtures may be measured (Figure B-5). The figure demonstrates that MMP values increase linearly with increase in the CH_4 fraction of the CO_2/CH_4 mixture. The MMP values vary from approximately 1400 psi for 0 mol% CH_4 to about 4000 psi for 100 mol% CH_4 in the mixture. The results indicate miscible gas flooding may still be attainable with up to 30 mol% CH_4 in the recycled gas stream if the reservoir pressure is maintained at or above 2500 psi (Figure B-5).

DISCUSSION

The use of three capillaries in each determination yields triplicate MMP values. With the capillary-rise VIT method described here, the MMP values from the three capillaries typically agree within a relative standard deviation (RSD) less than 2%, and rarely vary more than 5% RSD. In addition, replicate determinations of MMP with new samples of the same oil also typically agree within 2%, which demonstrates that the method is repeatable and robust (Ahmad and others, 2016; Hawthorne and Miller, 2014; Hawthorne and others, 2016).

The VIT process also gives insight as to how CO_2 recovers the oil remaining in the pore space after waterflooding. The oil is in residual condition relative to water and does not move if the IFT is not alleviated. Miscible CO_2 injection mobilizes some of this oil (based on the various

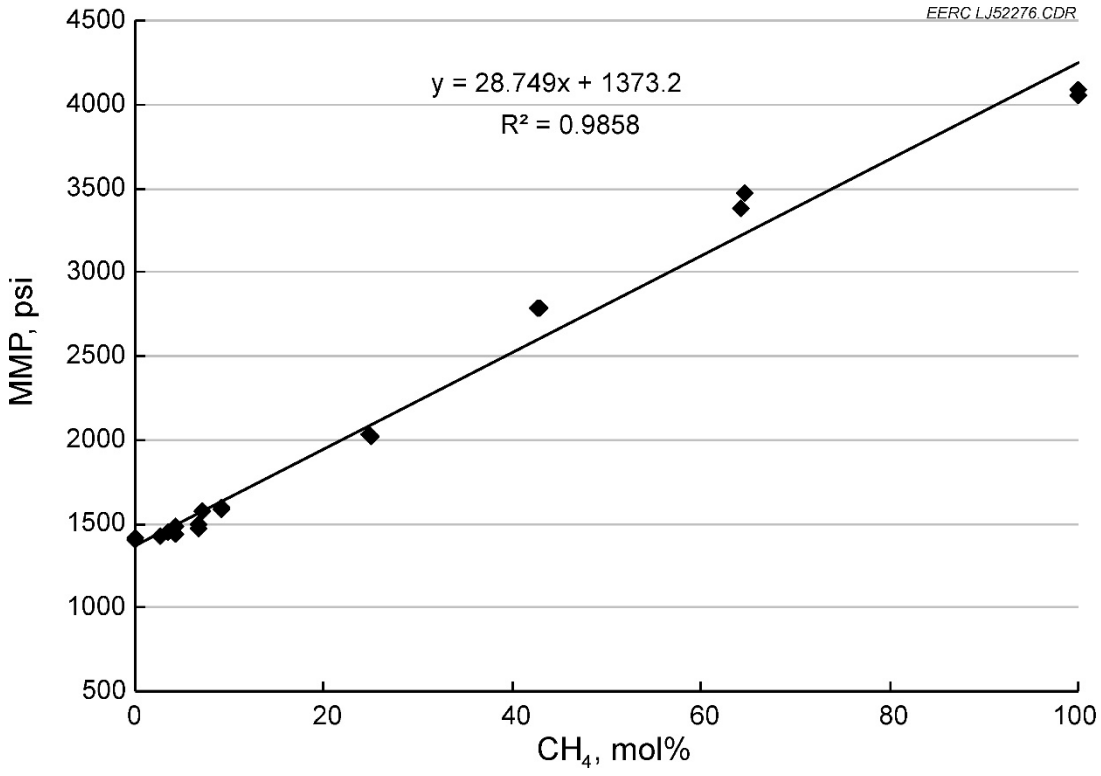

Figure B-5. MMP for Bell Creek oil with CO_2/CH_4 mixtures at 108°F.

mechanisms mentioned above) and drives the hydrocarbons into the CO_2 phase. The mobilized oil is then produced (with or without CO_2). Because water has higher density and viscosity than CO_2 (and CO_2 is highly soluble in water), in some scenarios it may be helpful to inject a slug of water to displace the hydrocarbon-saturated CO_2, potentially improving sweep efficiency and oil recovery. This process is referred to as WAG (water-alternating-gas) injection, which has been widely used in CO_2 EOR operations (Rogers and Grigg, 2000; Manrique and others, 2007; Chen and others, 2010; Uj and Fekete, 2011).

REFERENCES

Ahmad, W., Vakili-Nezhaad, G., Al-Bemani, A.S., and Al-Wahaibi, Y., 2016, Uniqueness, repeatability analysis and comparative evaluation of experimentally determined MMPs: Journal of Petroleum Science and Engineering, v. 147, November.

Chen, S., Li, H., Yang, D., and Tontiwachwuthikul, P., 2010, Optimal parametric design for water-alternating-gas (WAG) process in a CO_2-miscible flooding reservoir: Journal of Canadian Petroleum Technology, v. 49, no. 10.

Hawthorne, S.B., and Miller, D.J., 2014, Determining minimum miscibility pressure of an oil composition with a fluid: U.S. Patent 14/470,241, filed August 27, 2014.

Hawthorne, S.B., Miller, D.J., Jin, L., and Gorecki, C.D., 2016, Rapid and simple capillary-rise/vanishing interfacial tension method to determine crude oil minimum miscibility pressure – pure and mixed CO_2, methane, and ethane: Energy & Fuels, v. 30, p. 6365–6372; DOI: 10.1021/acs.energyfuels.6b01151.

Manrique, E.J., Muci, V.E., and Gurfinkel, M.E., 2007, EOR field experiences in carbonate reservoirs in the United States: SPE Reservoir Evaluation & Engineering. v. 10.

Rogers, J.D., and Grigg, R.B., 2000, A literature analysis of the WAG injectivity abnormalities in the CO_2 process, in Proceedings of the SPE/DOE Improved Oil Recovery Symposium, SPE-59329: Tulsa, Oklahoma, April 3–5.

Uj, I., and Fekete, T., 2011, CO_2 Gas + WAG + water injection in the same oil reservoir—case study, *in* Proceedings of the SPE Enhanced Oil Recovery Conference, SPE-143833: Kuala Lumpur, Malaysia, July 19–21.